

BRAIN OSCILLATORY ANALYSIS OF VISUAL WORKING MEMORY ERRORS

A THESIS SUBMITTED TO
THE GRADUATE SCHOOL OF INFORMATICS OF
THE MIDDLE EAST TECHNICAL UNIVERSITY
BY

IGOR MAPELLI

IN PARTIAL FULFILLMENT OF THE REQUIREMENTS FOR THE DEGREE OF
DOCTOR OF PHILOSOPHY OF SCIENCE
IN
HEALTH INFORMATICS DEPARTMENT

FEBRUARY 2019

BRAIN OSCILLATORY ANALYSIS OF VISUAL WORKING MEMORY ERRORS

Submitted by **Igor Mapelli** in partial fulfillment of the requirements for the degree of **Doctor of Philosophy of Science in the Health Informatics Department, Middle East Technical University** by,

Prof. Dr. Deniz Zeyrek Bozşahin
Dean, **Graduate School of Informatics**

Assoc. Prof. Dr. Yeşim Aydın Son
Head of Department, **Health Informatics**

Assoc. Prof. Dr. Tolga Esat Özkurt
Supervisor, **Health Informatics Dept., METU**

Examining Committee Members:

Prof. Dr. Ünal Erkan Mumcuoğlu
Health Informatics Department, METU

Assoc. Prof. Dr. Tolga Esat Özkurt
Health Informatics Department, METU

Assoc. Prof. Dr. Cengiz Acartürk
Cognitive Science Department, METU

Assoc. Prof. Dr. Tolga Çukur
Electrical and Electronics Engineering Department,
Bilkent University

Prof. Dr. Canan Kalaycıoğlu
Physiology Department, Medical School, Ankara
University

Date: 01/02/2019

I hereby declare that all information in this document has been obtained and presented in accordance with academic rules and ethical conduct. I also declare that, as required by these rules and conduct, I have fully cited and referenced all material and results that are not original to this work.

Name, Last Name: IGOR MAPELLI

Signature : _____

ABSTRACT

BRAIN OSCILLATORY ANALYSIS OF VISUAL WORKING MEMORY ERRORS

MAPELLI, IGOR

Ph.D., Health Informatics Department

Supervisor: Assoc. Prof. Dr. Tolga Esat Özkurt

February 2019, 130 pages

Brain dynamics of memory formation were explored throughout a working memory (WM) task. Electroencephalography data were acquired from participants while presented with grayscale photos of object categories (each category defined by images sharing a common gist). Following a short delay, two probes were shown to test memory accuracy. Time-frequency representations of successful and erroneous memories were contrasted. Additionally, brain connectivity was studied via coherency and phase-amplitude coupling (PAC). Where significant differences were identified, oscillatory properties of false memories (a novel item of the same category recognized as familiar) were compared with those of successful and erroneous memories. Spectral analysis revealed occipital theta power for encoding of successful and false memories to be smaller when compared to other memory errors. The reduced theta power indicates successful encoding and reflects efficient activation of the underlying neural assemblies. During the retention interval, prominent alpha-beta activity over right parieto-occipital channels was found to be larger for false memories and errors when compared to correct responses. High levels of alpha-beta oscillatory activity for errors indicate poor maintenance leading to inefficient allocation of WM resources. For false memories, they imply necessary cognitive effort to manage an extra semantic and perceptual load induced during encoding. Significant fronto-occipital coherency was measured: Possibly, theta and alpha band coherency reflect central executive functions of WM, whereas beta band coherency indicates coordination of local assemblies related to stimulus representations. Significant theta/gamma PAC, linked to WM retention of sequentially encoded stimuli, and alpha/gamma PAC, reflecting processing of visuo-spatial information, were also observed.

Keywords: Visual Working Memory, False Memory, memory errors, neural oscillations, EEG

ÖZ

GÖRSEL ÇALIŞMA BELLEĞİ HATALARININ BEYİN OSİLYON ANALİZİ

MAPELLI, IGOR

Doktora, Tıp Bilişimi Bölümü

Tez Yöneticisi: Doç. Dr. Tolga Esat Özkurt

Şubat 2019, 130 sayfa

Çalışma Belleği (ÇB) görevi boyunca, bellek oluşumunun beyin dinamikleri incelenmiştir. Nesne kategorilerine ait (her bir kategori, ortak bir özelliği olan görüntülerle tanımlanmıştır) gri skala fotoğraflar gösterildiği sırada deneklerden, elektroensefalografi (EEG) verileri toplanmıştır. Kısa bir aranın/bekletmenin ardından, belleği test üzere deneklere iki görüntü gösterilmiştir. Doğru ve yanlış anıların zaman-frekans temsilleri karşılaştırılmıştır. Bununla birlikte tutarlık ve faz-genlik kuplajı (FGK) bağlantısallık tahminleri yoluyla beyin bağlantısallığı çalışılmıştır. Önemli farklar tespit edildiğinde, sahte anıların salınımlı nitelikleri (aynı kategoriden yeni bir ögenin tanıdık gelmesi) doğru ve yanlış anılarınkilerle karşılaştırılmıştır. Spektral analiz, diğer bellek hatalarıyla karşılaştırıldığında, doğru ve yanlış anıların kodlanmasındaki oksipital Teta gücünün daha düşük olduğunu göstermiştir. Düşük Teta gücü, başarılı kodlamaya işaret etmekte ve altta yatan nöral kurulumların etkin şekilde aktive olduğunu göstermektedir. Akılda tutulma aralığı boyunca, sağ paryetal-okcipital kanallar üzerindeki baskın alfa-beta aktivitesinin doğru yanıtlarla karşılaştırıldığında sahte anı ve hatalardan daha büyük olduğu tespit edilmiştir. Hatalar için alfa-beta salınım aktivitesinin yüksek düzeylerde seyretmesi, ÇB kaynaklarının etkin olmayan bir şekilde atanmasına yol açan zayıf tutunmaya işaret etmektedir. Sahte anılar için bu, kodlama sırasında tetiklenen ek bir anlamsal ve algısal yükün yönetilmesi için gerekli olan bilişsel bir çabayı ifade edecektir. Önemli düzeyde bir frontookcipital tutarlık ölçülmüştür: Olasılıkla, Teta ve Alfa bandı tutarlığı, ÇB'nin merkezi yönetsel işlevlerini yansıtmakta; Beta bandı tutarlığı ise uyaran temsilleriyle ilgili lokal kurulumların koordinasyonunu göstermektedir. Sırayla kodlanan uyaranların ÇB tutunumuyla ilgili önemli Teta/Gamma FGK ile görsel-mekansal bilginin işlenişini yansıtan Alpha/gamma FGK gözlemlenmiştir.

Anahtar Sözcükler: Görsel Çalışma Belleği, Sahte Anı, bellek hataları, sinirsel salınımlar, EEG

To Luka and Ece, my Pillars of Creation

ACKNOWLEDGMENTS

I am wholeheartedly thankful to my supervisor, Tolga Esat Özkurt, whose patient guidance, enthusiastic encouragement and useful critiques of this research work enriched me beyond academic knowledge.

My gratitude to my (former) lab mate, Natalia Melnik, for her help with data acquisition and more importantly for having endured patiently my monologues (both neurosciences related and randomly triggered).

I am also thankful to Ece Çağlayan and Sibel Özer for their great contributions during experiment sessions.

Last but foremost my Turkish and my Italian families with their ∞ patience, but especially their intersection, Luka and Ece, you are my northern stars.

I want to acknowledge the main open-source software programs and communities that helped me throughout the whole doctoral period: Ubuntu, GNOME, Mozilla Firefox, Mozilla Thunderbird, GIMP, Krita, LibreOffice. These are only few among a multitude of amazing projects that contributed, directly or indirectly, to this research.

I would also like to acknowledge the financial support of the Scientific and Technological Research Council of Turkey under TÜBİTAK 3501 (#112E562).

TABLE OF CONTENTS

ABSTRACT	iv
ÖZ.....	v
DEDICATION	vi
ACKNOWLEDGMENTS.....	vii
TABLE OF CONTENTS	viii
LIST OF TABLES	xi
LIST OF FIGURES.....	xii
LIST OF ABBREVIATIONS	xv
CHAPTERS	
1. INTRODUCTION.....	1
2. LITERATURE REVIEW.....	3
2.1. Visual System: Human Eye and Pathways to the Visual Cortex	3
2.2. Theories of Vision: Framing the Problem of Visual Perception	8
2.2.1. Structuralism	8
2.2.2. Gestaltism.....	8
2.2.3. Ecological optics	9
2.2.4. Constructivism	10
2.3. Visual Attention: Directing Relevant Information into Awareness	10
2.4. Visual Memory: Preserving Information Pertaining to the Visual Experience.....	11
2.4.1. Iconic memory.....	12
2.4.2. Visual short-term memory	12
2.4.3. Visual long-term memory	12
2.5. Working Memory	13
2.5.1. Cowan’s embedded process theory.....	13
2.5.2. Individual difference-based theories	13

2.5.3.	Jonides and the mind and brain of short-term memory.....	13
2.5.4.	Computational models of working memory	13
2.5.5.	Baddeley and Hitch's working memory model	14
2.6.	Semantic Memory	14
2.7.	False Memory.....	15
2.8.	Cognitive Electrophysiology: Reflections of Cortical Functions.....	16
2.8.1.	Electroencephalogram.....	16
2.8.2.	Magnetoencephalogram	17
2.8.3.	Event-related potentials analyses	17
2.8.4.	Time-frequency based analyses	18
2.8.5.	Connectivity analyses.....	19
2.8.6.	Frequency bands.....	23
2.9.	Neural Correlates of Visual Working Memory	25
2.10.	Research Questions	28
3.	MATERIALS AND METHODS	31
3.1.	Participants	31
3.2.	Stimuli	33
3.3.	Paradigm.....	33
3.4.	Procedure.....	35
3.5.	Electroencephalographic Recordings	35
3.6.	Preprocessing and Time-Frequency Analysis	35
3.7.	Conditions and Trial Selection for the Oscillatory Analysis.....	39
3.7.1.	Correct and error	39
3.7.2.	False memory	39
3.8.	Channel Selection and Frequencies of Interest for the Encoding Interval	40
3.9.	Channel Selection and the Individual Central Frequency for the Retention Interval	41
3.10.	Gamma Band Analysis Within the Encoding and Retention Interval.....	42
3.11.	Statistical Analyses of Behavioral Measurements	44
3.12.	Cluster Permutation Statistics	44
3.13.	Connectivity Analyses.....	45

3.13.1.	Coherency	45
3.13.2.	Phase-amplitude coupling.....	49
4.	RESULTS.....	51
4.1.	Behavioral Analysis.....	51
4.1.1.	Six conditions: Correct, false memory and type I, II, III, IV errors.....	51
4.1.2.	Three conditions: Correct, false memory, error	53
4.2.	Oscillatory Analysis	56
4.3.	Connectivity Analysis.....	61
4.3.1.	Coherency.....	61
4.3.2.	Phase-amplitude coupling	67
5.	DISCUSSION AND CONCLUSION.....	71
5.1.	Correct and Error	71
5.2.	False Memory	74
5.3.	Connectivity.....	75
5.3.1.	Coherency.....	75
5.3.2.	Phase-amplitude coupling	75
5.4.	Limitations and Future Research.....	76
5.5.	Conclusions	76
	REFERENCES.....	79
	APPENDIX A	101
	APPENDIX B	103
	APPENDIX C	105
	APPENDIX D	107
	CURRICULUM VITAE	123

LIST OF TABLES

Table 1: Definition of the experimental conditions	34
Table 2: Subjects' rate distribution and response time	52
Table 3: Statistical results pertaining to the coherency investigation	67
Table 4: Participants' information and task performance	104
Table 5: Averaged response times for each condition and all subjects.....	106

LIST OF FIGURES

Figure 1: Anatomy of the human eye.....	4
Figure 2: Simplified diagram of retina cells layers.....	5
Figure 3: Pathways of the visual system.....	6
Figure 4: Major areas of the human brain and the visual cortex.....	7
Figure 5: Temporally localized frequency decomposition.....	18
Figure 6: Diagram illustrating the steps applied by the multitapering method.....	19
Figure 7: Bivariate measures in the presence of multivariate networks.....	20
Figure 8: Schematic of phase-amplitude coupling on a single electrode.....	21
Figure 9: Theta phase to gamma amplitude coupling in WM.....	22
Figure 10: Phase-amplitude coupling with frontal theta phase modulating parietal gamma power.....	23
Figure 11: Experiment design with example of encoded items and types of probes.....	32
Figure 12: Example of artifact-related component identified by using ICA.....	37
Figure 13: Example of a visual inspection from a representative subject.....	38
Figure 14: Grand average time course over occipital channels and topographical map of theta activity during encoding.....	40
Figure 15: Distribution of the individual central frequency, grand average topography following frequency alignment within the retention interval, and grand average time-frequency portraits prior and following frequency alignment.....	42
Figure 16: Time-frequency portraits of gamma frequencies from a representative subject while performing the experimental task outside of the Faraday room.....	43

Figure 17: Gamma band grand average for the encoding and retention intervals	44
Figure 18: An example of coherency distribution obtained via Monte Carlo simulation for a representative subject.....	47
Figure 19: (A) Example from a representative subject of connectivity between the frontal-right region and the seed channel O2. (B) To account for anatomical differences between subjects, channels were partitioned: Left, right and central locations for frontal, middle and posterior areas respectively	48
Figure 20: Participants' answer rate per condition and average response time considering six conditions (correct, false memory, type I, II, III, IV errors)	53
Figure 21: Participants' response time considering three conditions (correct, false memory, error), correlation between false memory and error rates, and serial position effect.....	55
Figure 22: Theta power difference within the encoding interval between the conditions correct and error: time-frequency plot, topographic contrast between the conditions, and variation of theta power within the encoding interval for correct, error, and false memory conditions	57
Figure 23: Lateralization of the alpha-beta pattern during the second half of the retention interval: Right parieto-occipital channels (P4, P8, O2) exhibited power values higher than the ones observed in the contralateral channels (P3, P7, O1)	58
Figure 24: Alpha-beta power difference within the retention interval between correct and error conditions: time-frequency portrait, topographic pattern, and variation of alpha-beta power within the retention interval for correct, error, and false memory conditions	59
Figure 25: Correlation between response time and power at the individual central frequency.....	60
Figure 26: Squared imaginary coherency for the alpha band (8 – 12 Hz) during the encoding interval.....	61
Figure 27: Squared imaginary coherency for the beta band (13 – 30 Hz) during the encoding interval.....	62
Figure 28: Squared imaginary coherency for the theta band (4 – 7 Hz) during the encoding interval.....	63

Figure 29: Squared imaginary coherency for the alpha band (8 – 12 Hz) during the retention interval64

Figure 30: Squared imaginary coherency for the beta band (13 – 30 Hz) during the retention interval65

Figure 31: Squared imaginary coherency for the theta band (4 – 7 Hz) during the retention interval.....66

Figure 32: Theta (3 – 5 Hz) to lower gamma (30 – 60 Hz) PAC levels68

Figure 33: Alpha (8 – 14 Hz) to upper gamma (60 – 120 Hz) PAC levels.....68

Figure 34: Cross-frequency coupling between the phase of theta (5 – 8 Hz) measured in F4 and the amplitude of gamma (50 – 80 Hz) measured on the remaining channels within the encoding interval69

Figure 35: Cross-frequency coupling between the phase of theta (5 – 8 Hz) measured in F4 and the amplitude of gamma (50 – 80 Hz) measured on the remaining channels within the retention interval.....70

Figure 36: Time-frequency representations and topographical plots highlighting the ICF for each subject.....107

LIST OF ABBREVIATIONS

ANOVA	Analysis of Variance
BOLD	Blood Oxygenation Level Dependent
DFT	Discrete Fourier Transform
DRM	Deese-Roediger-McDermott
EEG	Electroencephalography
ERP	Event-Related Potential
fMRI	Functional Magnetic Resonance Imaging
Hz	Hertz
ICA	Independent Component Analysis
ICF	Individual Central Frequency
ITC	Inferior Temporal Cortex
KHz	Kilohertz
LTM	Long-Term Memory
MEG	Magnetoencephalography
MT	Middle Temporal
PAC	Phase-Amplitude Coupling
PET	Positron Emission Tomography
RT	Response Time
s	Second(s)
SNR	Signal-to-Noise Ratio
STM	Short-Term Memory
TEO	Temporo-Occipital
TFR	Time-Frequency Representation
VLTM	Visual Long-Term Memory
VSTM	Visual Short-Term Memory
VWM	Visual Working Memory
WM	Working Memory

CHAPTER 1

INTRODUCTION

Cognition is an intricate process that gives us the ability to extrapolate information from the environment while assessing it with our senses. The newly acquired knowledge, alongside past experiences, contributes to the thoughts needed to resolve the task at hand. Despite successfully performing ordinary as well as unusual actions, cognitive failures (Broadbent et al., 1982), i.e., minor slips disrupting the activity underway, may occur sporadically.

While the majority of studies focused on memory and action slips, researchers also investigated errors in the context of perception, distractibility and interpersonal intelligence (Carrigan & Barkus, 2016). Cognitive factors, such as attention (i.e., the ability to allocate resources solely on task-related information), inhibition (i.e., the capacity to suppress interfering events) and working memory (WM) (i.e., the storage and maintenance of information within short time intervals), affect the rate to which cognitive failures occur. There are also others non-cognitive factors, such as dissociative experiences, schizotypy, biological, sleep-wake cycle and age, that have been reported to influence cognitive failures (for a review: Carrigan & Barkus, 2016). Studying the inherent causes of failures may allow to identify the most vulnerable sections of the population as well as widen the understanding of the human cognitive system. Furthermore, it may be possible to reduce the frequency of cognitive slips by attempting to control the underlying factors.

Featured among the factors affecting the rate of failures, WM encompasses short-term memory (STM), i.e., the temporary storage unit and all the processes responsible for monitoring, maintaining and manipulating task-relevant information over a brief period of time. Given the critical role played by WM in the cognitive apparatus, its efficiency comes with no surprise. Nevertheless, it is susceptible to distortions and thus investigating the cases where memory fails us can contribute to the understanding of its underlying mechanisms.

Neural oscillations are seen as a fundamental constituent of WM (Lisman & Idiart, 1995; Klimesch, 1996; Buzsáki & Draguhn, 2004; Eriksson et al., 2015). As cognitive dynamics related to WM unfold in mere seconds, it is important to use the appropriate tools to effectively conduct these investigations. For this reason, electroencephalography (EEG),

a relatively simple and inexpensive technology, became a common tool used to probe the oscillatory dynamics linked to WM. EEG provides an adequate temporal sensitivity, which is equatable to magnetoencephalography (MEG) and two orders of magnitude faster than the hemodynamic responses recorded via functional magnetic resonance imaging (fMRI). The neurophysiological factors contributing to EEG signals are yet to be fully understood. It is generally accepted that the voltage fluctuations recorded by EEG on the scalp reflect the macroscopic dynamics of populations of neurons in the cortex (Cohen, 2014). Whereas EEG provides data with high temporal resolution, it does not allow for the precise localization of the sources within the brain, particularly deep brain structures. Thus, the hypotheses to be tested should be defined bearing in mind these limitations.

The purpose of this study was to contrast scalp EEG oscillatory activity related to successful and erroneous STM of grayscale photos, belonging to distinct categories (e.g., “luggage”, “chair”, “car”). Each category was defined by a set of images sharing the general thematic information (*gist*) while differing in the details that characterize the individual items (*verbatim*) (Koutstaal & Schacter, 1997; Brainerd & Reyna, 2002). Among memory errors, it has been of further interest to investigate oscillatory traits of false memories – when a novel item (lure) like the encoded images (i.e., sharing some of their perceptual or semantic properties) is recognized as familiar. To conduct the investigation, we devised a challenging WM task with the intent to maximize the rate of erroneous memory responses by the encoding of visual stimuli presented sequentially at a fast-pace.

The remainder of the thesis is divided into four chapters. Chapter 2 introduces the human visual system, from its anatomical organization to the theoretical accounts of vision and perception. The role of human memory within the visual system is then examined with added emphasis on the phenomenon of false memory. To close chapter two, the most common brain imaging techniques are presented alongside with the relevant hemodynamic and electrophysiological studies covering VWM. Chapter 3 outlines the materials and methods adopted to carry out the experimental work. Chapter 4 details behavioral and EEG oscillatory results. Finally, Chapter 5 discusses the theoretical implications of the findings and provides the conclusive remarks.

Please note that the following chapters includes also paragraphs from Mapelli & Özkurt (2019).

CHAPTER 2

LITERATURE REVIEW

Life on Earth is strongly dependent from the energy released by the Sun that reaches the atmosphere in the form of light. Many organisms evolved to harvest light energy (e.g., photosynthesis) and convert it into chemical energy used to fuel their actions. The animal kingdom went further as the evolution of the eye allowed for the surveying of the landscapes. Some animals (e.g., box jellyfish) have no brain to further interpret the sensory data, thus their reactions are simply driven by the detected patterns of light intensity. Others, and humans among them, acquire advanced knowledge through the analysis of the light that enters the eye, a process known as visual perception. As such, visual perception is not a pristine window onto reality. Rather, it is a derived representation drawn to assist in the planning of the best course of actions aimed at increasing the chances of survival. Phenomena such as adaptations (e.g., after few minutes spent outside gazing at the night sky the number and brightness of the stars increase), altereffects (e.g., the temporary dark spot we experience following the flash of a photo camera) and illusions (e.g., the illusion of the moon being larger when it is close to the horizon) are evidence that, despite its proven evolutionary advantage, visual perception might not always provide a fully veridical experience.

2.1. Visual System: Human Eye and Pathways to the Visual Cortex

Everything we see reaches the brain as a flow of pulses traveling along the nerve fibers. All the information the brain uses to create a model of our surrounding comes from these stimuli. Given this perspective, it comes as no surprise that illusions, hallucinations and all kinds of failures affect our visual experience.

As described by Stone (2012), within the human eye (Figure 1), the scene is brought to focus onto the retina, a light-sensitive layer of tissue covered, not uniformly, by photoreceptors. The fovea, a small pit, is filled with cones, i.e., color-sensitive photoreceptors. It is the area associated with central vision where humans see in greater details. Three types of cones exist which are sensitive respectively to long (red), medium (green) and short (blue) wavelengths of light. The fovea contains only cones sensitive to long and medium wavelengths. On the outer regions, the number of cones decreases leaving space for the rods, photoreceptors more sensitive to light that work better under low-light conditions.

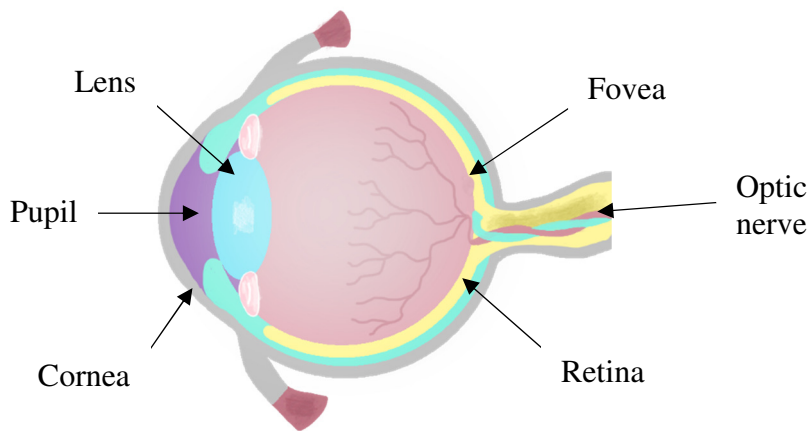


Figure 1: Anatomy of the human eye.

The light stimulus is converted into electro-chemical energy by the photoceptors; the stimuli are then transmitted to the ganglion cells through a series of neurons in the retina layer (Figure 2).

Decomposition of the image into important components (e.g., color, motion) begins from the retina. The M (magnocellular) and P (parvocellular) streams are two distinct flows of information that start from the retina and extend up to the cortex. In general, the left part of the visual field (i.e., left visual hemifield) is projected onto the right part of the retina. Similarly, the right part of the visual field (i.e., right visual hemifield) is projected onto the left part of the retina (Figure 3). Thus, the information of the right (left) hemifield is projected onto the left (right) side of both retinal images. Each hemisphere receives information from half visual field. Considering the right eye, retinal projections of the right visual hemifield cross to the left hemisphere at the optic chiasm. In contrast, information from the left visual hemifield remains on the right hemisphere. The retinal projections of the left eye follow an analogous but symmetrical pattern. Each newly created bundle (optic tract) connects to a six-layered structure called lateral geniculate nucleus (LGN). Each layer contains unique descriptions of the pertaining visual hemifield. As the layers are placed on top of each other, the same point of each layer corresponds to the same point in the visual field.

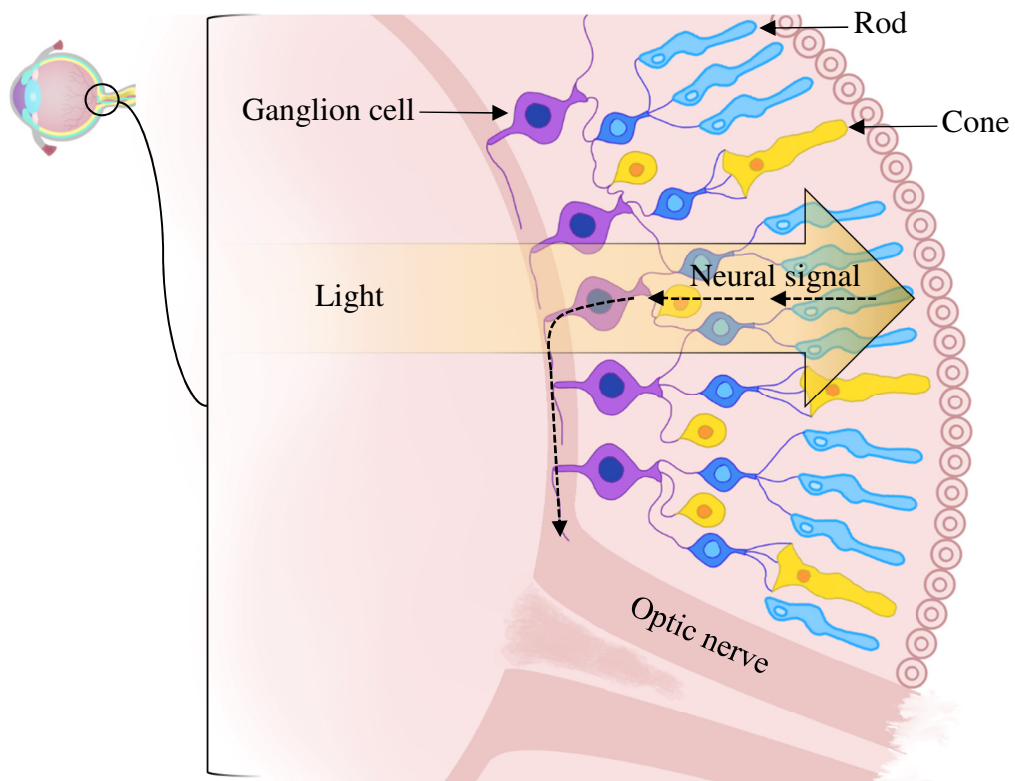


Figure 2: Simplified diagram of retinal cell layers.

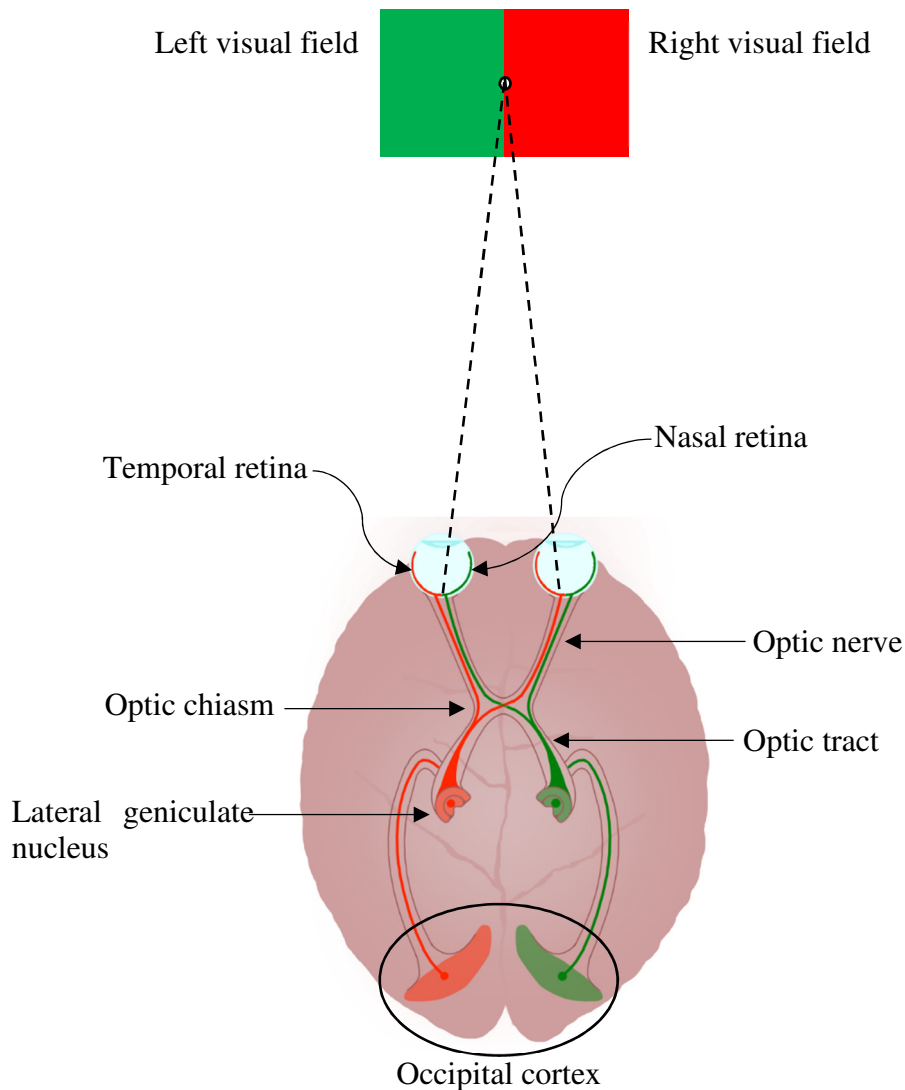


Figure 3: Pathways of the visual system.

In broad terms, the visual cortex (Figure 4) is organized retinotopically, i.e., contiguous points of the retinal image are projected onto contiguous areas in the cortex. The primary visual cortex (V1) is the main recipient of the visual signal coming from the retina. For every point in the retinal image, V1 extracts implicit features such as orientation, texture, motion, contrast, depth, color and brightness. The outgoing connections originate two pathways: The dorsal and ventral streams (Ungerleider & Haxby, 1994; Creem & Proffitt, 2001; Stone, 2012). The ventral stream begins from V1 and reaches the inferior temporal cortex (ITC) crossing through V2, ventral V3, V4 and TEO (located at the posterior border

of the ITC) (Milner & Goodale, 2006). Differently, the dorsal stream defines a more complex pattern from V1 to the posterior parietal cortex: While one set of inputs passes from the middle temporal region (MT/V5), additional visual information travels across V2 and V3 reaching the posterior parietal cortex either via V3A or via the parieto-occipital area (Milner & Goodale, 2006). Ventral and dorsal streams are associated with either object identification versus spatial relationships (Ungerleider & Haxby, 1994), or perception versus guidance of action (Milner & Goodale, 2008) respectively. Moreover, the two pathways are interconnected and information is mutually exchanged. As they move away from V1, the spatial/retinal organization is gradually supplanted by a features-based (e.g., color, shape, motion) cortical mapping.

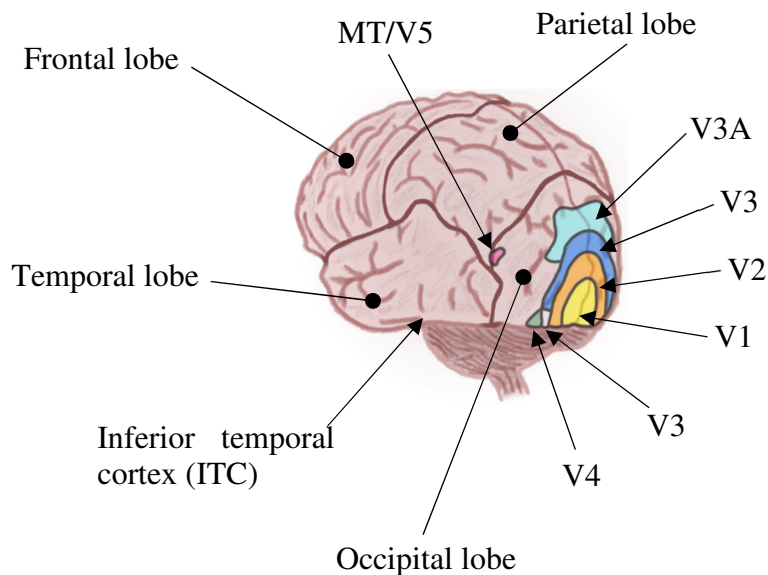


Figure 4: Major areas of the human brain and the visual cortex.

2.2. Theories of Vision: Framing the Problem of Visual Perception

Any newly formulated theory of vision must address four prominent issues (Palmer, 1999):

- Environment versus organism: Which factors influence the perception process? External elements and their condition in the environment, or internal properties of the organism, such as the visual nervous system. This dualism may not necessarily be mutually exclusive as both internal and external properties might influence perception.
- Empiricism versus nativism: Why are elements perceived as they are? Empiricism sees it as consequential to the learning process and knowledge accumulated through time. Nativism expects it to be readily available (or it surfaces through maturation) from the moment the organism is born and shaped by evolutionary processes.
- Atomism versus holism: How does perception emerge? By assembling each local element on the visual field, or the perception of a local element depends on all elements on the visual field.
- Introspection versus behavior: How to derive a theory of perception? From one's own reported experience or from objective measurements of performances.

Four classical psychological theories attempted to tackle the visual perception problem by providing specific answers to the aforementioned matters. Following, a brief account of each formulation.

2.2.1. *Structuralism*

Structuralism stands on the assumption that perception emerges from basic atomic elements of sensory experience. Memories from prior and recurrent experiences link together related atoms. In the context of vision, these atoms refer to small local regions of the visual field. They are singularly bound to a photoreceptor and subjected to a local experience of color. The concatenation of regions induces the activation of associated memories from other sensory modalities. Thus, perception is defined by a rapid execution of unconscious processes eliciting associated memories created via repeated interactions with the environment.

2.2.2. *Gestaltism*

This theory refutes atomism and empiricism, the basic principles of structuralism. It promotes instead a holistic idea suggesting that perception arises from considering the whole visual configuration. Less fundamental, the idea that perceptual organization is

innate and does not need learning from experience to mature. Another element introduced by the gestaltism is the psychophysiological isomorphism. It links statuses of mind and brain, i.e., subjects' perceptual (psychological) experiences are structurally identical to the related (physiological) events within the brain. An example to better illustrate the concept is given by the primary colors. They are grouped into three pairs: Red opposite to green, blue opposite to yellow and black opposite to white. The psychological experience of the primary colors and their opposites finds a neural correspondence with three specialized neurons decoding respectively red/green, blue/yellow and black/white (De Valois, 1960). Additional propositions that were put forward by gestaltists, such as the theory of electrical brain fields, were dismissed by the scientific community following experimental investigations.

2.2.3. *Ecological optics*

One of the most prominent pioneers in the field was James J. Gibson. Gibson's theory of perception (Gibson, 1950) proposed that the visual space is described by the ground, a continuous surface composed by connected sub-surfaces. Consequently, the visual space is not described by sets of objects but by the information laying on the ground. The theory asserts that the information used to build the perception is not collected from a stationary point of observation fixating a local isolated area. On the contrary, perception is built through an optic flow (a continuous transformation of the image on the retina) generated by the organism while exploring the environment. Yet, despite having a continuous flow of images on the retina, the relevant information remains mostly invariant. Examples of invariants introduced by Gibson are: *Density of texture*, which might allow the organism to understand the dimensions of the explored space; *flowing of patterns*, movement causes the surrounding patterns to flow except for the central point of direction, thus allowing to maintain the intended direction; *affordances*, i.e., provisions found in the environment that are relevant, in meaning and utility, to the organism (e.g., water affords to quench the thirst, air affords breathable oxygen). Gibson stated that invariants directly contribute to perception, as they are readily available without additional processes of transformation or extraction. From Gibson's perspective, perception can be built by evaluating the elements in the environment without the need of internal processing performed by the organism. A refinement of the first theory, which was based upon the notion of retinal image, was later proposed: The *ecological approach to visual perception* (Gibson, 2015) was based on the array of ambient light, a set of visual solid angles (or connected components) given a point of observation. The author affirmed that perception should not be considered as a process of manipulation of sensory inputs, but as a process of extrapolation of invariants from the environment. Affordances emerge as assembled invariants following minimal learning efforts. They are directly bound to perception, i.e., both physical features and affordances of the elements are immediately perceived. The direct perception, Gibson clarified, operates on the environment itself (a single-step process) and it is not mediated by sense-related data (multi-steps process). In general, Gibson distinguished between two types of information: Afferent-input information, which refers to information represented as impulses in the optic-nerve; and optic-array information, i.e., information in form of light,

which is not inside the observer but available from the environment. The latter is the information readily available for perception.

2.2.4. *Constructivism*

Constructivism asserted that human visual perception, despite being affected by errors and illusions, regularly provides the correct perceptual experience of one's surrounding. To explain such efficiency, the use of additional information, which is dynamically integrated with the retinal image by the visual system, must be accounted for. One of the most relevant properties pertaining to the constructivist model is the process of *unconscious inference*. As the optical information available from the retinal image is not sufficient to resolve the perceptual inverse problem, an additional unconscious process is enrolled. It is responsible for the integration and transformation of the two-dimensional information, available from the retinal image, into a three-dimensional representation of the environment. The inferences made by this unconscious process are based on the likelihood principle. Thus, the selected interpretation is the one which provides the higher probability of generating the specific retina content (heuristic interpretation process).

The advent of the digital computer era enabled scientists to develop synthetic simulations to test theories, to integrate information processing ideas in the classical domain of psychology and to design alternative models likening the brain to a biological processor. The ability to generate computer simulations gave rise to connectionist models based on neural networks. The idea behind this approach was to create synthetic networks mimicking neural circuitry of the brain. Hence, the system would be composed of networks of artificial synapses densely interconnected. These artificial synapses would work as simplified versions of biological neurons, whose behavior, defined by either inhibitory or excitatory states, would depend on nonlinear mathematical equations. As the analytical interpretation of such models was not trivial, the study of its behavior had to be done through automatized simulations.

2.3. **Visual Attention: Directing Relevant Information into Awareness**

Attention refers to a mental resource that is allocated among competing sources of information. Its objective is to facilitate the processing of the relevant information and use it to produce a behavioral response or a memory (Lamme, 2003). The sources could be externally (e.g., perception of stimuli) or internally (e.g., thoughts, memories) generated. Thus, trivially, visual attention accounts for the attention allocated to process visual inputs. Visual attention is characterized by two significant properties: The limited capacity of the brain for data processing and the ability to filter out unwanted information (Desimone & Duncan, 1995).

Many models have been proposed to explain the selection mechanisms through which relevant information reaches awareness (for a detailed review on visual attention, see Friedenberg, 2013). Broadbent's filter theory (1958) originally suggested that non-selected

sensory data is completely excluded from subsequent processing. Differently, Treisman's attenuation theory (1964) does not strictly filter out non-selected information. It posited that unattended but relevant data will still be processed. These are named *early selection* models as the filtering is performed prior recognition/categorization and based solely on sensory data. In contrast, *late selection* models hypothesize a delayed process of selection whose criteria may be influenced by a variety of properties such as meaning or semantic (Deutsch & Deutsch, 1963; Norman, 1968). As for *early* models, *late* ones initially filter the sensory input. However, following the recognition and prior transferring the information into STM, another selection process is performed. At this point, it is influenced by the interpretation given to the sensory data. Another proposition describes a shifting filter, whom, according to task requirements, can be applied at different stages of processing (Posner & Snyder, 1975).

How competing elements get access to attentional resources? Bundesen (1990) proposed that the item with greatest salience, at any given time, is selected and thus included in awareness. Top-down directives (e.g., based on context, knowledge, or task instructions) could also bias the process favoring specific items. The described mechanism includes *filtering*, i.e., the selection of relevant inputs rather than distracters, and *pigeonholing*, the classification of selected inputs with respect to pertaining categories. As Bundesen formulated the theory through mathematical equations, its model could be tested thoroughly and accounted adequately for the experimental data. Alternatively, the global workspace theory (Baars, 1997) approaches consciousness and selective attention through the metaphor of a theater. In this context, the attentional spotlight shines on the stage focusing on different actors. The contents under the spotlight reflect the conscious experience. While partial awareness is associated with elements at the fringe of the spotlight, outside of it there is no awareness. The information brought to awareness by the spotlight is broadcasted to the audience. People behind the scenes may influence whatever is brought under the light. Information comes from external (sensory input) or internal (imagination) sources and compete to access the stage. The audience is composed by different unconscious cognitive components responsible for processing information.

2.4. Visual Memory: Preserving Information Pertaining to the Visual Experience

Visual memory refers to stored information produced by the visual system that concerns perceptual properties of the encoded stimuli. The memory content may range from low-level information extracted in early visual areas to more abstract higher-level representations. As described by Luck & Hollingworth (2008) the visual system is composed by three subsystems: Iconic memory, visual short-term memory (VSTM) and visual long-term memory (VLTM). Following, an overview of each subsystem.

2.4.1. *Iconic memory*

Research suggests the existence of two types of iconic memory: The *visible persistence* and the *informational persistence*. The visible persistence identifies the sustained activity associated with photoreceptors and neurons at low-levels of the visual system (probably through area V1). It reflects a detailed representation of the visual scene which rapidly fades over time. The informational persistence refers to the content which endures the offset of the stimulus and it is not part of the fading visual experience. The informational persistence encloses two distinct components. The first one is dedicated to spatially organized and pre-categorical representations, which reflects the decaying activity in intermediate visual regions such as V4. The second component is responsible for more abstracts, categorized and amodal representations. The iconic memory is unlikely to maintain the available information for the duration required by post-perceptual processing. New incoming perceptual information masks the current content, thus preventing any comparison or integration with previous visual elements. Iconic memory supports higher-level systems (e.g., VSTM) by acting as a temporal smoother of the input signal, thus facilitating the consolidation of memories.

2.4.2. *Visual short-term memory*

VSTM stores information concerning a limited number of items. Its capacity varies in accordance with the complexity of the stimuli to encode. While VSTM representations are not as precise as early visual ones, they are immune to saccades, blinks and brief occlusions. Thus, VSTM allows for comparisons with elements separated in space and time. The VSTM-related activity generated in response to a stimulus is sustained over several seconds following the offset of the stimulus. The limited storage capacity and the active maintenance of oscillatory nature prevent any meaningful accumulation of information over long periods. Research suggests that VSTM has two subcomponents responsible respectively for spatial and object identity information. As discussed in the Section 2.3, VSTM appears to be the recipient of information processed by visual attention. Furthermore, it helps to keep track of previously attended locations, thus biasing attention towards new areas. VSTM plays a role also in transsaccadic integration to ensure perceptual continuity as saccadic eye movements disrupt the visual stream. Possibly, it is even responsible for creating the correspondence between objects in the presaccade and postsaccade input.

2.4.3. *Visual long-term memory*

VLTM contrasts with VSTM in that it possesses a larger storage capacity. Whilst VLTM representations are less detailed than the ones of VSTM, they are reliably stored thanks to changes in the pattern and strength of synaptic connections. Studies suggest that LTM memories are kept within the same systems that underlie perception. VLTM plays a role in object and scene categorization via retention of visual features.

2.5. Working Memory

Working memory (WM) is a fundamental constituent of the cognitive system. It encompasses short-term memory (STM), i.e., the temporary storage unit and all the processes responsible for monitoring, maintaining and manipulating task-relevant information over brief intervals (Baddeley, 2003). Following, a brief overview of the most common theoretical approaches and WM models.

2.5.1. *Cowan's embedded process theory*

The theory suggests that WM is structured in two components. The first component responsible for activated LTM representations (with no limit of activations). The second one, namely the *attentional focus*, operates across activated LTM areas. It has a suggested limited capacity of four chunks, i.e., activated representations and it may contain more than a single item per chunk (Cowan, 1999).

2.5.2. *Individual difference-based theories*

Individual difference-based theories rely on a framework that focuses primarily on processes linked to WM capacity (Engle & Kane, 2004). Prominence is given to inhibitory processes, responsible for protecting memories from interferences. The typical approach considers individual differences among subjects by separating them into two groups: High and low WM span. The groups differ in accuracy as well as in a variety of experimental measurements (e.g., susceptibility to interference, ability to produce lists of items given a semantic category).

2.5.3. *Jonides and the mind and brain of short-term memory*

This model is strongly influenced by neuroimaging studies (Jonides et al., 2008). It suggests that, across a variety of modalities, perception, STM and LTM activations are all located in the same anatomical structures. Supporting evidence and presented conjectures are still considered controversial.

2.5.4. *Computational models of working memory*

This class of theories focuses on producing detailed predictions on how the WM functions. Thus, each model provides also its own computer simulation. Among several computational models, the *interactive cognitive subsystems* (Barnard, 1985) is regarded as the class representative due to its accurate predictions in certain contexts.

2.5.5. *Baddeley and Hitch's working memory model*

WM is a system with limited resources and modality-specific components (e.g., *phonological loop*) coordinated by a control-committed component, namely the *central executive*. The model has been updated since its first definition made by Baddeley and Hitch in 1974. It defines four core components (Baddeley, 2012). The phonological loop works with verbal information. It has a limited capacity and stores the information sequentially. Vocal or subvocal rehearsal assists the maintenance mechanism. The *visuospatial sketchpad* is an analogue of the phonological loop which concerns visuospatial information. The central executive coordinates the activities and it monitors, maintains and manipulates task-relevant information.

How could distinct codes (e.g., phonological and visual code, or LTM and WM information) be integrated in the absence of a common storage? To address these theoretical concerns the authors further refined their model. A new component was introduced, the *episodic buffer*, which functioned as the necessary common storage used to combine information of different origins.

2.6. **Semantic Memory**

The memory component responsible for general knowledge is known as semantic memory. As described by Baddeley et al. (2009), the semantic memory shares similarities with the episodic memory. Yet, while the latter refers to content bound to a precise episodic instance, semantic memory lacks this sense of conscious recollection of the past.

A considerable amount of research has been done to better understand the relationship between semantic and episodic memory. Patients diagnosed with anterograde amnesia displayed episodic memory impairment while their semantic memory was mildly affected. Differently, retrograde amnesia patients exhibited a compromised episodic memory, but they still showed more stable performances when semantic memory was probed. Brain imaging techniques contributed to the study of semantic and episodic memories by revealing how they activated different neural areas. All these findings consolidate the idea that semantic and episodic memory are two distinct components.

Questions involving general knowledge can be answered quickly: This observation would suggest that semantic memory is well organized. Different models have been proposed in the attempt to delineate the structure of semantic memory, with the most notable one being the *spreading activation model* (Collins & Loftus, 1975). It hypothesizes a semantic memory organized by semantic relatedness – which can also be interpreted as a distance measure, i.e., the closer the more related two elements are. Whenever a concept is produced, either internally thought or externally stimulated, the pertaining semantic node of the network is activated. The activation then spreads towards connected semantic elements with a strength that is inversely related to the semantic proximity. Other

experiments provided further evidence in support of this model whose general concepts allow for different interpretations yet limiting its ability to make accurate predictions.

In general, information pertaining to a specific object is not stored in a unique brain region. Reports suggest that details of an object (e.g., visual properties, tactile information, its functionality) may be stored in different brain regions. How this information is quickly retrieved and integrated remains an open debate.

Semantic memory can also store complex information. To reflect this ability, Bartlett, F.C. (Bartlett & Kintsch, 1995) introduced the concept of *schemas*. A schema is a well-defined chunk of knowledge describing a sequence of events and associated consequences (*scripts*) or structures and properties of objects (*frames*). *Expectation* is an emerging functionality associated with the prediction of upcoming events and actions from a given script. Schemas also enable the drawing of inferences, thus enhancing the comprehension through learning processes. Ultimately, schematic knowledge contributes to an enhanced interpretation of visual perception.

The schematic knowledge appears to facilitate the perception and predictability of the surroundings. Yet, it also carries undesired side effects. Schemas influence the way things are remembered. In general, people tend to bias information in favor of a consistent personal view, to the detriment of accuracy of maintained information (consistency bias).

Theories based on schemas have been proven useful. Yet, their definitions remain too generic and fail to make accurate predictions. Furthermore, memory representations seem to be more complex than the given descriptions. The schema theory predicts an error rate which is higher than experimental measures, thus highlighting how human memory processes are more flexible than the current theoretical account.

2.7. False Memory

False memory distortions refer to novel events that a person falsely believes having experienced in the past. The term was initially used in the context of childhood abuse cases and was popularized by the media (Beckett, 1996). To reproduce this phenomenon in a controlled environment, where experimental measurements could be reliably collected, the focus shifted towards more specific memory errors for which various paradigms were devised (e.g., novel words or pictures falsely recognized as familiar). Moreover, nuances in the definition of the term false memory were introduced which, at times, were considered controversial (DePrince et al., 2004).

A common experimental procedure used to induce false memories in LTM is the Deese-Roediger-McDermott (DRM) paradigm (Deese, 1959; Roediger & McDermott, 1995). Typically, sets of words, each grouped according to a common theme, were constructed – e.g., “jazz”, “piano”, “note” and “orchestra” all associated with the critical lure “music”. These sets, but not the lure, were presented to the participants. Later, during the

recognition (or free recall) session, participants would consistently misrecognize (or list) the lure as previously studied.

While the vast majority of research investigated false memories in long-term, some recent studies have designed variations of DRM paradigms to explore them over short-term periods, mostly through behavioral measurements (Coane et al., 2007; Atkins & Reuter-Lorenz, 2008; Flegal et al., 2010; Flegal & Reuter-Lorenz, 2014, Olszewska et al., 2015). There have also been few studies examining BOLD (blood oxygenation level dependent) responses (Atkins & Reuter-Lorenz, 2011) and electrophysiological characteristics (Chen et al., 2012; Melnik et al. 2017) in order to determine neuronal markers linked to these events. One fMRI study assessed neural correlates of false memory in VWM, while subjects performed a modified delayed match-to-sample test with human faces as stimuli (Iidaka et al., 2014). Unlike the DRM-like paradigms, the relationship between stimuli was defined by perceptual similarities and not by semantic associations.

2.8. Cognitive Electrophysiology: Reflections of Cortical Functions

Cognitive electrophysiology investigates the relations between cognitive functions and the electrical activity generated by populations of neurons (Cohen, 2014). Beyond behavioral data, electrophysiological measures provide additional knowledge to better understand cognitive processes of interest. They also provide insight on functional properties of neural networks, thus contributing to the development of computational models simulating neurobiological or neurophysiological systems.

2.8.1. Electroencephalogram

The electroencephalogram (EEG), a noninvasive technology to study human electrophysiology, was pioneered by the German psychiatrist Hans Berger in the early 20th century (Millett, 2001). Since then, both technical and methodological advancements contributed to a rapid expansion of the field.

EEG records electrical activity on the scalp through electrodes that are placed on the subjects' head. As EEG possesses a high temporal resolution, it is ideal to monitor cognitive processes evolving within tens to hundreds of milliseconds. The voltage fluctuations measured by EEG are influenced by the underlying populations of neurons, thus they are a direct reflection of cortical activity (Wang, 2010; Buzsáki & Wang, 2012). The recorded signal is multidimensional inasmuch as time, space, frequency, power and phase are beneficial to the characterization of cognitive functions or to the testing of theoretical concepts.

The neurophysiological basis of the EEG signal is yet to be fully explained. The postsynaptic responses of pyramidal neurons, predominantly located in the human cortex and hypothesized to be central to cognitive processes, are believed to strongly influence the EEG signal (Luck, 2005).

The electrical activity generated by the neurons leaks through different tissue layers prior to be detected by the electrodes on the scalp. Each layer, defined by unique electrical properties and structures, contributes to the smearing of the traveling signal (Lopes da Silva, 2013). Thus, in contrast with the temporal resolution, EEG spatial resolution is poor and does not allow for the precise localization of the sources within the brain.

2.8.2. *Magnetoencephalogram*

The magnetoencephalography (MEG) is a noninvasive technology that records magnetic fields generated by neuronal activity within the brain. Cohen (1968) firstly reported of the human magnetic alpha rhythm detected by a single magnetic sensor, thus demonstrating the feasibility of recording MEG in the proximity of the human head. MEG is closely related to EEG since both signals possess analogous time resolution and they both originate from synchronized neuronal activity. Like EEG, the measured fluctuations recorded by MEG are a direct reflection of cortical activity (Hämäläinen et al., 1993).

Any flowing electric current generates a magnetic field which is perpendicular to the flow and whose direction is determined by the right-hand rule, i.e., while the thumb points in the direction of the flow, the remaining fingers show the direction of the magnetic field. Within the brain, generated magnetic fields travel unchanged through the different tissue layers and skull. The signal generated by the fields are weak, nevertheless the sophisticated sensors of MEG systems are still able to detect them.

Contrary to EEG, MEG has a high spatial resolution. However, the source localization based on the analysis of the spatial distributions of the magnetic fields, namely the inverse problem, relies on source models (e.g., current dipoles) and assumptions that, if ill-conceived, may return contrasting results as multiple sources configurations could give rise to the magnetic fields detected nearby the head (e.g., the inverse problem has multiple solutions) (van Oosterom, 1991).

2.8.3. *Event-related potentials analyses*

Event-related potentials (ERP) are calculated by averaging the EEG signal over many trials. The assumption behind this approach is that the brain systematically responds to the events of the studied task in a time-locked fashion. This methodology retains a high temporal accuracy as there is no temporal filtering (contrary to time-frequency based analyses, see Section 2.8.4) or complicated preprocessing steps. While computing ERPs one should consider that task-modulated information which is time-locked but non-phase-locked with task events will no longer be observable following trials averaging. Despite the wide literature covering ERPs, their underlying neurophysiological mechanisms are still not clearly understood (Pfurtscheller & Lopes da Silva, 1999; Cohen, 2014).

2.8.4. Time-frequency based analyses

Time-frequency based analyses aim at the identification of oscillatory components in neural time-series. Furthermore, dependences between oscillations across distinct brain regions (connectivity), as well as relations amid oscillations (for frequency, amplitude, or phase) and cognitive processes or behavior can also be assessed (Gross, 2014).

To obtain a time-frequency representation (TFR), the neural time-series need to be translated into the frequency domain via, for instance, non-parametric methods such as Fourier transform, wavelet transform, or Hilbert transform.

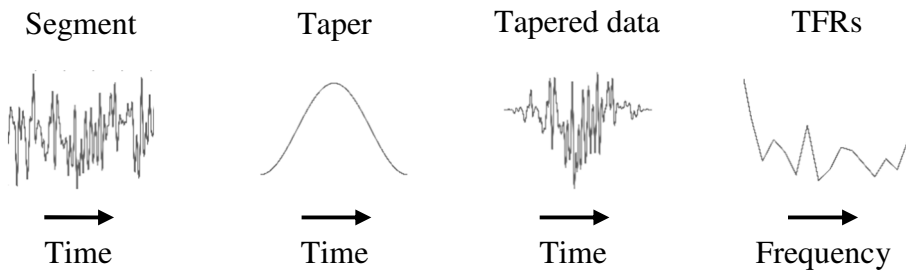


Figure 5: Temporally localized frequency decomposition: Diagram of the processing of a segment of the trial.

Concerning the Fourier transform, one fundamental requirement is that the input data must be stationary, i.e., the statistics of the data do not change over time. As this assumption is not valid for EEG recordings, which reflect brain activity in the context of a cognitive task, a temporally localized frequency decomposition method is used instead (Cohen, 2014). By using these methods, the assumption, which is considered acceptable for EEG recordings, is that for short time intervals the signal is stationary (Florian & Pfurtscheller, 1995). Another reason to use temporally localized frequency decomposition is that the Fourier transform does not reflect changes over time. Thus, for any given trial, following the selection of the short time interval (segment), its data are weighted by a tapering function (Figure 5). Tapering prior the application of the Fourier transform is recommended as it reduces spectral leakages by attenuating the amplitude values at the beginning and at the end of the segment (Cohen, 2014; Gross, 2014). Next, another segment, which overlap for the most part with the previous one, is selected and the procedure is repeated until the end of the trial (for all trials). For each segment separately, the absolute value is averaged thus leading to a TFR of each trial. It should be highlighted that tapering reduces the temporal resolution of the EEG data, this side effect can be mitigated by temporally overlapping the segments. This approach is helpful when studying activity at lower frequencies, as opposed to higher frequencies, considering the

higher SNR that characterizes the former. For the latter, multitapering extends the aforementioned method as it aims at increasing the SNR of the frequency portraits by using multiple tapers each with slightly different temporal settings. More specifically, the trial is divided into overlapping segments which are then processed individually. Each segment is multiplied by a series of tapers producing tapered time series that concentrate the input signal over different time intervals. Time-frequency representations are then generated for each tapered set of data and then averaged to produce the final TFR of the segment (Figure 6). Once again, for each segment separately, the absolute value is averaged thus leading to the TFR of the whole trial.

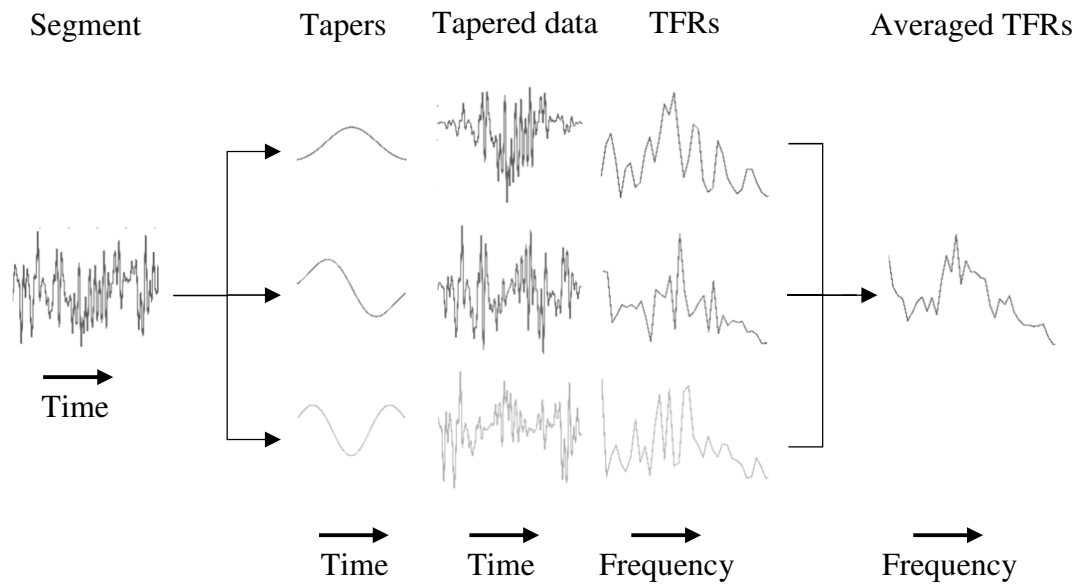


Figure 6: Diagram illustrating the steps applied by the multitapering method.

2.8.5. Connectivity analyses

Brain networks, and more specifically the role they cover for cognition, is a growing topic of interest in the field of neuroscience. Research suggests that oscillatory synchronization is instrumental to the transfer of information throughout large networks (Sporns, 2010).

Connectivity indicates the study of two or more signals, from one (e.g., signals in distinct frequency bands) or multiple electrodes/regions, based on specific measures such as phase and power. The most common connectivity measures are bivariate, e.g., they only assess the relationships between two signals, given their simplicity, as opposed to a greater complexity of multivariate approaches. It is important to consider that given multivariate

relationships within a network, bivariate correlations may return inflated estimates (Cohen, 2014) (Figure 7A). This effect is partially alleviated when comparing different conditions of a studied task as both estimates are similarly inflated.

In the following paragraphs an introduction to the measures of connectivity that were of interest in our study: *phase-based connectivity* and *cross-frequency coupling*.

Phase-based connectivity accounts for the distribution of the phase difference between two electrodes. The rationale behind this approach is that whenever two areas are functionally coupled the timing of their oscillations synchronizes and it can be measured by the phase value. Importantly, the phase lag between the two signals is not considered, but only the strength of the synchronization is. Furthermore, one should be careful when interpreting nonzero-phase lag as it doesn't imply neither causal nor direct relationship (Figure 7).

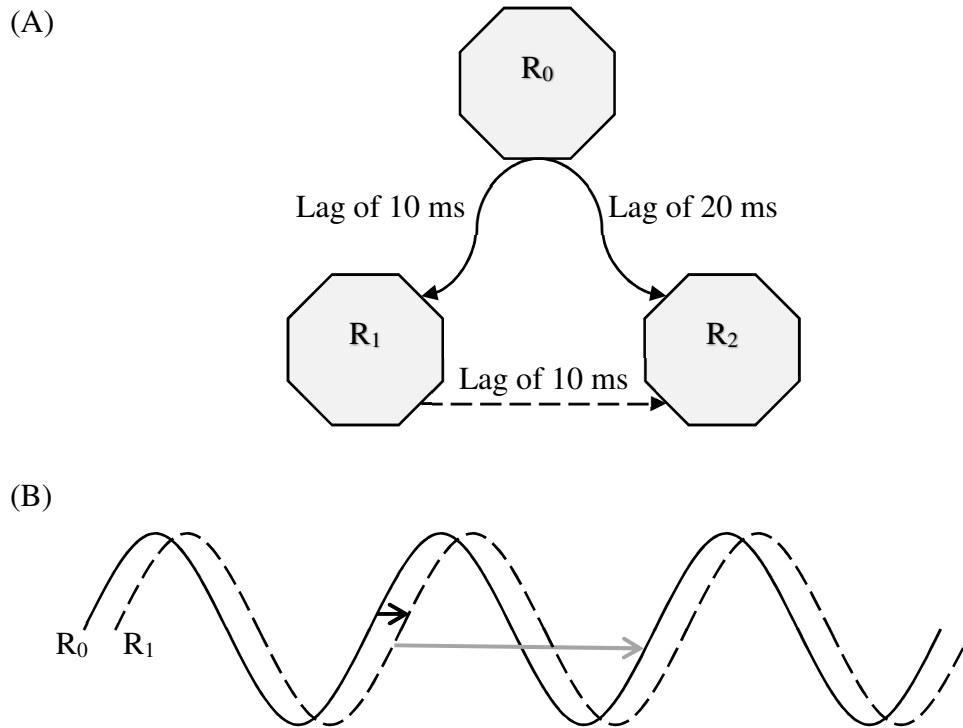


Figure 7: One should be careful in interpreting bivariate measures in the presence of multivariate networks. **(A)** A bivariate measure would report a nonzero-phase lag between R_1 and R_2 regions, though there is neither causal nor direct relationship between R_1 and R_2 . **(B)** Considering the two synchronized signals for R_0 and R_1 , it might not be possible to understand whether R_0 leads R_1 or R_1 leads R_0 , without additional information.

When investigating connectivity, it is important to account for spurious effects induced by volume conduction: A single source may generate electrical fields that are large enough

to be picked up by more than one (usually neighboring) electrode, thus resulting in a deceptive zero-phase lag synchronization. However, not all zero-phase lag connectivity is explained by volume conduction effects, as it can also reflect real brain synchrony.

Cross-frequency coupling provides a statistical measure of the relationship between brain activities in two distinct frequency bands. It has been associated with many cognitive processes and among them, of relevance to our study, those related to WM, i.e., phase-amplitude coupling (PAC), see Section 2.9. PAC (Figure 8) measures the relationship between the phase of a frequency band (usually low frequencies) and the power of another (usually high frequencies).

In the context of WM, as originally hypothesized by Lisman & Idiart (1995), a sequence of presented items would be encoded in WM by single gamma cycles (one per item) in turn nested within theta periods, thus retaining the sequential structure of the presentation (Figure 9). Indeed, recent oscillatory findings support this idea showing significant presence of theta phase to gamma amplitude coupling throughout WM tasks (Canolty et al., 2006; Axmacher et al., 2010).

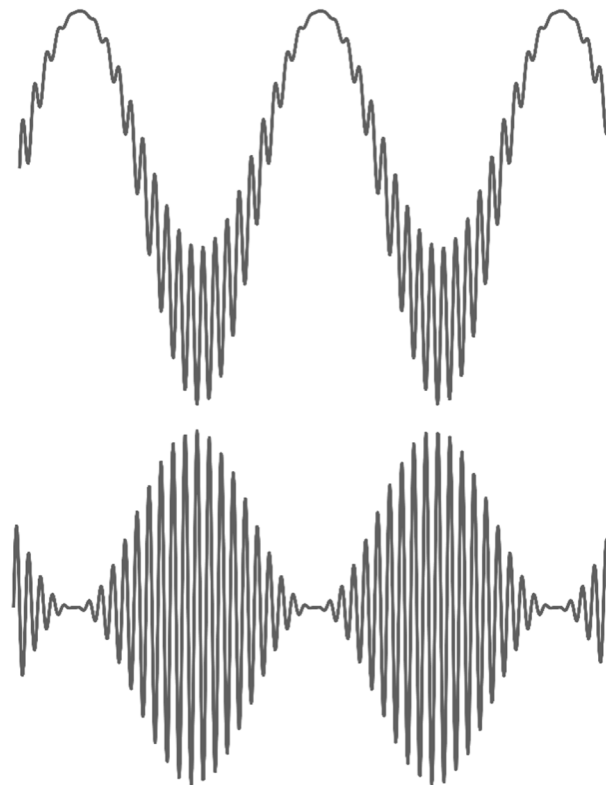


Figure 8: Schematic of phase-amplitude coupling on a single electrode. The signal at the top is composed by two (fast and slow) oscillations. The power of the fast oscillation varies in accordance with the phase of the slow oscillation. The signal at the bottom highlight the variation of power of the fast oscillation.

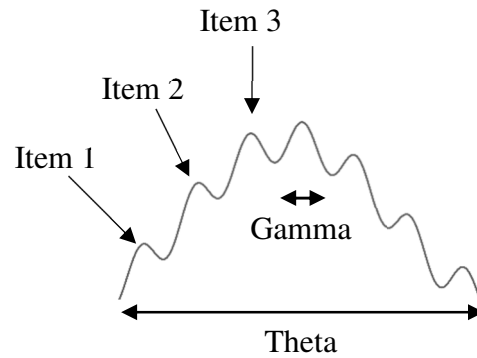


Figure 9: Theta phase to gamma amplitude coupling in WM. Exemplification of how sequential memories are retained in the same network. Each memory item is represented by distinct groups of active cells (i.e., the associated neural code within the network) that fire in different gamma cycles within a theta cycle. Thus, each item is associated with a specific theta phase. During WM retention, the described pattern repeats every theta cycle. Adapted from Lisman (2010).

When studying PAC, low and high frequencies signals can be extracted not only from a single electrode but also from two different locations (Figure 10). Relevant to WM, frontal theta to posterior gamma PAC has been reported to differentiate between later remembered and later forgotten stimuli (Friese et al., 2013), thus supporting the idea that the interactions between frontal and posterior regions play an important role during the formation of new memories.

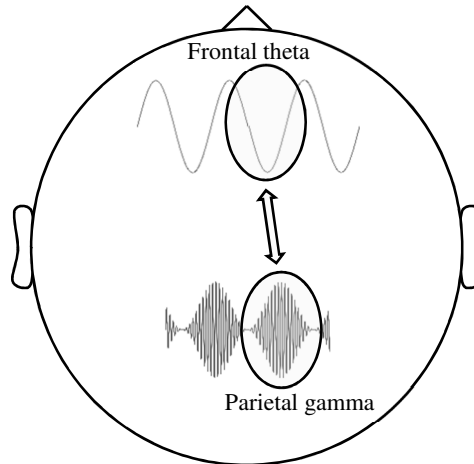


Figure 10: Phase-amplitude coupling with frontal theta phase modulating parietal gamma power. Adapted from Frieese et al. (2013)

2.8.6. Frequency bands

Traditionally, EEG activity is divided into frequency bands, each linked to a wide set of perceptual, sensorimotor and cognitive operations. However, these ranges may seem artificial at times as they vary on a subject basis and are influenced by task-related factors such as cognitive and memory loads (Klimesch, 1997, 1999; Klimesch et al., 1998; Haegens et al., 2014). The typical ranges, more commonly found in the literature, are defined as follows: Delta (0.5 – 3.5 Hz), theta (4 – 7 Hz), alpha (8 – 12 Hz), beta (13 – 30 Hz) and gamma (> 30 Hz). Delta, theta and alpha oscillations spread over large portions of the cortex and have been hypothesized to reflect integration of cerebral activity across distributed neural assemblies via synchronization of coherent activity and phase coupling. Conversely, beta and gamma oscillations show lower power values and are topographically restricted over smaller regions.

- *Delta band (0.5 – 3.5 Hz)*

Spontaneous slow-waves have been reported propagating throughout the cortex during the sleep (SWS). Functionally, SWS may indicate memory consolidation realized through a dialog between the hippocampus and neocortical areas (Marshall & Born, 2007). Beyond sleep-related functionalities, delta power has been reported to increase during concentration, while performing tasks such as mental calculations (Fernández et al., 1995; Harmony et al., 1996), semantic tasks

(Fernández et al., 2012) and the Sternberg paradigm (Harmony et al., 1996). Possibly, the reported delta power increase observed during mental tasks indicates functional cortical deafferentation, or inhibition of the sensory inputs, thus preventing interference with the internal concentration (Harmony, 2013).

- *Theta band (4 – 7 Hz)*

Theta oscillations have been extensively linked to memory processes (Klimesch, 1999; Kahana et al., 2001) and they are hypothesized to reflect cortico-hippocampal communication (Buzsáki, 1996; Mitchell et al., 2008). Furthermore, it has been suggested that top-down coordination exerted by frontal networks over recruited subsystems could be reflected by theta phase synchronization (Sauseng et al., 2010).

- *Alpha band (8 – 12 Hz)*

Modulation of alpha oscillations has been widely associated with memory (Klimesch, 1997; Jensen & Mazaheri, 2010) and attention (Hanslmayr et al., 2011). A possible functional interpretation is given by the inhibition-timing hypothesis (Klimesch et al., 2007) which attributes to alpha oscillations the role of protecting relevant cognitive processes from non-related task interferences. Specifically, an alpha power decrease reflects cortical excitability of task-related regions (Lange et al., 2013). Conversely, an increase in alpha power is associated with an inhibition effect over task-irrelevant areas to avert interferences. The inhibitory account is further supported by the BOLD signal recorded with fMRI which has been shown to negatively correlate with alpha power (Goldman et al., 2002; Laufs et al., 2003).

- *Beta band (13 – 30 Hz)*

Modulation of beta oscillations has been observed throughout the planning and execution of voluntary motor movements (Neuper & Pfurtscheller, 2001). Enhanced beta oscillations have been hypothesized to reflect the maintenance of the current sensorimotor state. In contrast, a beta decrease would indicate an anticipated, or already undergoing, status change (Engel & Fries, 2010). However, the beta rhythm has also been reported in tasks that did not require neither planning nor performing motor movements. Specifically, when participants performed attentional tasks, strengthened phase synchronization within the beta band has been hypothesized to reflect communications among task-relevant regions (Gross et al., 2004).

- *Gamma band (> 30 Hz)*

Gamma oscillations are considered to reflect cortical activation and they contrast with inhibitory characteristics linked to various low-frequency bands (Merker,

2013). They have been associated with perception (Crone et al., 2001; Meador et al., 2002; Demiralp et al., 2007; Wyart & Tallon-Baudry, 2009), attention (Müller et al., 2000; Fries et al., 2001; Jensen et al., 2007) and memory (Tallon-Baudry et al., 1998; Herrmann et al., 2004; Gruber et al., 2004; Jensen et al., 2007) processes.

2.9. Neural Correlates of Visual Working Memory

In the recent years, the study of human memory through the analysis of brain oscillations has linked a wide range of frequencies – from 3 Hz to 100 Hz – to the formation of memory traces. Occasionally, depending on the task, contradictory oscillatory behaviors have also been observed. In an attempt to reconcile the numerous conflictual observations, Hanslmayr & Staudigl (2014) hypothesized that the relationship between cognitive processes enrolled during encoding and processes engaged at retrieval, would influence the outcome of a studied task. Consequently, also oscillatory markers linked to successful memory formation could vary in accordance with task requirements.

Following this cautionary note about neural correlates of memory traces, in the remaining part of this paragraph we proceed by providing the reader with the relevant literature covering the visual memory in STM.

Visual WM refers to visual sensory information that is encoded into internal neural representations and subsequently maintained by WM processes.

Encoding and retention are two critical VWM phases, where improper neural activations may lead to memory failures. The initial factor that influences memory performance is the translation of the sensory input into VWM representations (Cohen et al., 2012; Killebrew et al., 2018). Yet, successful performances do not solely depend on optimal encoding of the to-be-remembered information but also the maintenance of it. The efficiency of memory processes relies on a tight synchronization of neural oscillations with a precision in the millisecond range (Lisman & Idiart, 1995; Klimesch, 1996; Buzsáki & Draguhn, 2004; Singer, 2009; Palva et al., 2010; Eriksson et al., 2015). Both EEG and MEG, due to their higher temporal resolution, have been important tools for the investigation of oscillatory dynamics related to encoding and retention of visual information in STM.

A wide range of studies reported amplitude modulation of theta (for a review Sauseng et al., 2010) and alpha (for a review Jensen & Mazaheri, 2010 and Klimesch et al., 2011) bands during VWM tasks.

Intracranial EEG studies demonstrated specifically the occurrence of theta oscillations in the human cortex during the encoding interval of a Sternberg task (Howard et al., 2003; Rizzuto et al., 2003). Raghavachari et al. (2001) reported event-related theta band activity gated at many sites widely dispersed over the cortex. The amplitude of theta oscillations increased sharply at the beginning of each trial of the Sternberg task and returned to baseline level only after the subject's response. In a subsequent investigation conducted by the same group, the theta power increase was found to be mostly situated in the parieto-

occipital and temporal cortical regions (Raghavachari et al., 2006). In another study by Sederberg et al. (2003), successful memory encoding of words was associated with a significant theta power increase predominantly located in the right temporal and frontal sites. It has been suggested that cortico-hippocampal feedback loops (Buzsáki, 1996) may drive theta activity into cortical regions, reflecting encoding of novel information, by maintaining cortical areas of interest into a state of resonance (Klimesch 1996, 2000; Klimesch et al., 1997a; Miller, 1991; Mölle et al., 2002). Beyond hippocampal functions, the strength of the frontal midline theta activity, a rhythmic activity that reaches its maximum around the Fz electrode site, has been linked to sustained attention (Sauseng et al., 2007) and found to be positively correlated to WM load and cognitive effort (Gevins et al., 1997; Jensen & Tesche, 2002; Onton et al., 2005). For an in-depth review on human and animal studies pertaining to WM and the frontal midline theta activity, we refer the reader to Hsieh & Ranganath (2014).

Relevant to WM, the phase of theta has been shown to cover a significant role during encoding and retention of sequences. Specifically, the interaction between the phase of theta and the amplitude of gamma, namely cross-frequency coupling – originally described by Lisman & Idiart (1995) – was proposed as the oscillatory mechanism through which sequentially encoded items were retained in WM (see also Section 2.8.5). The theta-gamma coupling (for a review see Lisman & Jensen, 2013) has been demonstrated in both cortex (Canolty et al., 2006) and hippocampus (Maris et al., 2011) while subjects were performing WM tasks. For the latter, within WM retention, gamma power has been shown to be modulated by the phase of theta and the strength of the coupling was linked to WM performance (Axmacher et al., 2010). Notably, the locations associated with significant PAC vary according to the content of WM (Jacobs & Kahana, 2009; Fuentemilla et al., 2010). Additionally, cross-frequency coupling between the phase of theta in frontal regions and the amplitude of gamma in posterior areas has been shown to predict encoding performance as the strength of coupling was able to discriminate between later remembered and later forgotten stimuli (Friese et al., 2013).

WM is a complex system that might recruit, depending on task requirements, a wide range of distinct cognitive processes (e.g., sensory, manipulation, attentional, LTM and multi-modal integrations). It has been suggested that synchronous theta phase coherence may reflect the control exerted by central executive networks over the enrolled sub-systems (Sauseng et al., 2004; Sauseng et al., 2010).

In the context of ERP studies, the ERP-P2 (or P200), a positive electrical potential that peaks at around 200 ms after stimulus onset, has been associated to WM (Luck & Hillyard, 1994; Anllo-Vento & Hillyard, 1996; Tallon-Baudry et al., 1998; Federmeier & Kutas, 2002; Lefebvre et al., 2005). In a visual semantic priming paradigm that used photographic stimuli, the ERP-P2 component was linked to human theta oscillations (phase-lock index and power) (Freunberger et al., 2007).

Complementary to EEG theta power increase observed during encoding, studies also reported an alpha power decrease (Klimesch, 1996, 1999; Mölle et al., 2002), which

presumably reflects increased excitability of the involved cortical areas (Klimesch et al., 1997a, Stipacek et al., 2003; Lange et al., 2013). Conversely, a power increase in alpha activity is associated with low excitability. For instance, when attention shifts towards external visual information, alpha band activity in occipital areas was shown to decrease (Worden et al., 2000; Sauseng et al., 2005b) enhancing perceptual performance (Thut et al., 2006; Van Dijk et al., 2008; Hanslmayr et al., 2007). On the other hand, when attention is directed inwards for maintenance of VWM internal representations, alpha power increases (Jensen et al., 2002; Tuladhar et al., 2007) preventing external interferences (Rihs et al., 2007; Foxe & Snyder, 2011). Studies using EEG/MEG source modeling provided further evidence in support of the inhibition-timing hypothesis by observation of alpha power increase over task-irrelevant regions during WM tasks (Haegens et al., 2010; Roux et al., 2012). Importantly, alpha frequency was shown to vary across individuals (Klimesch, 1999) and the peak frequency in occipital areas was reported to increase along with the cognitive load leaking in some cases into the beta band (Haegens et al., 2014). Inhibitory alpha power levels during WM maintenance were also reported to positively correlate with memory load (Jensen et al., 2002; Tuladhar et al., 2007).

The functional role of the phase of alpha frequencies was also investigated in the context of WM. Specifically, the synchronization of alpha phase has been theorized to facilitate cortico-cortical communications (Sauseng et al., 2005a; Klimesch et al., 2007). Moreover, alpha/gamma PAC has been suggested to facilitate the formation and maintenance of sensory-spatial WM items (Roux & Uhlhaas, 2014; Park et al., 2016).

Less explored, cortical beta oscillations observed for visual tasks were suggested to reflect visual attention (Wróbel, 2000) and were associated with STM processes (Tallon-Baudry et al., 1999; Medendorp et al., 2007; Palva et al., 2011) hypothesized to support the endogenous reactivation of WM content (Spitzer & Haegens, 2017). Theoretical works based on studies on rats suggest that beta rhythms in the association cortex – involved in higher-level sensory information processing – complement gamma frequencies during the creation and manipulation of cell assemblies. More specifically, the emergent beta activity that follows the removal of sensory input (Tallon-Baudry et al., 1999), could reflect the transient coordination of excited cell assemblies (Kopell et al., 2011). Additionally, beta band oscillations are hypothesized to facilitate the integration of sensory information in connecting distinct local networks (Tallon-Baudry et al., 2001; Siegel et al., 2011). In relation to visual imagery ability, beta levels were reportedly higher for subjects with vivid, in contrast with inadequate, imagery skills.

Gamma band activity in visual regions has been shown to increase during processing of sensory inputs. This increase, that is accompanied by a decrease in lower frequency ranges, is sustained until the stimulus offset. Studies linked local gamma activity to the processing of individual features of the presented stimulus (Tallon-Baudry et al., 2001; Siegel et al., 2011), or to visual awareness and spatial attention (Wyart & Tallon-Baudry, 2008). As mentioned in earlier paragraphs, gamma amplitudes play a role of interest in the context of PACs. Namely theta/gamma PAC and alpha/gamma PAC, with the first being linked to the sequential retention of items (Canolty et al., 2006; Axmacher et al.,

2010) and the latter associated to the formation and maintenance of sensory-spatial inputs (Roux & Uhlhaas, 2014; Park et al., 2016). Finally, gamma power in retention has also been found to correlate with WM load (Howard et al., 2003).

The processing of visual information, prior to being transferred into WM, occurs through the ventral and dorsal streams (Milner & Goodale, 2006). These are associated with either object identification versus spatial relationships (Ungerleider & Haxby, 1994), or perception versus guidance of action (Milner & Goodale, 2008) respectively. Functional magnetic resonance imaging (fMRI) studies have also contributed to the mapping of cortical regions associated with VWM. Reportedly, frontal and parietal BOLD activity reflected executive functions (Carpenter et al., 2000; Linden et al., 2003; Osaka et al., 2004; Brass et al., 2005; Yuan & Raz, 2014; Bettcher et al., 2016) and selective attention (Kastner & Ungerleider, 2000; Mayer et al., 2007; Gazzaley & Nobre, 2012). Among the different visual-related areas, sustained activity in temporal and occipital regions reflected the maintenance of object representations (Grill-Spector et al., 2001; Kourtzi & Kanwisher, 2001; Bell et al., 2009). Moreover, two studies applied pattern classification techniques to BOLD activity obtained from the visual cortex during the delay period of delayed discrimination tasks. They were able to predict, on a trial basis, which type of orientation (Harrison & Tong, 2009) and color (Serences et al., 2009) were held in VWM. These results supported the view that sensory cortical areas contribute to VWM retention of fine-tuned feature information (Pasternak & Greenlee, 2005).

2.10. Research Questions

Visual WM, like other critical memory components, is susceptible to distortions. Investigating memory failures with respect to successful performances may help to understand the underlying neural mechanisms in memory formation. False memories, unlike common errors, may arise due to pre-existing semantic associations (Koutstaal et al., 2003) and/or prototypical perceptual features (Gutchess & Schacter, 2012) additionally elicited by the encoded sequence. Paradigms were devised to study false memories by introducing novel items (lures) similar to the encoded items sharing perceptual or semantic properties and trapping subjects into erroneous responses (DePrince et al., 2004; Brainerd & Reyna, 2005).

Most of the studies on visual false memories were conducted in the domain of long-term memory (Israel & Schacter, 1997; Koutstaal & Schacter, 1997; Seamon et al., 2000; Koutstaal et al., 2001; Jones et al., 2006; Baioui et al., 2012), some recent studies have explored them over short-term periods. As suggested by the aforementioned theoretical accounts based on LTM studies, additional LTM activations induced by the encoded set contribute to the occurrences of false memories. This assumption remains valid in the STM context where LTM activations may interfere with WM content. Typically, LTM investigations use longer lists of stimuli to be studied and longer delays between encoding and recognition sessions. An advantage of having trials that last only a few seconds is that

participants can be continuously monitored throughout all three main intervals, i.e., encoding, retention, recognition.

In STM, Iidaka et al. (2014) studied visual false memory by presenting subjects with human faces as stimuli. The authors reported an active role played by the amygdala amid short-term false memory events. Two studies investigated electrophysiological properties (Chen et al., 2012; Melnik et al. 2017) in an attempt to identify neural markers of these events. Specifically, in a STM DRM study using Chinese words to be encoded (Chen et al., 2012), they reported a prominent ERP N400 effect over frontal, central and parietal midline electrodes for correctly recognized probes when compared to that of false memories. In a modified Sternberg paradigm with short lists of words presented auditorily, Melnik et al. (2017) identified prominent alpha band activity in posterior regions corresponding to false memories induced by semantic interference.

To the best of our knowledge, oscillatory correlates associated with visual memory errors including false memories in WM have not been investigated, yet. The current study was realized to explore the temporal dynamics of EEG oscillatory activity reflecting VWM performance. Specifically, we aimed at identifying time-frequency windows and locations distinguishing successful and erroneous short-term memories of grayscale photos of commonly seen object categories (e.g., “luggage”, “chair”, “car”). Each category was defined by a set of images sharing the general thematic information (*gist*) while differing in the details characterizing the individual items (*verbatim*) (Koutstaal & Schacter, 1997; Brainerd & Reyna, 2002). The analysis was primarily concentrated on low frequencies (4 – 32 Hz), particularly theta and alpha bands, as the aforementioned studies (see Section 2.9) suggested that they played prominent roles in the encoding and maintenance intervals of VWM.

Observing meaningful EEG gamma band (> 30 Hz) activity is problematic given technical limitations and the nature of the signal. As microsaccades and muscle movements generate artifacts within the gamma band, it is difficult to discriminate genuine cortical activity from artifacts (Yuval-Greenberg et al., 2008; Hipp & Siegel, 2013). Nevertheless, given the reports provided by previous VWM studies (see Section 2.9) we intended to explore the gamma band looking for discriminatory characteristics at higher frequencies.

When evaluating WM performance, the investigation of connectivity measures may reveal useful information concerning top-down modulation deficiencies, inefficient sequential organization, or poor formation of sensory-spatial elements, potentially reflected by phase synchronization, theta/gamma PAC and alpha/gamma PAC respectively (see Section 2.9).

Furthermore, we attempted to induce false memories over short-term periods and looked for potential oscillatory markers differentiating them from other types of errors. To this end, we devised a challenging VWM task with the intent to maximize the rate of erroneous memory responses by the encoding of visual stimuli presented sequentially at a fast-pace.

CHAPTER 3

MATERIALS AND METHODS

3.1. Participants

A total of 40 volunteers partook in this study. Six participants were excluded: One due to technical problems, one reported to have given random answers due to drowsiness and four provided a selection between two alternatives whenever faced with the paired probes, not following the given instructions (see the experimental design provided in Section 3.3). Hence, there remained 34 participants (mean age $M = 24.88$, $SD = 4.77$, 16 females) for the analysis.

Six subjects contributed only with behavioral data. For the remaining 28 subjects (mean age $M = 23.54$, $SD = 3.77$, 12 females), EEG data were also recorded. Eligibility criteria included right-handedness and no use of medications that may affect the central nervous system. All subjects reported normal or corrected-to-normal visual acuity. They were informed about the experimental procedure and provided written informed consent prior to data collection in accordance with the Declaration of Helsinki. The METU ethics committee approved all experimental procedures.

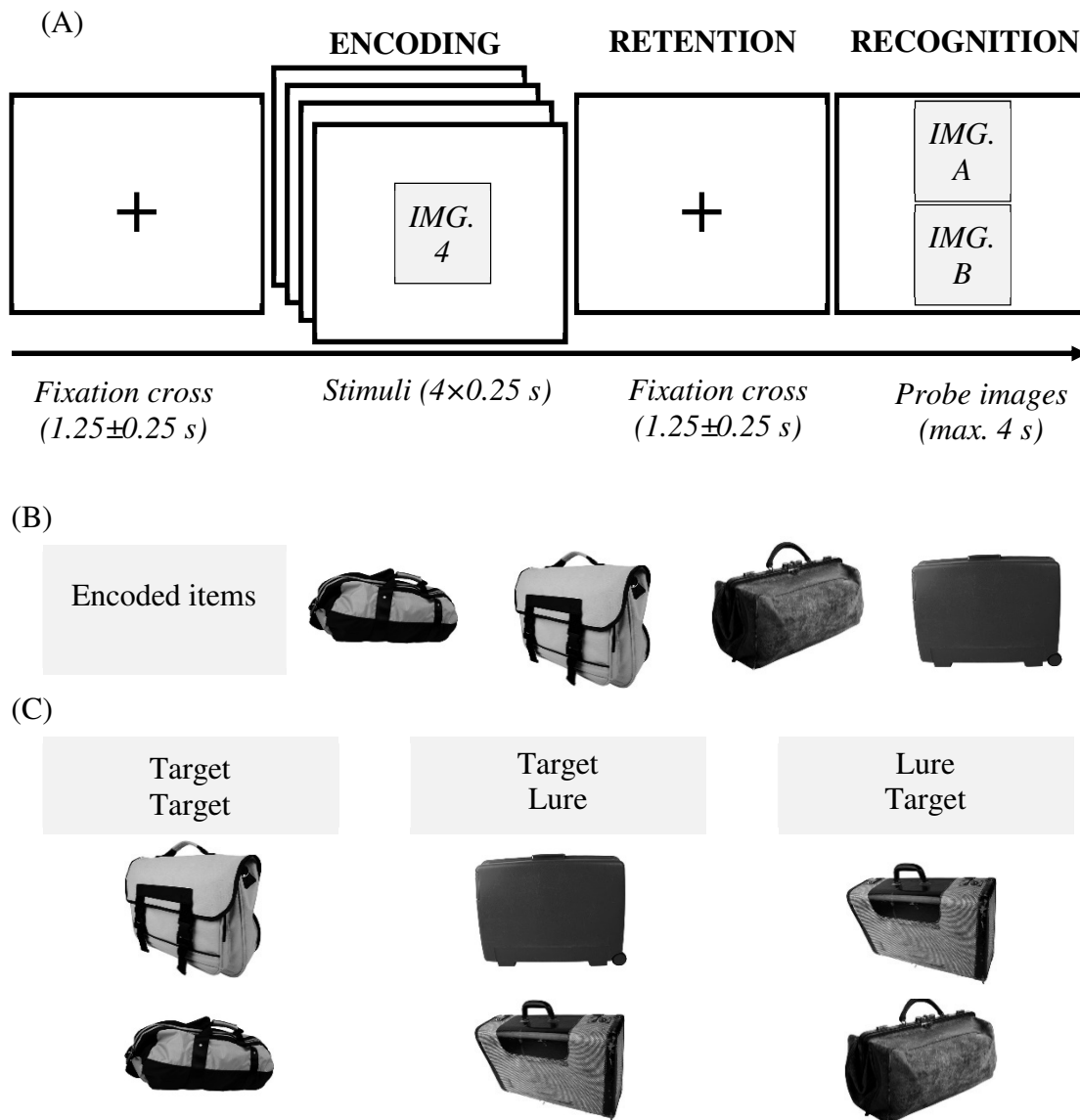


Figure 11: (A) Experimental procedure. At the beginning of each trial, a fixation cross was displayed at the center of the screen for 1.25 ± 0.25 s. Next, four images were sequentially presented for 0.25 s each. After a retention interval lasting for 1.25 ± 0.25 s, two probe images were shown. Participants had a maximum time of four seconds to decide whether they had previously seen one (or both) image(s) (“yes” answer) or none (“no” answer). Following the “yes” answer, subjects provided additional details identifying the remembered images (not shown in the diagram). Feedback was given after each trial. (B) An example of encoded items (targets) for the category “bag”. (C) Three types of probes were utilized – i.e., two previously studied items (i.e., target, target), one previously studied item and the lure presented in the lower slot of the presentation screen (i.e., target, lure), one previously studied item and the lure presented in the upper slot of the presentation screen (i.e., lure, target).

3.2. Stimuli

Dataset used in the experiments consisted of 216 sets of commonly seen object categories (e.g., “carpet”, “ball”, “flower”), each comprising four target images to be encoded (Figure 11B) and a lure image belonging to the category but being never shown during encoding (Figure 11C). All images were converted to grayscale and downsampled to a resolution of 500×500 pixels. Pictures were obtained either from the Hemera Photo DVD (Hemera Technologies Inc., Gatineau, Québec) or via Google Images.

3.3. Paradigm

The experimental procedure can be described as follows (Figure 11A): At the beginning of each trial, a fixation cross was shown for 1.25 ± 0.25 s. In the following encoding interval, four target images were presented sequentially. Each stimulus was displayed, centered on the screen, for 250 ms. Please note that neither a mask nor a blank screen was shown during the transition between images. During the ensuing retention interval, a fixation cross was shown for 1.25 ± 0.25 s and subsequently, two probe images were presented. Participants provided their responses using a gamepad. They had four possible answers to classify both probe images labelled as: *[new item, new item]*, *[old item, new item]*, *[new item, old item]* and *[old item, old item]* (Table 1). They had a maximum time of four seconds to respond. They were asked to press the “yes” button if they had previously seen one (or both) image(s), meaning at least one image was recognized as old. Whereas “no” corresponded to *[new item, new item]*, i.e., both images were identified as new. Following the “yes” response, subjects were further required to highlight the remembered image(s) using the gamepad joystick as *[old item, new item]*, *[new item, old item]* or *[old item, old item]*. Notably, the “yes/no” answer was always given with the right hand, whereas the joystick was controlled with the left hand. A feedback was given at the end of each trial. Subjects were instructed to respond as quickly and accurately as possible and they were asked not to yield an answer if they were not sure.

There were three distinct types of probes (Figure 11C): Lure in the lower slot (target in the upper slot), lure in the upper slot (target in the lower slot) or two targets. No trial included two novel images in the recognition interval. These properties of the probe images were not made explicit to the subjects.

Many STM studies reported higher rates of memory errors for related versus unrelated items, e.g., words (Coane et al., 2007; Atkins & Reuter-Lorenz, 2008; Flegal et al., 2010; Melnik et al., 2017) and faces (Iidaka et al., 2014). In order to induce false memories, the lure was an exemplar semantically related to the studied category.

Table 1: Definition of conditions. Different answers given by the participants – i.e., *[new item, new item]*, *[old item, new item]*, *[new item, old item]* and *[old item, old item]* – coupled with the types of probes, allowed for the characterization of the studied three conditions: *Correct*, the subject successfully recognized the probes; *false memory*, the lure is presented together with a target – i.e., an encoded item – and the subject mistakenly remembers of seen both images; *error*, the remaining combinations where the subject fails to recognize one or both presented images. The *error* condition was originally subdivided into four additional types, but the small number of trials associated with each condition (i.e., *type I, II, III, IV*) did not allow to conduct a meaningful oscillatory analysis. Thus, the *error* condition groups all these trials together which were anticipated to be characterized by poor encoding or retention.

Types of Probes <i>Upper slot</i> <i>Lower slot</i>	Conditions					
	<i>correct</i>	<i>false memory</i>	<i>error</i>			
			<i>type I</i>	<i>type II</i>	<i>type III</i>	<i>type IV</i>
<i>Target</i> <i>Lure</i>	<i>Old item</i> <i>New item</i>	<i>Old item</i> <i>Old item</i>	-	<i>New item</i> <i>Old item</i>	<i>New item</i> <i>New item</i>	-
<i>Lure</i> <i>Target</i>	<i>New item</i> <i>Old item</i>	<i>Old item</i> <i>Old item</i>	-	<i>Old item</i> <i>New item</i>	<i>New item</i> <i>New item</i>	-
<i>Target</i> <i>Target</i>	<i>Old item</i> <i>Old item</i>	-	<i>Old item</i> <i>New item</i> OR <i>New item</i> <i>Old item</i>	-	-	<i>New item</i> <i>New item</i>

It is also important to point out that while in principle it is possible to include trials with two new probes, we intended to maximize the number of opportunities to get false memory responses by never presenting two new images. As defined by our study (Table 1), only the types of probes *[target, lure]* and *[lure, target]* could have ended with a false memory response. Our definition of false memory is not only based on the misrecognition of the lure but also on proper encoding by successfully recognizing the accompanying target. With two lures we wouldn't be able to confirm whether the induced false memory response was genuine. A further consideration is that in laboratory settings, nuances in the definition of the term false memory were introduced (DePrince et al., 2004).

216 trials of images were randomly presented. Types of probes were randomized and balanced throughout the experiment. Three conditions were defined as follows: *Correct* indicating the successfully answered trials; *false memory*, whenever a lure was misrecognized as previously seen and the concomitant target probe was correctly identified; and *error*, whenever either one or both probed targets were not recognized (Table 1).

In its original definition, the experiment had six conditions as *error* was subdivided into four additional types, i.e., *type I, II, III, IV* (Table 1). However, the small number of trials associated with each error type didn't allow us to perform a meaningful oscillatory analysis, as each type would have been characterized by low signal-to-noise ratio (SNR). Thus, the *error* condition merges together all these trials which we anticipated to be characterized by poor memory encoding or retention. Nevertheless, in the following chapter we are briefly summarizing behavioral results pertaining to the six conditions (see Section 4.1.1).

The experimental paradigm was implemented in MATLAB® (2014a, The Mathworks, Inc., Natick, MA) using the publicly available Psychophysics toolbox extensions (Brainard, 1997).

3.4. Procedure

EEG recordings were performed in an acoustically insulated and electrically shielded room. Images were presented foveally on a 21" monitor positioned 90 cm from the subject's eyes, thus resulting in a visual angle of 8.41° in both dimensions. Participants completed a preparatory session to become acquainted with the task. On average, electrodes placement over subjects' head and training session took one hour. The experiment was divided into blocks, each of which composed of ten trials (except for the last block made by six trials). Blocks were separated by self-paced rest breaks in between. The average duration of the experiment was measured to be 37 min (SD = 10 min).

3.5. Electroencephalographic Recordings

EEG data were acquired using a 32-channel BrainAmp amplifier (Brain Products, Munich, Germany). Electrodes were mounted in an elastic cap (EasyCap, Herrsching, Germany) and positioned according to the standard international 10-20 system. Mastoids served as reference, while ground electrodes were placed on the earlobes. Electrooculogram data were recorded from a pair of electrodes placed respectively below (for vertical movements) and to the right (for horizontal movements) of the right eye. All impedance levels were kept below 10 kΩ. Data were sampled at the frequency of 1000 Hz.

3.6. Preprocessing and Time-Frequency Analysis

Data analyses were performed using MATLAB® with the aid of the open-source Fieldtrip toolbox (Oostenveld et al., 2011) and in-house scripts.

We chose the Fieldtrip toolbox as it offers an extended library of high-level functions that allow to perform advanced analysis of electrophysiological data while giving full control over all the data processing details.

Recordings were bandpass filtered offline using a 4th order Butterworth filter with cut-off frequencies of 0.2 Hz and 100 Hz. Epochs of three seconds, from -1.00 s to 2.00 s around the onset of the first stimulus, were extracted and demeaned.

During preprocessing of EEG recordings, it is important to consider the presence of artifacts that could undermine the quality of the data. One of the most common sources of artifacts in EEG studies is eye activity. While subjects are instructed to avoid or to restrict blinking during the task, it still remains difficult to obtain artifact-free recordings. The simplest solution to tackle the problem is to reject all the segments of the data which are affected by artifacts. However, large portion of data could end up being discarded thus impacting negatively the study. More advanced techniques have been developed in the attempt to limit the damaging effect caused by artifacts, among them the ones based on independent component analysis (ICA) (Bell & Sejnowski, 1995; Makeig et al., 1996) has been proven effective. Among several ICA algorithms (Hyvärinen & Oja, 2000), our analysis used the fastICA implementation (Hyvärinen, 1999). In general terms, ICA is typically described in the context of audio recordings at a cocktail party. In this chaotic scene, all the voices at the party are recorded through a series of microphones distributed across the room. Each microphone will record a cacophony of conversations and background noise. Nevertheless, it is possible to isolate an individual voice by considering weighted combinations of the recordings of each microphone. Within our domain, ICA derives independent sources from EEG signals without considering physical location, or structure and extent of the sources. EEG is seen as the output of statistically independent and spatially steady potential-generating sources. Given N (= 32 in our case) scalp electrodes that pick up correlated signals, ICA separates N sources. Even though ICA is generally fit to be used on EEG data, the assumption that the recorded signal is a linear mixture of exactly N sources is dubious. Not knowing the exact number of sources generating the scalp signal, one should be careful when interpreting the returned ICA components. The topographical distribution of each component (Figure 12A) assists its interpretation, i.e., whether a component reflects cortical activity, or other activity related to, for instance, muscle movements, eye blinks, heartbeats, or even external, such as line noise. Besides spatial topographies, the time course of the components (Figure 12B) can also contribute to the successful identification of artifactual components. Thus, EEG data can be cleaned by identifying artifacts-related components and then subtracting them from the data. Components associated with eye blink artifacts are characterized by topographical representations with frontal activity (Figure 12A) and by time courses which are mostly flat but occasionally interrupted by high-amplitude spikes in correspondence of a blink (Figure 12B). In removing spurious component, we adopted a conservative approach, i.e., components were removed only when we were convinced of their artifactual origin, not to lose meaningful cortical activity.

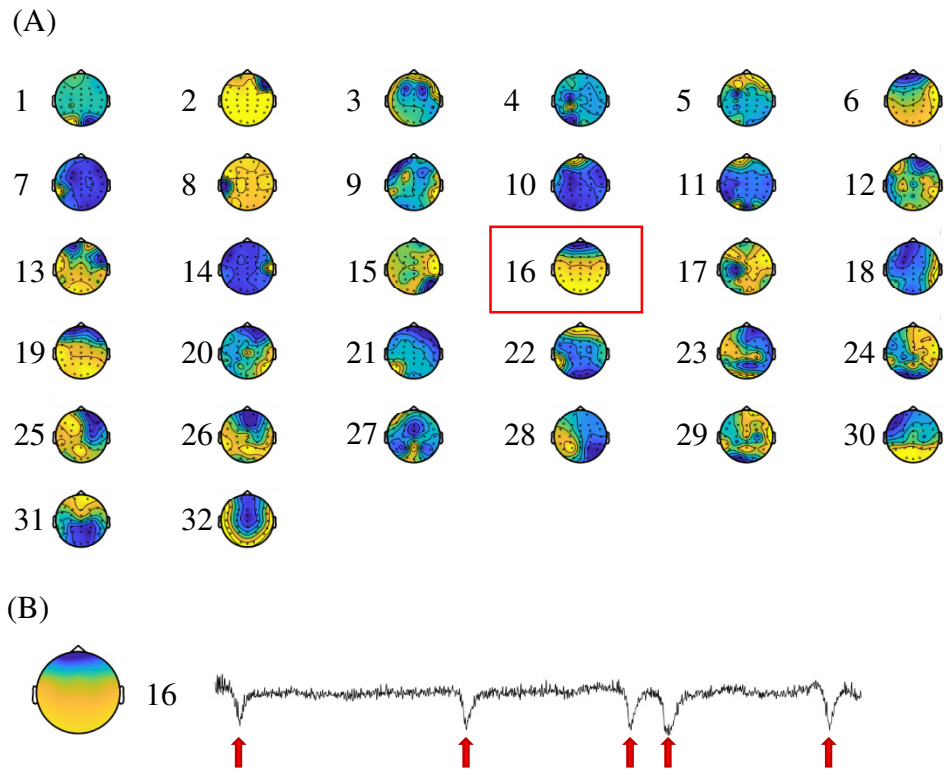
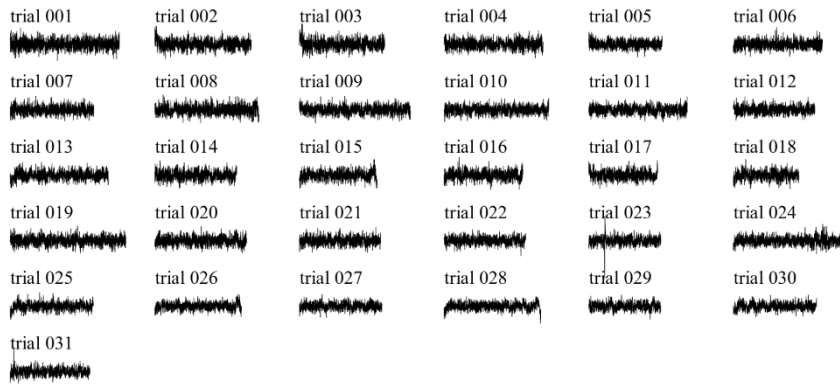


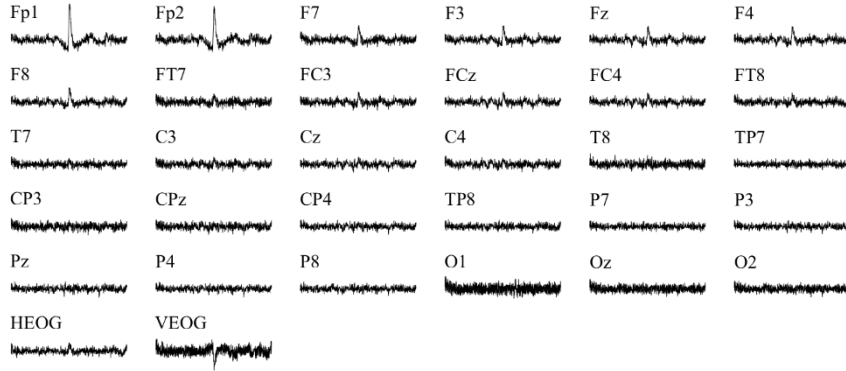
Figure 12: Example of artifact-related component identified by using ICA. **(A)** The topographical representations of the components returned by the ICA algorithm. The component 16, highlighted by the red rectangle, is an example of topography associated with eye blink artifacts. **(B)** Time-series linked to the component 16: Clearly visible, the generally flat pattern interspersed by high-amplitude spikes generated by the blinks (marked with red arrows).

After removing spurious components, trials (Figure 13A) and channels (Figure 13B) were inspected individually and as a visual summary of their variances (Figure 13C). Those still heavily affected by artifacts were discarded.

(A)



(B)



(C)

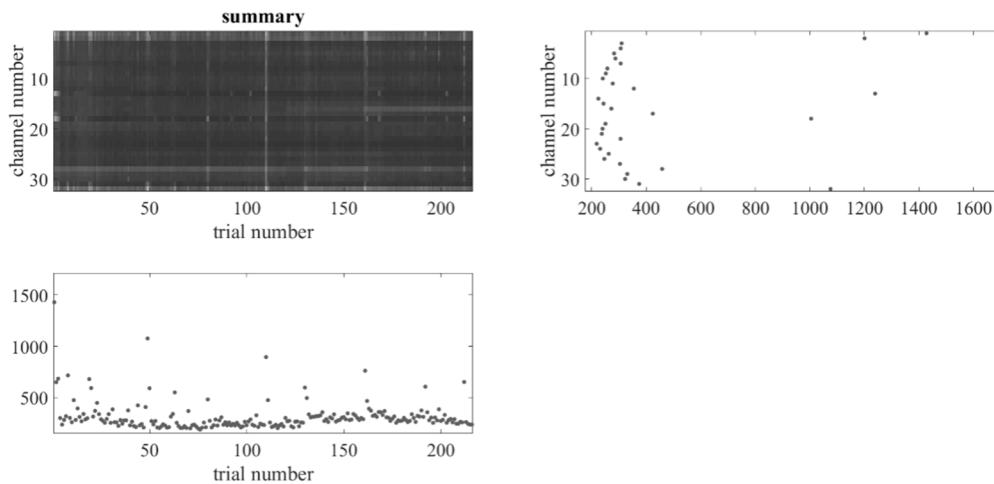


Figure 13: Example of a visual inspection from a representative subject. (A) Time courses of sample of trials for channel O2. (B) Time courses of a single trial for all the 32 channels. (C) Top-right plot: The variance of the recorded signals (considering the non-rejected trials) per channel. Bottom-left plot: The variance associated with each trial (considering the non-rejected channels). Top-left plot: Representation of the variances computed for both (non-rejected) trials and (non-rejected) channels.

Following the removal of noisy trials and components, the average number of trials per participant was $M = 202.39$, $SD = 11.96$ (*correct*: $M = 105$, $SD = 13.98$; *error*: $M = 78.57$, $SD = 14.97$; *false memory*: $M = 18.82$, $SD = 11.09$). Time-frequency power estimates were computed using Fourier basis with an Hanning window of 500 ms (Figure 5 and see Section 2.8.4). Frequencies ranging from 2 Hz to 32 Hz with 2 Hz increments were considered. The time window slid across trials in steps of 50 ms. Power estimates were normalized for each subject and condition, as a percentage of variation from baseline:

$$P_{norm}(f_i, t_j) = 100 \times \frac{P(f_i, t_j) - P_{baseline}(f_i)}{P_{baseline}(f_i)}$$

where f_i is the i^{th} frequency bin and t_j is the j^{th} time point. $P_{norm}(f_i, t_j)$ and $P(f_i, t_j)$ denote respectively the normalized power value (reported as a percentage) and the original power estimate for the specific frequency bin f_i and time point t_j . $P_{baseline}(f_i)$ is the average power value within the baseline for the specific frequency bin f_i . Baseline values were estimated considering all trials, regardless of the condition, within the time interval ranging from -1.00 s to -0.30 s prior to the onset of the first stimulus.

3.7. Conditions and Trial Selection for the Oscillatory Analysis

3.7.1. Correct and error

The oscillatory investigation contrasted initially correct and error conditions. To control for SNR differences, an equal number of trials was selected for each studied condition prior to the estimation of the time-frequency portraits. Accordingly, a pseudorandomized process selected a subset for the condition with a higher number of trials. Initially, trials having response time (RT) lying within one standard deviation from the mean RT of the condition were given priority. When the number of trials having RT inside the defined range was not enough, trials with RT outside of that range were also considered in order to complete the selection process. With this approach we intended to prioritize oscillatory data associated with participants' typical behavioral responses. Possibly, uncommon RTs could have been symptomatic of occasional lack of engagement throughout the trial. Thus, it was a precautionary step we took to ensure the inclusion of genuine trials in the oscillatory analysis.

3.7.2. False memory

After assessing the differences between correct and error conditions, the focus shifted to false memory trials. Notably, channels, frequencies and time intervals relevant to the correct and error investigation – Section 3.12 – were retained in these subsequent analyses.

The study of false memory was separated as a small number of *false memory* occurrences across participants resulted into low SNR that did not allow for a reliable direct comparison with *correct* and *error* conditions. As a remedy, for each analysis (i.e., encoding and retention), all *false memory* trials were combined with those of the *error* condition (*error + false memory*), which was then compared with the *correct* condition. Conversely, all *false memory* trials were then merged with the *correct* condition (*correct + false memory*) and the contrast with *error* condition was re-evaluated. Importantly, false memory trials were added in turn to each condition and statistical results were Bonferroni corrected to account for multiple comparisons. The rationale behind this approach was to use these newly defined conditions, with increased SNR, to highlight pattern similarities of *false memory* with *correct* and *error* conditions.

The trial selection process (analogous to the one described in Section 3.7.1) for the combined conditions – i.e., *correct + false memory* and *error + false memory* – would ensure to retain all *false memory* trials.

3.8. Channel Selection and Frequencies of Interest for the Encoding Interval

Given the perceptual nature of our task, occipital channels were anticipated to play a prominent role during the encoding of the visual stimuli. Time-frequency estimates (regardless of the condition) revealed conspicuous occipital power increase within theta band range with simultaneous power decrease of alpha power immediately after the onset of the first stimulus (Figure 14). Thus, we decided to focus the analysis of the encoding interval on the occipital channels (O1, Oz, O2) for theta (4 – 8 Hz) and alpha (10 – 14 Hz) bands.

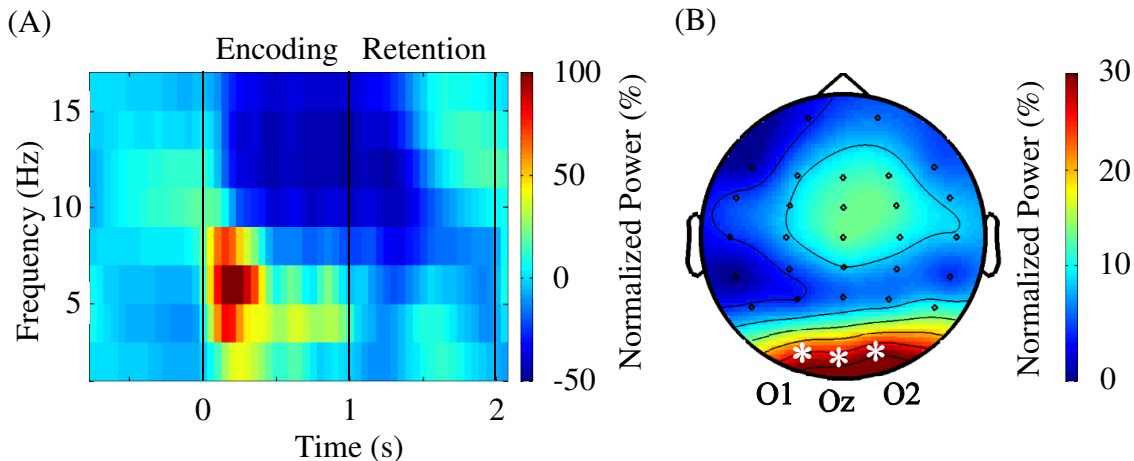


Figure 14: **(A)** Grand average time course averaged over occipital channels O1, Oz, and O2. **(B)** Topographical map of theta activity (4 – 8 Hz) during encoding ([0, 1] s). A theta power increase, more prominent in occipital regions, was clearly visible.

3.9. Channel Selection and the Individual Central Frequency for the Retention Interval

Visual inspection of time-frequency portraits consistently identified alpha-beta band activity within the second half of the retention interval, i.e., [1.5, 2.0] s, more prominently on the right parieto-occipital channels. Yet, its central frequency and associated bandwidth were shown to be subject-dependent – with values ranging from 10 Hz to 26 Hz (Figure 15A). Accordingly, for each participant, we decided to ascertain the individual central frequency (ICF), i.e., the frequency yielding the strongest power increase being consistent with the aforementioned pattern. To assess the significance of the right lateralization of the observed pattern we performed a dependent t -test considering the mean power from each hemisphere computed within the second half of the retention interval, [1.5, 2.0] s, for the frequency range [ICF – 2, ICF + 2] Hz over the right (P4, P8, O2) and left (P3, P7, O1) channels respectively. Given the found lateralization ($t(27) = 4.69$, $p < 0.0001$, $r = 0.67$, see Section 4.2 and Figure 23 for the details), the analysis of the retention interval focused on the channels (P4, P8, O2) for the frequency band [ICF – 2, ICF + 2] Hz. Figure 15B and C show the effect of the ICF alignment on grand average plots.

As the ICF values ranged within the alpha and beta bands, throughout the article we will be referring to that as the “alpha-beta band”. Visual cognition studies such as Waldhauser et al. (2012) and Michalareas et al. (2016) also reported individual frequency peaks spreading over broad alpha and beta band ranges.

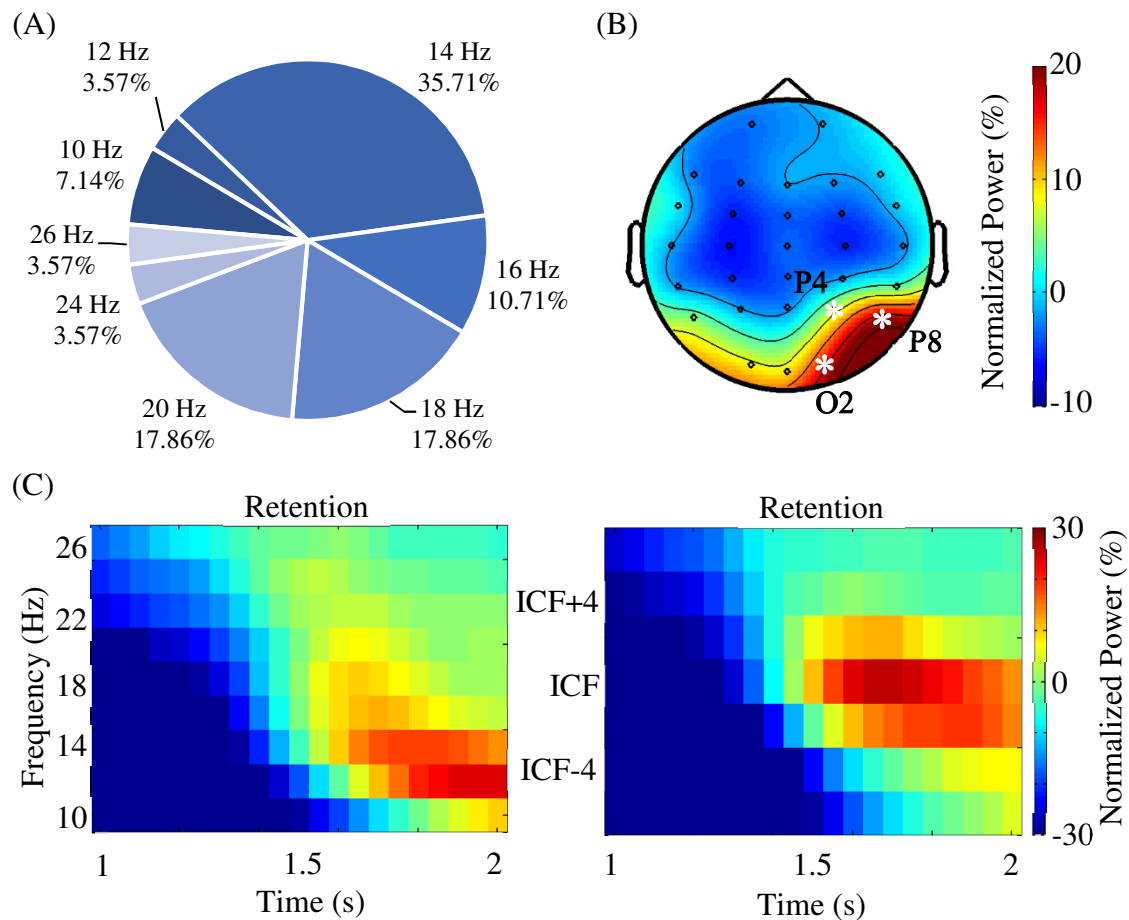


Figure 15: **(A)** Distribution of the individual central frequency (ICF) across all participants. ICFs were spanning across the alpha and beta bands, between 10 Hz and 26 Hz. **(B)** Grand average topography, following the alignment of ICFs, for the frequency range [ICF - 2, ICF + 2] Hz and for the second half of the retention interval ([1.5, 2.0] s). A conspicuous activity in parieto-occipital regions, lateralized in the right hemisphere, was notable. **(C)** Grand average time-frequency portraits prior (left) and following (right) ICF alignment averaged over the channels O2, P4 and P8.

3.10. Gamma Band Analysis Within the Encoding and Retention Interval

To explore time-frequency patterns at higher frequencies, an additional preprocessing step and different analysis settings were required. A discrete Fourier transform (DFT) filter was used to remove residual line noise (50 Hz) and related harmonic (100 Hz). The DFT filter needs to be very sharp in order to be effective. Consequently, the data were padded up to 10 seconds (mirrored data were used as filling not to bias the estimation of the noise). The padding ensured a filtering frequency bin of 1/10 Hz wide. The DFT filter generated a constant sine wave (its amplitude estimated from the noise) with a frequency of 50 Hz and harmonic which were later subtracted from the original data. As the majority of the

participants performed the experiment in the Faraday room, no line noise presence was observable in the recordings. However, three subjects had performed the experiment outside of the Faraday room. Following the filtering of the data, a residual line noise was still noticeable (Figure 16). This is caused by the non-stationarity of the line noise in the recordings. Time-frequency power estimates for the gamma band (30 Hz to 100 Hz) were computed using Fourier basis with the multitaper method (see Section 2.8.4). Discrete prolate spheroidal sequences (Slepian sequences) taper was used with a fixed window length of 0.2 s and smoothing of the frequencies of ± 10 Hz (three tapers) (Figure 6). Note that the multitapering in the frequency domain smoothed out the notch introduced by the DFT filter.

Grand average topographical patterns for both encoding and retention intervals (Figure 17) revealed gamma activity more prominent in temporal sites that were consistent across subjects – 22 out of 28 subjects showed visible activity on at least one temporal location.

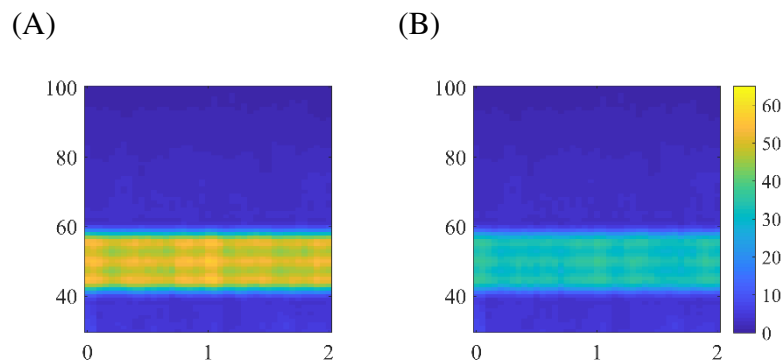


Figure 16: Time-frequency portraits of gamma frequencies for channel O1 from a representative subject while performing the experimental task outside of the Faraday room. **(A)** The task grand-average TFR prior line noise filtering. **(B)** The task grand-average TFR following the filtering. The line noise has been reduced, nevertheless it still remains noticeable.

Frontal gamma activity was less common being observed in 15 out of 28 subjects. Finally, 7 out of 28 subjects exhibit pronounced gamma activity in occipital areas.

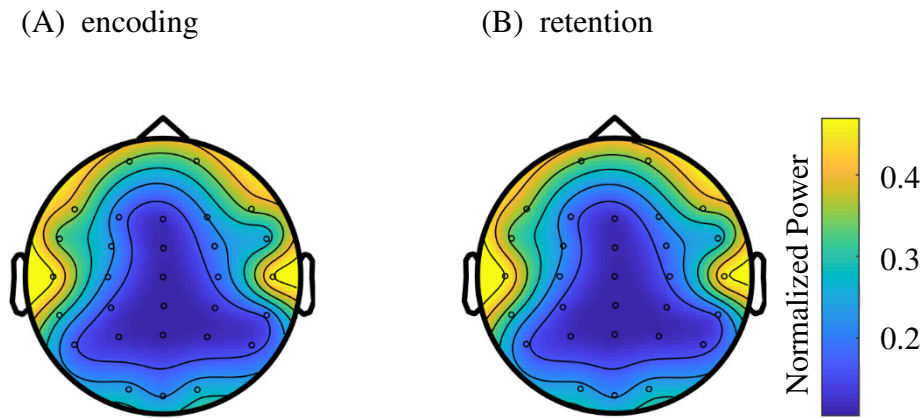


Figure 17: Grand average for the gamma band (40 – 100 Hz) for (A) encoding and (B) retention interval.

3.11. Statistical Analyses of Behavioral Measurements

Statistical analyses pertaining to behavioral data were conducted via IBM SPSS[®] Statistics 22.0 (IBM Corp., Armonk, NY). Friedman's ANOVA was used to investigate RT differences across conditions as the Kolmogorov-Smirnov test showed that the RT distribution was non-normal. When required, post hoc analyses were realized via Wilcoxon tests and Bonferroni correction was applied to account for multiple comparisons.

Correlations between RTs (averaged independently from the conditions) and task accuracies (i.e., *correct* response rate) were investigated. Moreover, relationships between the rates of the conditions (i.e., correct, false memory and error rates) were also assessed. As for the RTs, the Kolmogorov-Smirnov test showed that distributions of the rates of conditions were non-normal and hence Spearman's coefficient was used to estimate the correlations.

3.12. Cluster Permutation Statistics

Statistical analyses of oscillatory data were conducted using the non-parametric cluster-based permutation test (Maris & Oostenveld, 2007), which controls for the multiple comparisons problem. Clusters were defined as two or more contiguous channel-frequency-time triplets, each showing $p < 0.05$ (two-sided dependent samples t -test) with respect to the conditions. Cluster-level statistics were computed taking the sum of the t -values within each cluster. The reference distribution was approximated by means of the Monte Carlo method with 30000 permutations. The test statistic was defined as the maximum of the cluster-level statistics. A cluster was deemed significant if its Monte

Carlo probability exceeded the threshold of 0.025 for each tail when compared to the distribution.

Analysis of the encoding interval ([0, 1] s) primarily focused on the elicited pattern, i.e., theta power increase ([4, 8] Hz) and alpha power decrease ([10, 14] Hz), that was more prominent in the occipital areas (O1, Oz and O2) (Figure 14B). Furthermore, during the retention interval ([1, 2] s), a conspicuous alpha-beta increase was observed in the right parieto-occipital channels (P4, P8 and O2) (Figure 15B). Notably, time-frequency estimates of each subject were shifted to align all ICFs and the range of [ICF-2, ICF+2] Hz was explored.

The investigation of the gamma band focused on temporal locations for both the encoding and retention intervals. As mentioned in Section 3.10, temporal sites exhibited higher gamma power levels. Furthermore, activity in medial temporal lobe (MTL) regions has been observed during WM encoding and maintenance (Aggleton et al., 1992; Nichols et al., 2006; Axmacher et al., 2007; Race et al., 2013). MTL was also hypothesized to be recruited whenever relations between items, or sequences of items were encoded (Eichenbaum, 2004; Kumaran & Maguire, 2006).

As WM studies reported significant correlations between alpha band power values and RTs (e.g., Obleser et al., 2012; Bonnefond & Jensen, 2012; Melnik et al., 2017), we investigated also potential relationships between oscillatory data within the significant clusters and behavioral measures. The correlation was realized via Spearman's coefficient as the Kolmogorov-Smirnov test determined the distributions of the oscillatory parameters as non-normal.

3.13. Connectivity Analyses

3.13.1. Coherency

Coherency was selected as a measurement of interest to investigate linear relationships across the different EEG channels at a specific frequency (Nolte et al., 2004). In order to define coherency, we should consider $X(f)$ and $Y(f)$, the Fourier transforms of $x(t)$ and $y(t)$, time series for electrodes x and y respectively. Then, the cross-spectral density is defined as follows:

$$P_{xy}(f) = \langle X(f)Y^*(f) \rangle$$

Where $*$ refers to the complex conjugation and $\langle \rangle$ indicates the expectation value, which can only be estimated by averaging a large enough number of epochs. Thus, the coherency is defined as follows:

$$\tilde{C}_{xy}(f) = \frac{P_{xy}(f)}{\sqrt{P_{xx}(f)P_{yy}(f)}}$$

Coherency measures the synchronization between two signals – i.e., time series of power values for different electrodes – by quantifying the strength of their phase lock. This quantity, represented by a complex number $A + Bi$, is non-directional, hence one can only estimate the degree of synchrony between two signals without being able to infer the leading source. Coherency estimates at electrode level suffer from volume conduction, a spurious contribution to the measured synchronization caused by neural activity from a unique source recorded by both channels. The real component A of coherency is mostly affected by the false synchrony. Therefore, we decided to keep only B^2 , the squared imaginary part of the coherency, to minimize the effect of volume conduction. It is important to note that genuine zero-phase synchrony, which is also a contributing factor to the real value A and indistinguishable at a channel level from volume conduction effects, is lost.

The connectivity investigation was conducted on the encoding and retention intervals for theta, alpha and beta frequency bands. At first, the analysis attempted to identify differences between *correct* and *error* conditions. Later, as for the time-frequency study (Section 3.7), differences have been reassessed following the inclusion of *false memory* trials in both conditions.

Time-frequency power values, for the computation of coherency, were estimated using Fourier basis and a Hanning window of 1000 ms, thus covering the entire encoding ([0, 1] s) and retention ([1, 2] s) times respectively. Frequencies ranging from 2 Hz to 32 Hz with 1 Hz increments were considered.

To discriminate genuine coherency estimates from noise, a coherency distribution was determined via Monte Carlo method: For each combination of channels, 200 runs were executed where coherency between two channels was estimated by shuffling their trials. The objective was to determine a confidence level, for each frequency bin, sets as the value under which lied 95% of the distribution (Figure 18).

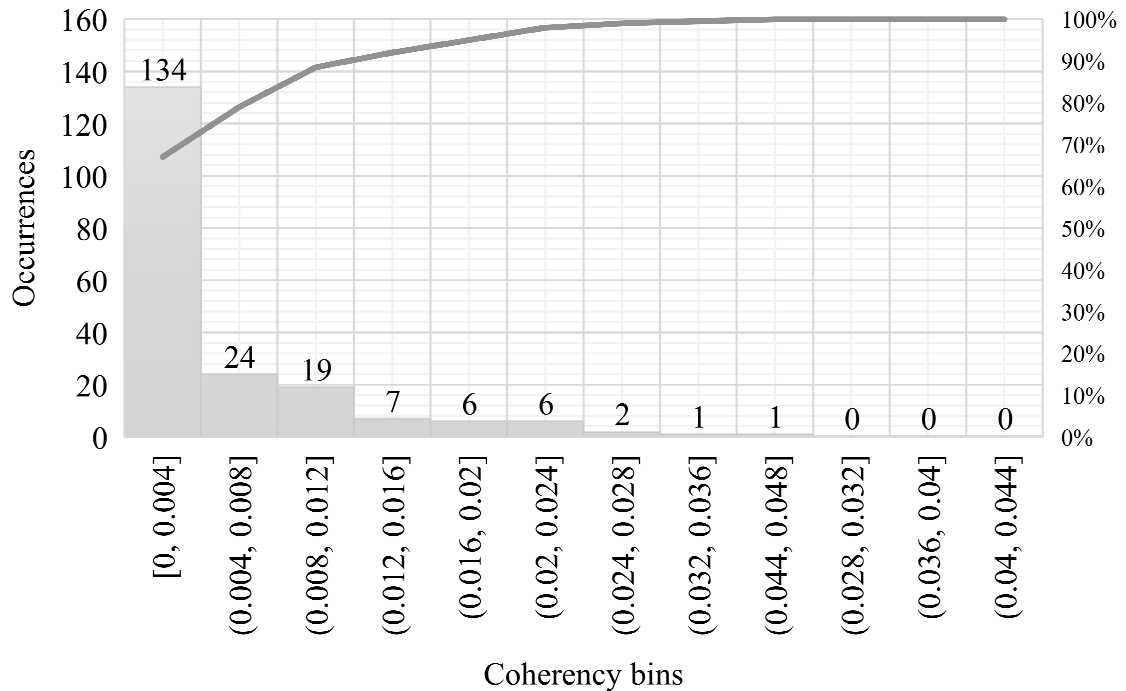


Figure 18: An example of coherency distribution obtained via Monte Carlo simulation for a representative subject. The objective of the simulation was to estimate the confidence level of the coherency measure. In this example the connectivity between the channels O2 and F4 at a frequency of 4 Hz for the condition *correct* was assessed. The Monte Carlo simulation (200 iterations) was repeated for each of the 28 subjects and for each condition. It considered the coupling between the seed channels (O1 for encoding and O2 for retention) and the remaining 29 channels for each of the 31 frequency points (from 2 Hz to 32 Hz). The objective was to determine a confidence level, for each frequency point (see also Figure 19), sets as the value under which lied 95% of the distribution (for the current example the value is 0.0196). For clarity of visualization, the coherency values were grouped in bins with a width of 0.004.

As this process revealed to be computationally expensive, the initial focus verted on a single seed channel selected a priori for each studied interval. More specifically, time-frequency portraits of the encoding interval highlighted significant power differences (see Section 4.2) in the theta band in occipital channels. As the difference was more pronounced in channel O1, it was selected as seed channel for the coherency analysis in encoding. Similarly, as the time-frequency study for the retention interval revealed power differences in posterior-right regions (see Section 4.2), O2 was the selected seed as it carried the stronger difference.

To approximate for anatomical differences across subjects, channels were divided into groups: Left, right and central locations for frontal, middle and posterior areas respectively (Figure 19B). The stronger coherency peaks across each region were selected and differences evaluated with a paired-sample *t*-test.

As one prominent location representing the WM central executive is hypothesized to be in frontal regions, we expected to see significant synchronization between occipital and

frontal areas. Hence, the analysis primarily focused on the relations between the seed channels (O1 for encoding and O2 for retention) and frontal regions, for which frequency coherency peaks were identified on a subject basis (Figure 19). Coherency values lower than the threshold defined by the confidence level were considered spurious and set to zero. Subjects not showing any significant coherency for both conditions were excluded from the analysis.

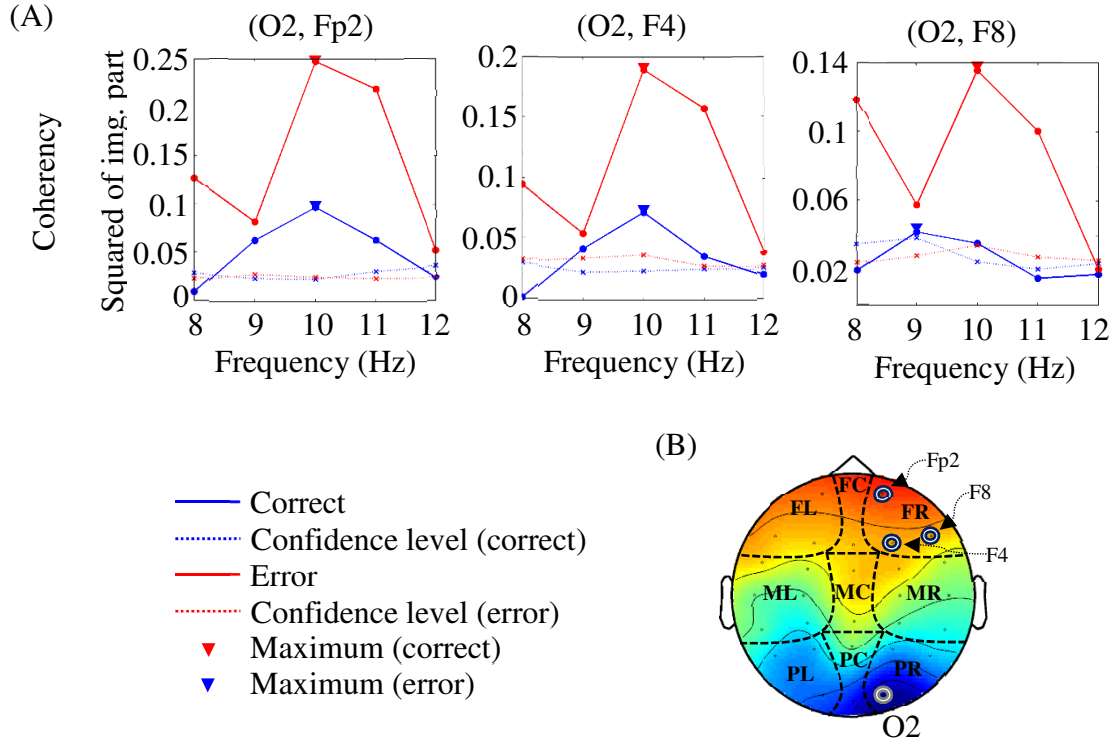


Figure 19: (A) Example from a representative subject of connectivity between the frontal-right (FR) region (Fp2, F4, F8 channels) and the seed channel O2. The stronger coherency peak is identified – in this case for (O2, Fp2) – and then we verified that it passed the confidence level thus indicating a genuine measurement of connectivity. In this specific example, an alpha phase synchrony between O2 and FR region is observed which is significant for both conditions and record the stronger values for (O2, Fp2). (B) To account for anatomical differences between subjects, channels were partitioned: Left (L), right (R) and central (C) locations for frontal (F), middle (M) and posterior (P) areas respectively.

Finally, a conclusive exploratory analysis accounting for potential differences in middle and occipital regions was also performed. Further examinations were conducted considering the seed channel Oz (for both the encoding and retention intervals) as the produced topographical distribution of coherency revealed stronger levels of synchronization (see Figure 29A and Figure 31A). The previous simulations estimated a confidence level which could be conservatively approximated being around 80% of the confidence level of coherence (the square of the coherency and hence a real value) and computed as described by Halliday et al. (1995):

$$1 - (1 - 0.95)^{\frac{1}{L-1}}$$

Where L is the length of the window in terms of number of samples (i.e., in our case 1 s corresponding to 1000 samples).

Therefore, in this latter analysis, we didn't perform the computationally expensive process of identifying the confidence level from a generated distribution. We used instead the aforementioned conservative approximation.

3.13.2. Phase-amplitude coupling

Phase-amplitude coupling (PAC) (Figure 8) is a measure of cross-frequency synchronization and provides an estimate of dependence between distinct frequency bands of a recorded signal (e.g., data from one or two EEG channels). More specifically, in our study, the dependence between the bands is defined by the phase time series $\varphi_L(n)$ of a low-bandpass filtered signal $z_L(n)$ and the amplitude envelope time series $a_H(n)$ of a high-bandpass signal $z_H(n)$. We used the direct PAC estimate (Özkurt & Schnitzler, 2011) as cross-frequency index and it is defined as follows:

$$\rho_D = \frac{1}{\sqrt{N}} \frac{|\sum_{n=1}^N a_H(n) e^{i\varphi_L(n)}|}{\sqrt{\sum_{n=1}^N a_H(n)^2}}$$

Where N is the length of the time series, and the phase and amplitude time series $\varphi_L(n)$ and $a_H(n)$ are extracted via Hilbert transform. Finally, PAC estimates are corrected, as described by Özkurt (2012), in order to retain only genuine cross-frequency coupling. More specifically, given a confidence level p (for our study set to 0.01 and Bonferroni corrected by the number of low frequency bins times the number of high frequency bins), x_{lim} , used to determine the significance of PAC, is defined as follows:

$$x_{lim} = N \times [erf^{-1}(r)]^2$$

Where N is the length of the time series, $r = 1 - p$, and erf is the error function.

In order to compute the confidence level for each frequency pair, the amplitude time series a_H is normalized, i.e., by dividing it for its standard deviation and subtracting its mean. The statistics for each frequency pair are then computed as follows:

$$s = \left| \sum_{n=1}^N \tilde{a}_H(n) e^{i\varphi_L(n)} \right|^2$$

Where \tilde{a}_H is the normalized time series of the amplitude values.

Only when $s > 2x_{lim}$ the associated coupling estimate is accepted, otherwise it is nullified.

Given the aforementioned literature concerning PAC (see Sections 2.8.5 and 2.9), it is of interest to investigate if significant differences between *correct*, *errors* and *false memory* conditions might be detected in PAC estimates during the encoding and retention intervals of our task. Once again, to approximate for anatomical differences across subjects, channels were grouped into regions of interest (Figure 19B): Frontal (left, central and right) and parietal (central), hypothesized to be recruited by central executive processes (Sauseng et al., 2005a); temporal sites (left and right), where the main gamma activity was observed in our task; posterior areas (left, central and right), as visual-related locations.

Two different analyses were performed. First, PAC values were estimated individually for each channel, i.e., low-frequency and high-frequency components were extracted from the same site. Next, PAC estimates were computed considering couples of channels, i.e., a low-frequency source channel was defined as seed and PAC computed considering the high-frequency components from the remaining channels. As the latter analysis was computationally expensive, only channels from frontal and occipital locations were selected as seed given their relevance to the study.

PAC estimates within a low-frequency interval ranging from 3 Hz to 14 Hz (with 1 Hz increment) and a high-frequency band ranging from 30 Hz to 120 Hz (with 2 Hz increment) were computed. In order to explore gamma frequencies up to 120 Hz, the initial preprocessing filtering (4th order Butterworth filter) was widened, i.e., cut-off frequencies of 0.2 Hz and 200 Hz. Next, for PAC on a single channel, theta (3– 5 Hz) to lower gamma (30 – 60 Hz) PAC and alpha (8 – 14 Hz) to upper gamma (60 – 120 Hz) PAC portraits were studied for higher coupling levels had been observed. When couples of channels were considered, the analysis focused on low frequencies ranging from 3 Hz to 8 Hz and high frequencies within 30 Hz and 80 Hz given the finding reported by Fries et al. (2013) (Section 2.9).

For each analysis, the PAC peaks across each defined region were selected and differences between conditions were assessed with a paired-sample *t*-test.

CHAPTER 4

RESULTS

4.1. Behavioral Analysis

In its original form, the experiment had defined six conditions, i.e., *correct*, *false memory*, *type I*, *type II*, *type III* and *type IV* errors. As the number of trials for each error type were not enough to perform a meaningful analysis of oscillatory properties, we decided to merge the four error types into one condition, namely *error*. Nevertheless, few behavioral results have been gathered from the six condition settings and they are reported in Section 4.1.1. Differently, in Section 4.1.2 behavioral results from the three conditions analysis are summarized.

4.1.1. Six conditions: Correct, false memory and type I, II, III, IV errors

For the investigation of potential differences in the rates of conditions, the Mauchly's test indicated that the assumption of sphericity had been violated, $\chi^2(14) = 124.579$, $p < 10^{-5}$, therefore degrees of freedom were corrected using Greenhouse-Geisser estimates of sphericity ($\epsilon = 0.575$). The results show a significant effect of the conditions on the distribution rate, $F(2.876, 97.775) = 487.078$, $p < 10^{-5}$. Significant differences among the conditions revealed by Bonferroni corrected post hoc tests are summarized in Table 2A and the distribution of the rate across conditions is shown in Figure 20A.

The analysis demonstrated an effect of task conditions over response time, $\chi^2(5) = 102.71$, $p < 0.00000001$. Post hoc analyses were performed with Wilcoxon tests and results were Bonferroni corrected thus setting the threshold for significance at 0.0033. Results are summarized in Table 2B while median (IQR) RTs are plotted in Figure 20B.

Table 2: (A) Subjects' rate distribution, significant differences of the post hoc investigation. (B) Subjects' RT post hoc analysis results. All effects are reported at a 0.0033 level of significance (significant *p* values are highlighted by an asterisk).

Subjects' rate distribution (post hoc comparison)	<i>p</i>
<i>correct – false memory</i>	< 10 ⁻⁵
<i>correct – type I error</i>	< 10 ⁻⁵
<i>correct – type II error</i>	< 10 ⁻⁵
<i>correct – type III error</i>	< 10 ⁻⁵
<i>correct – type IV error</i>	< 10 ⁻⁵
<i>false memory – type I error</i>	< 5·10 ⁻⁵
<i>false memory – type IV error</i>	< 10 ⁻⁵
<i>type I error – type II error</i>	< 10 ⁻⁵
<i>type I error – type III error</i>	< 10 ⁻⁵
<i>type I error – type IV error</i>	< 10 ⁻⁵
<i>type II error – type IV error</i>	< 10 ⁻⁵
<i>type III error – type IV error</i>	< 10 ⁻⁵

(A)

Subjects' RT (post hoc comparison)	<i>p</i>	<i>Z</i>	<i>r</i>
<i>false memory – correct</i>	0.966	-0.043	-0.005
<i>type I error – correct</i>	0.871	-0.162	-0.020
<i>type II error – correct</i>	< 0.00001*	-4.522	-0.548
<i>type III error – correct</i>	< 0.000001*	-4.937	-0.599
<i>type IV error – correct</i>	< 0.00001*	-4.623	-0.561
<i>type I error – false memory</i>	0.700	-0.385	-0.047
<i>type II error – false memory</i>	0.001*	-3.308	-0.401
<i>type III error – false memory</i>	< 0.000001*	-4.937	-0.599
<i>type IV error – false memory</i>	< 0.00001*	-4.554	-0.552
<i>type II error – type I error</i>	< 0.00001*	-4.676	-0.567
<i>type III error – type I error</i>	< 0.00001*	-4.937	-0.599
<i>type IV error – type I error</i>	< 0.00001*	-4.623	-0.561
<i>type III error – type II error</i>	< 0.00001*	-4.937	-0.599
<i>type IV error – type II error</i>	< 0.00001*	-4.577	-0.555
<i>type IV error – type III error</i>	0.909	-0.114	-0.014

(B)

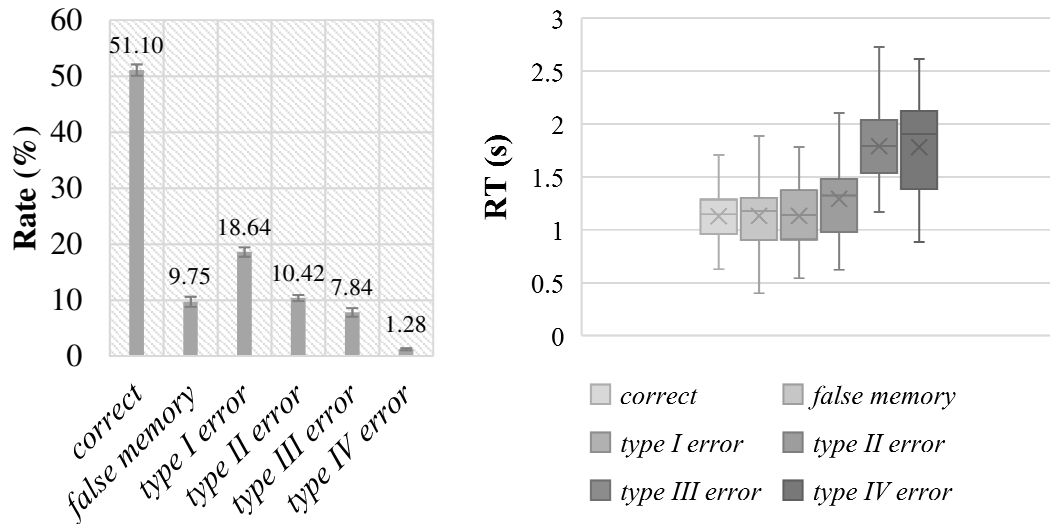


Figure 20: (A) Participants' answer rate (percentage) grouped by conditions. The analysis suggested that there was a significant effect of the condition on the distribution rate ($p < 10^{-5}$). the unanswered trials accounted for the remaining $M = 0.97\%$ ($SD = 1.80\%$). (B) Boxplot for the median (IQR) response time (RT) for the conditions. *correct*: 1.145 (0.957 to 1.285) s; *false memory*: 1.176 (0.900 to 1.302) s; *type I error*: 1.139 (0.906 to 1.372) s; *type II error*: 1.324 (0.977 to 1.478) s; *type III error*: 1.794 (1.535 to 2.039) s; *type IV error*: 1.903 (1.382 to 2.122) s. For these post hoc tests, a Bonferroni correction was applied and so all effects are reported at a 0.0033 level of significance, the results are summarized in Table 2B.

4.1.2. Three conditions: Correct, false memory, error

Participants' task performance, i.e., *correct* rate, was $M = 51.10\%$, $SD = 5.88\%$ in average. While the *error* rate was $M = 38.18\%$, $SD = 7.64\%$, *false memory* occurrences rated at $M = 9.75\%$, $SD = 5.30\%$. Finally, the unanswered trials accounted for the remaining $M = 0.97\%$, $SD = 1.80\%$.

The response time was significantly influenced by task conditions, $\chi^2(2) = 28.294$, $p < 0.000001$. Wilcoxon tests were used to follow-up this finding. A Bonferroni correction was applied and so all effects are reported at a 0.017 level of significance. Median (IQR) response time for *correct*, *false memory* and *error* conditions were 1.145 (0.957 to 1.285) s, 1.176 (0.900 to 1.302) s and 1.330 (1.055 to 1.581) s, respectively. There were significant differences between the *error* and *correct* trials ($Z = -5.001$, $r = -0.606$, $p = 0.0000006$) and between *error* and *false memory* trials ($Z = -3.753$, $r = -0.455$, $p = 0.000175$). However, there was no statistically significant difference in response time when comparing *correct* and *false memory* conditions ($Z = -0.043$, $r = -0.005$, $p = 0.966$) (Figure 21A). Notably, considering only the behavioral data from the 28 subjects that provided also EEG data, the aforementioned results remained valid.

A negative correlation was found between *false memory* and *error* rates (Figure 21B, Spearman's $\rho = -0.69$, $p = 0.000027$).

When the recognition rate of each single stimulus was evaluated according to its serial position, we found that the fourth stimulus ($M = 92.55\%$, $SD = 3.71\%$) was successfully recognized with a rate that was higher ($p < 10^{-6}$) than the ones of the other items (Figure 21C). Please note that the rates were $65.58 \pm 9.23\%$, $65.56 \pm 8.48\%$ and $67.83 \pm 8.98\%$ for the first, second and third items, respectively. Importantly, as we presented two images during recognition, these rates do not reflect the *global* task performance as for a correct response subjects need to properly classify both probes (Table 1). Please note that when only those 28 subjects having EEG data were considered in the behavioral analysis, all aforementioned behavioral results remained statistically valid.

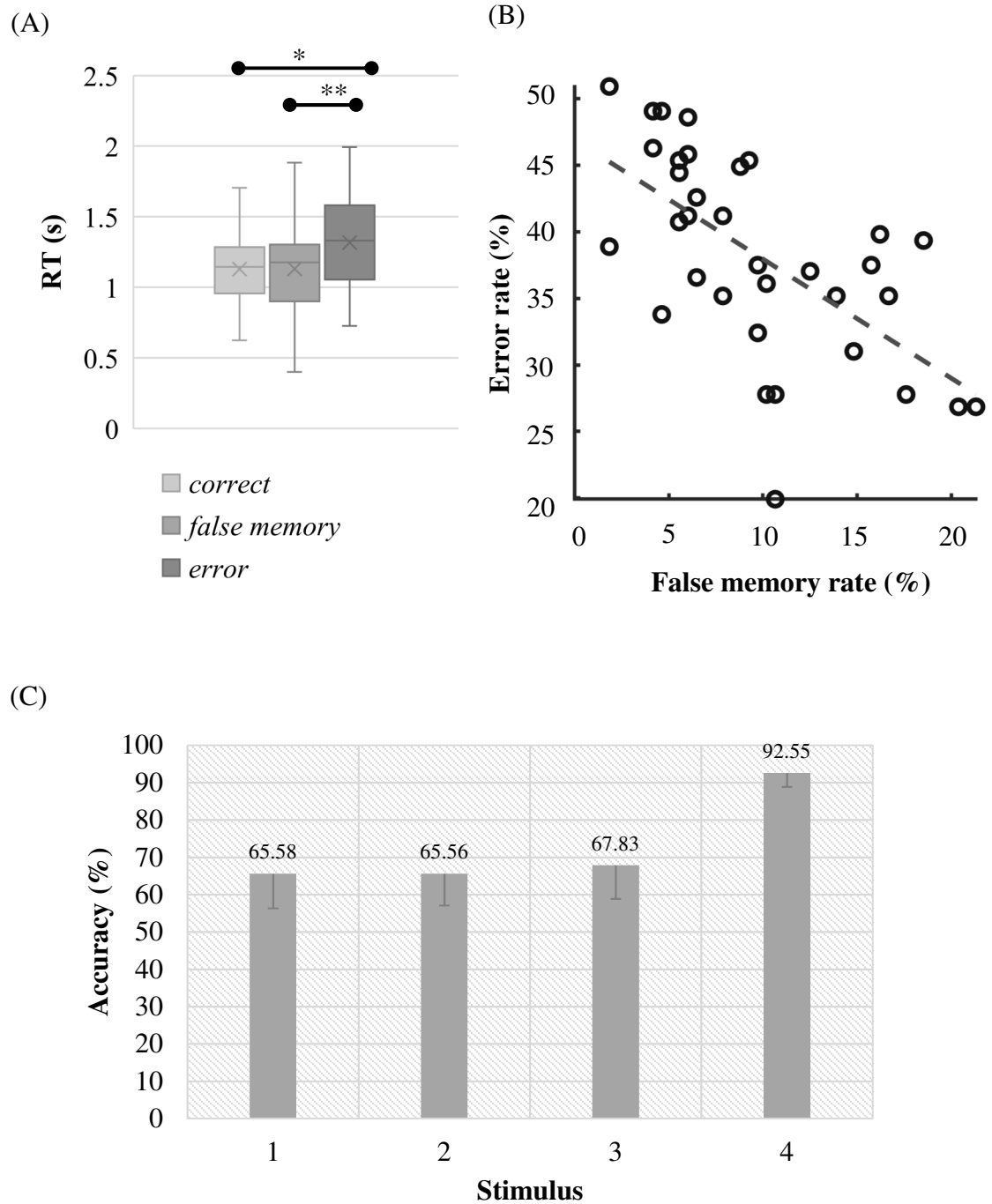


Figure 21: **(A)** Boxplot for the median (IQR) response time (RT) for *correct*, *false memory* and *error* conditions were 1.145 (0.957 to 1.285) s, 1.176 (0.900 to 1.302) s and 1.330 (1.055 to 1.581) s, respectively. *Correct* and *false memory* conditions recorded significantly faster RT when compared to the *error* condition (* $p = 0.0000006$, ** $p = 0.000175$). **(B)** *False memory* and *error* rates correlated negatively (Spearman's $\rho = -0.69$, $p = 0.000027$). Participants who made more errors had lower *false memory* rate. **(C)** Average accuracy rate and standard deviation as a function of serial position. When probed, the fourth stimulus in the series was recognized with significantly higher accuracy ($p < 10^{-6}$) in comparison to the other elements in the sequence.

4.2. Oscillatory Analysis

The non-parametric statistical analysis was used to investigate the prominent theta power increase and alpha power decrease during the encoding of the stimuli (Figure 14). Furthermore, the conspicuous alpha-beta activity in parieto-occipital regions during the retention interval (Figure 15B) was assessed.

The cluster-based permutation test revealed a significant difference between *correct* and *error* conditions ($p_{(corrected)} = 0.0112$) in the encoding interval ([0.40, 0.60] s), with *error* eliciting higher theta power ([6, 8] Hz) in all three occipital channels (Figure 22A, B, C). When trials from *false memory* and *correct* were grouped together and compared with *error*, a significant difference was still identified for [6, 8] Hz and [0.40, 0.55] s ($p_{(corrected)} = 0.0200$), with *error* showing higher theta activity (Figure 22D). Inversely, no significant cluster was found when trials from *false memory* were added to the *error* condition and differences with *correct* were reassessed.

Following the frequency shift for aligning the subjects' ICF, the analysis within the retention interval showed that the reported alpha-beta activity over right parieto-occipital channels was significantly higher than the activity over the contralateral channels (Figure 15B), $t(27) = 4.69$, $p < 0.0001$, $r = 0.67$ (Figure 23). Furthermore, the analysis revealed a significant difference between *correct* and *error* conditions ($p_{(corrected)} = 0.0203$), with *error* showing higher power values than those for *correct* in O2 (at the ICF, [1.50, 1.75] s) and P4 (at the ICF, [1.70, 1.80] s; Figure 24A, B, C). The addition of trials from *false memory* to the *error* condition produced, contrary to the encoding interval, a significant cluster ($p_{(corrected)} = 0.0393$), when compared to *correct*, in O2 (at the ICF, [1.55, 1.90] s) and P4 (at the ICF, [1.75, 1.80] s; Figure 24D). However, no significant difference was found out when trials from *false memory* and *correct* were merged and compared with *error*.

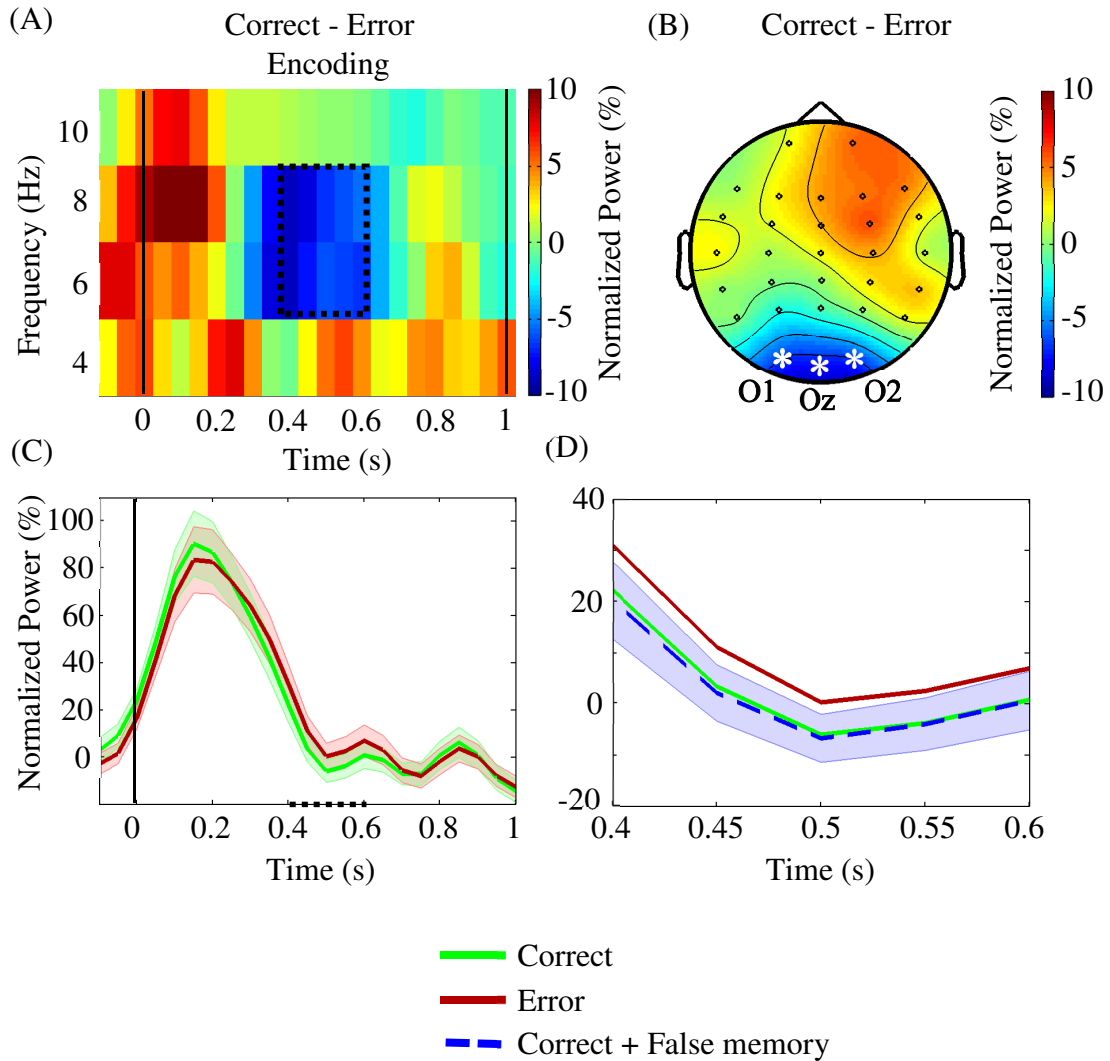


Figure 22: The statistical study of the encoding interval for the conditions *correct* and *error* revealed a significant difference ($p_{(corrected)} = 0.0112$) in the upper theta frequencies (6 – 8 Hz) within [0.40, 0.60] s. The analysis focused on the occipital channels O1, Oz and O2. **(A)** Time-frequency plot of the difference in power between the conditions averaged across the occipital channels. The area enclosed by the dotted line indicates the significant cluster. **(B)** The topographic contrast between the conditions within the cluster (asterisks and labels denote the channels showing significant differences). **(C)** Variation of upper theta power (and standard error), during encoding, averaged over the occipital channels. Within the cluster (dotted line on the x-axis), *error* power values were significantly higher than *correct* ones. **(D)** Variation of upper theta power (and standard error) within the cluster: When *false memory* trials were added to the *correct* condition, a significant difference was still observed on the channels O1, Oz and O2 ($p_{(corrected)} = 0.0200$) at [6, 8] Hz within [0.40, 0.55] s – inversely, no significant cluster was observed when *false memory* trials were added to the *error* condition.

Investigation of the relationships between behavioral and oscillatory properties revealed a positive correlation between average ICF power (estimated within the significant cluster of the retention interval) and mean RT (Figure 25, Spearman's $\rho = 0.60$, $p = 0.002$; three subjects were excluded as their parameters fell out of the 95 % confidence interval).

Concerning the gamma band investigation, neither the encoding nor the retention analyses revealed significant differences over the investigated temporal locations.

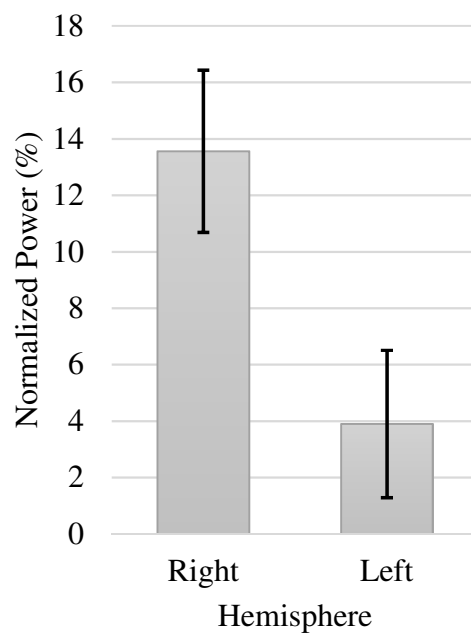


Figure 23: The analysis of the alpha-beta pattern during the second half of the retention interval revealed a significant lateralization – $t(27) = 4.69$, $p < 0.0001$, $r = 0.67$ – with power values for the frequency range [ICF – 2, ICF + 2] Hz over right parieto-occipital channels (P4, P8, O2) that were higher than the ones observed in the contralateral channels (P3, P7, O1).

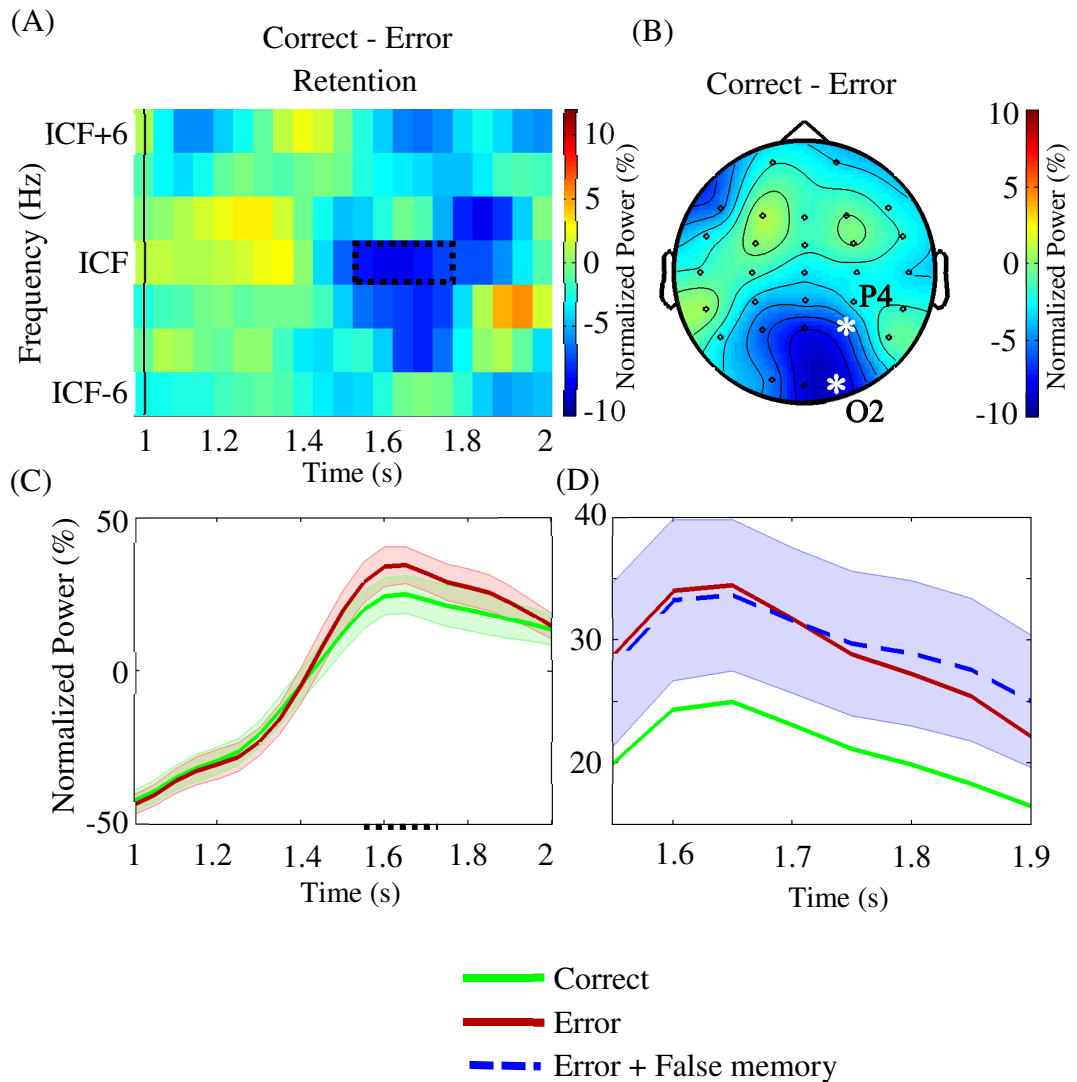


Figure 24: The analysis of the retention interval investigated differences between *correct* and *error* conditions in the right parieto-occipital channels (P4, P8, O2) considering the subjects' individual central frequencies (ICFs). A significant cluster ($p_{(corrected)} = 0.0203$) was found for the ICF in O2 (at [1.50, 1.75] s) and P4 (at [1.70, 1.80] s). **(A)** Time-frequency portrait of the difference between the conditions for the representative channel O2. The region enclosed by the dotted line highlights the significant cluster. **(B)** Topographic pattern of the difference between the conditions within the discovered cluster (asterisks and labels denote the channels showing the significant difference). **(C)** Variation of ICF power (and standard error) within the retention interval for the representative channel O2. Inside the significant region (dotted line on the x-axis), *error* power values were higher when compared to the *correct* ones. **(D)** Variation of ICF power (and standard error) within the cluster for the representative channel O2: When *false memory* and *error* trials were merged, a significant difference ($p_{(corrected)} = 0.0393$) was still measured for the ICF in O2 (at [1.55, 1.90] s) and P4 (at [1.75, 1.80] s) – inversely, no significant cluster was observed when *false memory* trials were added to the *correct* condition.

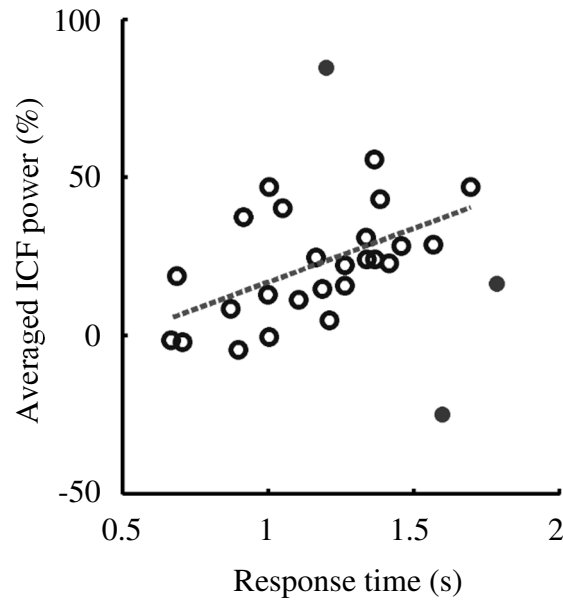


Figure 25: RT and ICF power showed a positive correlation (Spearman's $\rho = 0.60$, $p = 0.0020$). Participants with higher ICF power responded, on average, slower to the probes. Subjects included in the correlation analysis are denoted by empty circles. Outliers, highlighted with filled circles, were removed from the analysis as their values fell out of the 95 % confidence interval.

Preliminary results of the time-frequency investigation pertaining to the study of visual working memory errors were presented at the 1st Joint Turkish-German Symposium on Human Neuroscience in Berlin, “*Brain oscillatory analysis of gist-based short-term false memory for visual stimuli: a preliminary study*” (2014) and at OHBM in Hawaii, “*Alpha activity in the posterior regions distinguishes visual false memories and other memory errors*” (2015).

4.3. Connectivity Analysis

4.3.1. Coherency

The study of the coherency during the encoding interval considered O1 as seed channel. The investigation primarily focused on the connectivity between the seed channel and frontal regions (left, central, right). Significant levels of alpha phase synchrony were observed for many subjects (i.e., left, 25; right, 22; central, 18 out of 28), yet none of the regions yielded any significant difference (left, $p = 0.9271$; right, $p = 0.5449$; central, $p = 0.7859$) between conditions (Figure 26).

Similarly, the coherency measured within the beta band reached significant levels for most of the subjects (i.e., left, 27; right, 25; central, 21 out of 28) but once again no significant difference was detected when comparing the conditions (left, $p = 0.5283$; right, $p = 0.6796$; central, $p = 0.3130$) (Figure 27).

Only half of the subjects showed theta band coherency values that were higher than the confidence level (i.e., left, 14; right, 16; central, 14 out of 28): No significant differences were observed (Figure 28) when contrasting the studied conditions (left, $p = 0.6035$; right, $p = 0.4836$; central, $p = 0.8980$).

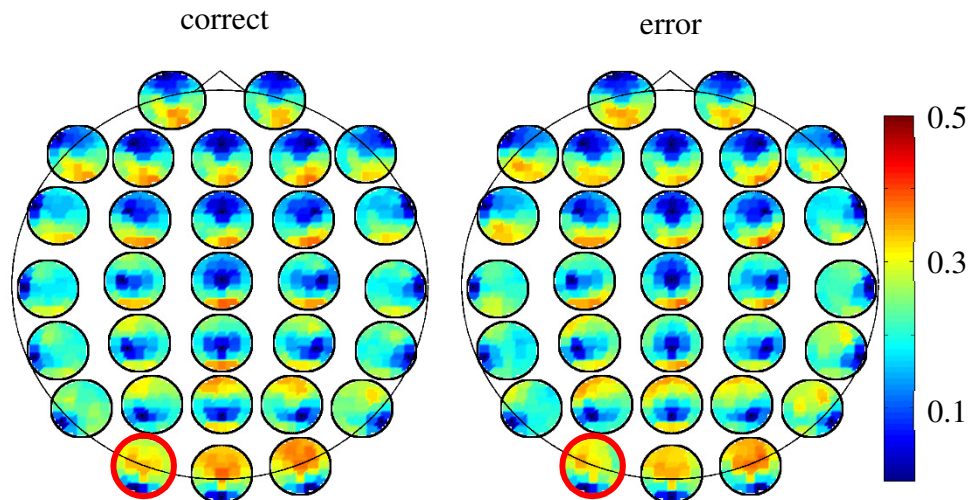


Figure 26: Squared imaginary coherency for the alpha band (8 – 12 Hz) during the encoding interval. The plots show the grand-averaged topographic maps of coherency (Nolte et al., 2004) for the condition *correct* (left) and *error* (right) considering in-turns all channels as seed channels. Highlighted by a red circle is the channel O1 which was selected a priori as seed channel for the subsequent statistical investigation (see Section 3.13.1). Coherency values were averaged within the entire alpha band. Values were normalized considering the maximum coherency level, independently from the condition, within the encoding interval for the alpha frequencies.

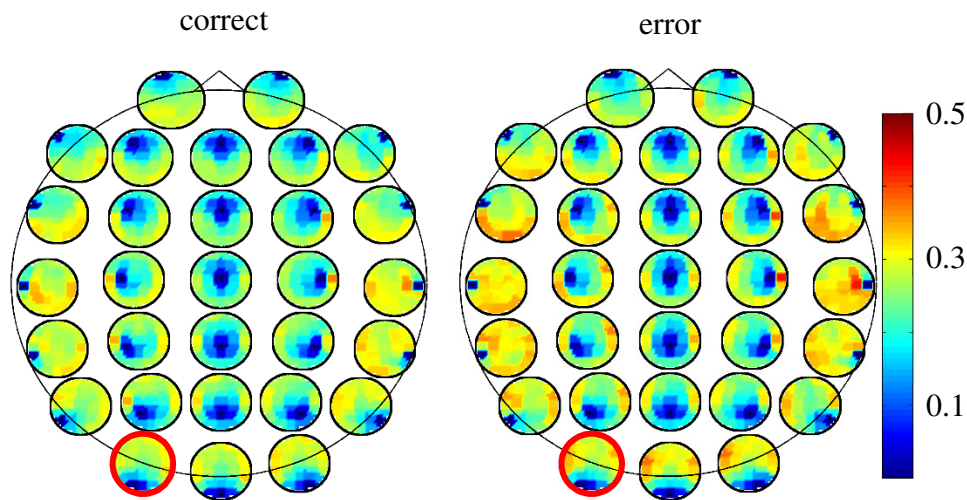


Figure 27: Squared imaginary coherency for the beta band (13 – 30 Hz) during the encoding interval. The plots show the grand-averaged topographic maps of coherency (Nolte et al., 2004) for the condition *correct* (left) and *error* (right) considering in-turns all channels as seed channels. Highlighted by a red circle is the channel O1 which was selected a priori as seed channel for the subsequent statistical investigation (see Section 3.13.1). Coherency values were averaged within the entire beta band. Values were normalized considering the maximum coherency level, independently from the condition, within the encoding interval for the beta frequencies.

Concerning the study of the coherency within the retention period, O2 was the seed channel chosen a priori. Significant levels of alpha phase synchrony were observed for most of the subjects (i.e., left, 27; right, 27; central, 27 out of 28), yet none of the regions yielded any significant difference (left, $p = 0.3931$; right, $p = 0.1280$; central, $p = 0.1785$) between conditions (Figure 29).

Regarding the beta coherency, values reached significant levels for the great majority of the subjects (i.e., left, 28; right, 28; central, 25 out of 28) but without showing significant difference among conditions (left, $p = 0.2359$; right, $p = 0.4544$; central, $p = 0.6521$) (Figure 30).

Finally, many subjects showed significant theta band coherency level (i.e., left, 26; right, 24; central, 15 out of 28) and no significant differences were reported (Figure 31) when contrasting the studied conditions (left, $p = 0.3699$; right, $p = 0.0849$; central, $p = 0.8524$). The investigation for differences of coherency estimates considering Oz as seed channel – observed to have the higher coherency levels, see Figure 29A and Figure 31A – didn't reveal any significant results. More specifically, for the alpha band: Left, $p = 0.6824$ (27 subjects); right, $p = 0.5780$ (28 subjects); central, $p = 0.8992$ (26 out of 28 subjects). Concerning the theta band: Left, $p = 0.9458$ (23 subjects); right, $p = 0.1923$ (28 subjects); central, $p = 0.4431$ (18 out of 28 subjects). Table 3 provides a detailed account of the statistical results pertaining to the coherency investigation.

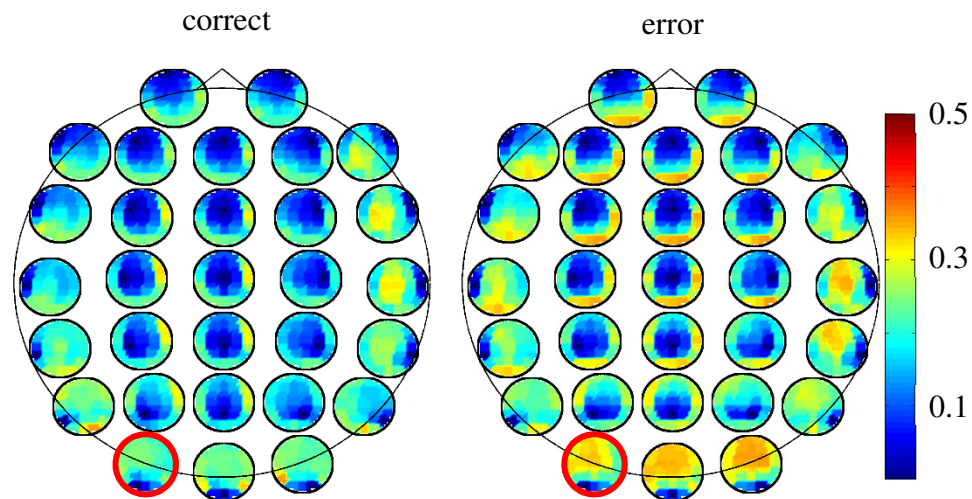


Figure 28: Squared imaginary coherency for the theta band (4 – 7 Hz) during the encoding interval. The plots show the grand-averaged topographic maps of coherency (Nolte et al., 2004) for the condition *correct* (left) and *error* (right) considering in-turns all channels as seed channels. Highlighted by a red circle is the channel O1 which was selected a priori as seed channel for the subsequent statistical investigation (see Section 3.13.1). Coherency values were averaged within the entire theta band. Values were normalized considering the maximum coherency level, independently from the condition, within the encoding interval for the theta frequencies.

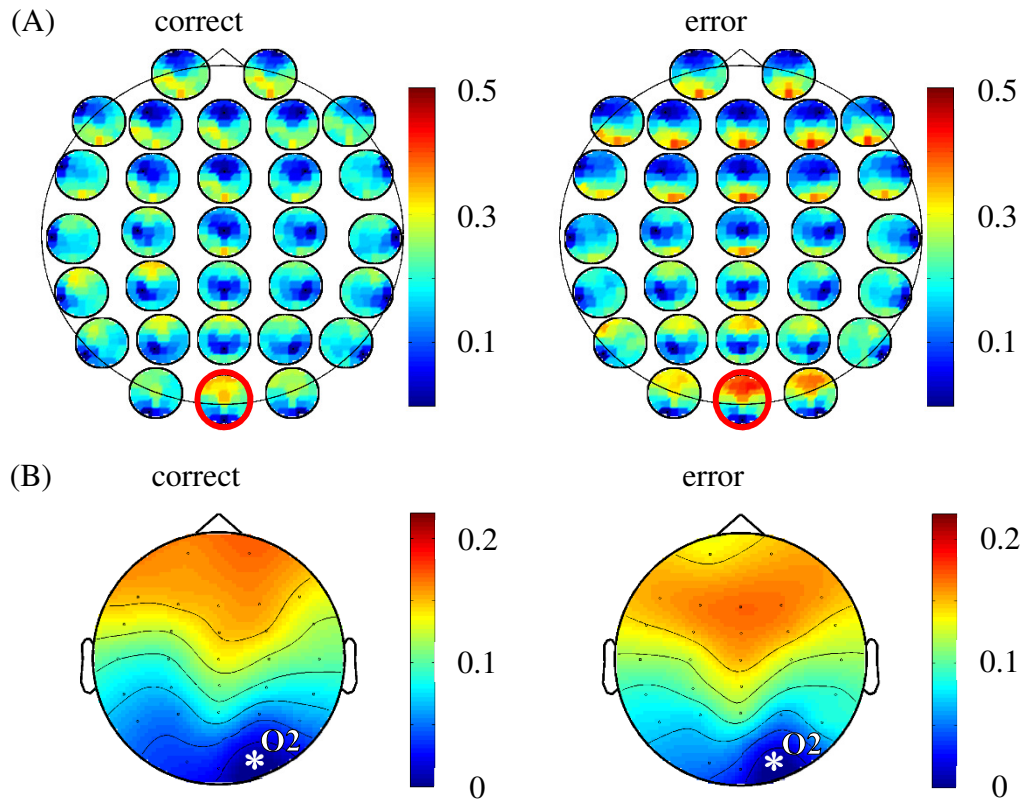


Figure 29: Squared imaginary coherency for the alpha band (8 – 12 Hz) during the retention interval. **(A)** Grand-averaged topographic maps of coherency (Nolte et al., 2004) for the condition *correct* (left) and *error* (right) considering in-turns all channels as seed channels. Coherency values are averaged within the entire alpha band. Values are normalized considering the maximum coherency level, independently from the condition, within the retention interval for the alpha frequencies. Highlighted by a red circle is the channel O2. **(B)** Grand-averaged topographic map of the squared imaginary coherency for *correct* and *error* conditions selecting O2 as seed channel. Please note that contrary to the plots (A), the averaging is performed considering only the alpha coherency peak and without normalization (identified on a subject basis, see also Figure 19).

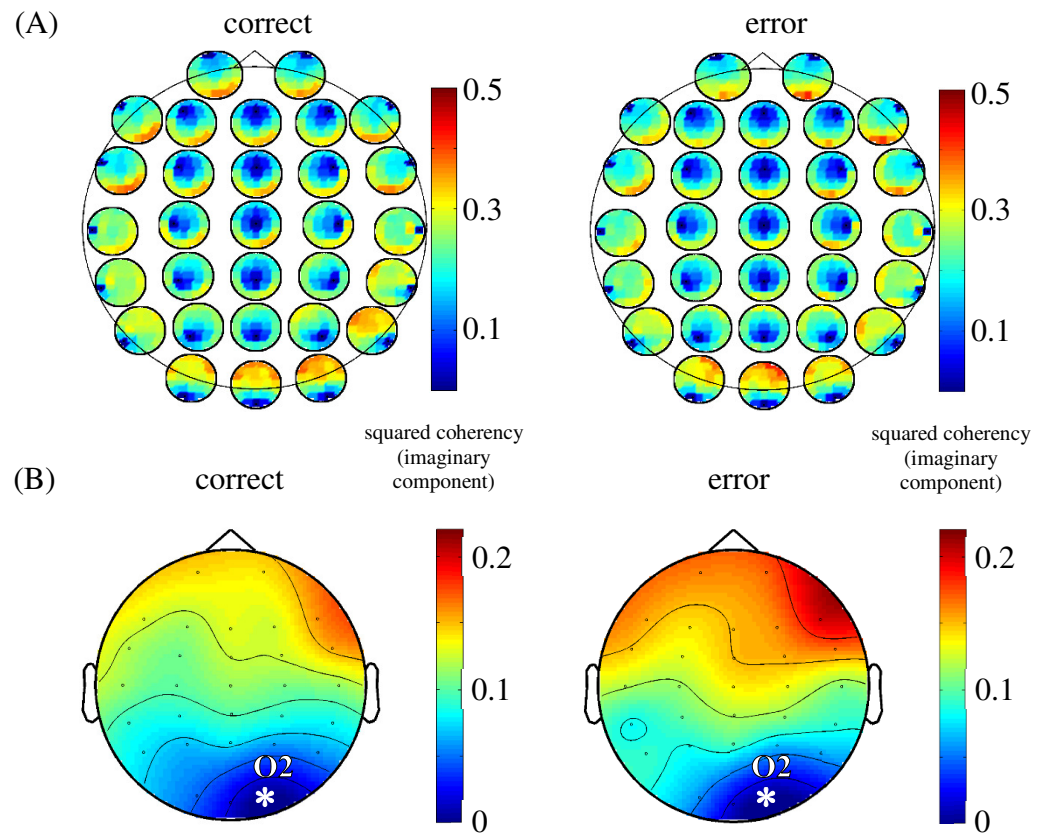


Figure 30: Squared imaginary coherency for the beta band (13 – 30 Hz) during the retention interval. **(A)** Grand-averaged topographic maps of coherency (Nolte et al., 2004) for the condition *correct* (left) and *error* (right) considering in-turns all channels as seed channels. Values are normalized considering the maximum coherency level, independently from the condition, within the retention interval for the beta frequencies. Coherency values are averaged within the entire beta band. **(B)** Grand-averaged topographic map of the squared imaginary coherency for *correct* and *error* conditions selecting O2 as seed channel. Please note that contrary to the plots (A), the averaging is performed considering only the beta coherency peak and without normalization (identified on a subject basis, see also Figure 19).

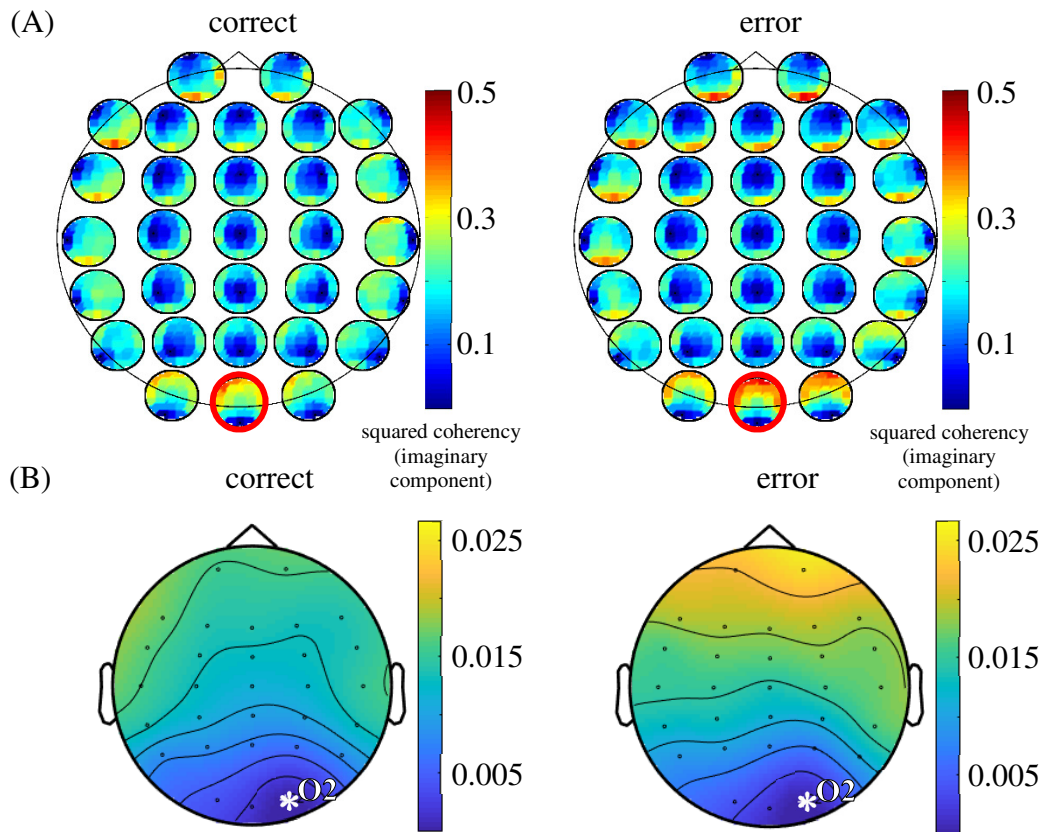


Figure 31: Squared imaginary coherence for the theta band (4 – 7 Hz) during the retention interval. **(A)** Grand-averaged topographic maps of coherence (Nolte et al., 2004) for the condition *correct* (left) and *error* (right) considering in-turns all channels as seed channels. Coherency values are averaged within the entire theta band. Values are normalized considering the maximum coherency level, independently from the condition, within the retention interval for the theta frequencies. Highlighted by a red circle is the channel Oz. **(B)** Grand-averaged topographic map of the squared imaginary coherence for *correct* and *error* conditions selecting O2 as seed channel. Differently from the plots (A), the averaging is done by taking only the theta coherency peak and without normalization (selected individually for each subject, see also Figure 19).

Table 3: Statistical results pertaining to the coherency investigation. Both encoding and retention intervals were probed. Mainly, the connectivity between the seed channels (O1 for encoding and O2 for retention) and frontal regions was investigated. In a follow-up analysis the connectivity between the seed channel Oz and frontal regions was also studied. The table reports all the p values obtained from the t -test analyses (Bonferroni corrected). In parenthesis, under the p value, the number of subjects (out of a maximum of 28) that showed significant connectivity levels and were therefore kept for the analysis of the specific frequency band and region.

	Encoding			Retention			seed
	<i>frontal left</i>	<i>frontal central</i>	<i>frontal right</i>	<i>frontal left</i>	<i>frontal central</i>	<i>frontal right</i>	
Alpha band (8 – 12 Hz)	$p = 0.9271$ (25)	$p = 0.7859$ (18)	$p = 0.5449$ (22)	$p = 0.3931$ (27)	$p = 0.1785$ (27)	$p = 0.1280$ (27)	O2
Beta band (13 – 30 Hz)	$p = 0.5283$ (27)	$p = 0.3130$ (21)	$p = 0.6796$ (25)	$p = 0.2359$ (28)	$p = 0.6521$ (25)	$p = 0.4544$ (28)	O2
Theta band (4 – 7 Hz)	$p = 0.6035$ (14)	$p = 0.4836$ (14)	$p = 0.8980$ (16)	$p = 0.3699$ (26)	$p = 0.8524$ (15)	$p = 0.0849$ (24)	O2
Alpha band (8 – 12 Hz)				$p = 0.6824$ (27)	$p = 0.8992$ (26)	$p = 0.5780$ (28)	Oz
Theta band (4 – 7 Hz)				$p = 0.9458$ (23)	$p = 0.4431$ (18)	$p = 0.1923$ (28)	Oz

Preliminary coherency results concerning the studied task were presented at the BIOMAG international conference in biomagnetism in Seoul, "Alpha and Theta Synchronization Between Occipital and Frontal Regions Distinguish Errors in a Visual Working Memory Task" (2016).

4.3.2. Phase-amplitude coupling

Significant theta (3 – 5 Hz) to lower gamma (30 – 60 Hz) PAC levels were observed, independently from the conditions, in fronto-parietal regions during the encoding of the stimuli and in fronto-occipital areas during the retention interval (Figure 32). Yet, the assessment of differences between *correct*, *error* and *false memory* did not highlight meaningful results. Additionally, a significant alpha (8 – 14 Hz) to upper gamma (60 – 120 Hz) PAC pattern was detected in both the encoding and retention intervals. More specifically, in occipital channels during the encoding of the stimuli and in fronto-occipital

areas during the retention interval (Figure 33). Ultimately, following statistical analyses, no significant differences were detected between conditions.

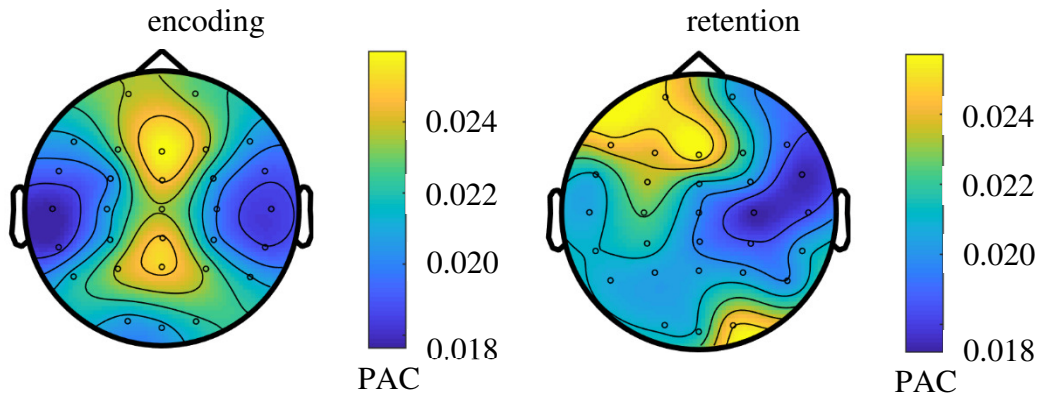


Figure 32: Theta (3 – 5 Hz) to lower gamma (30 – 60 Hz) PAC levels. Significant values were observed (independently from the conditions) yet, no significant difference was observed when comparing *correct*, *error* and *false memory* conditions.

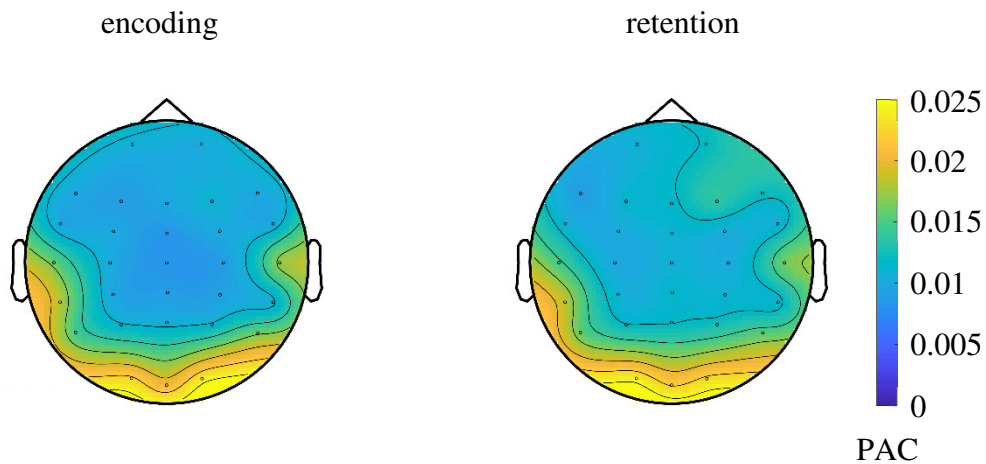


Figure 33: Alpha (8 – 14 Hz) to upper gamma (60 – 120 Hz) PAC levels. Significant values were observed (independently from the conditions) yet, no significant difference was observed when contrasting *correct*, *error* and *false memory* PAC levels. A significant difference was measured in O1 ($p_{(corrected)} = 0.0036$) with encoding showing higher alpha/gamma PAC when compared to the retention interval.

Finally, PAC estimates computed considering couples of channels (see Sections 2.8.5 and 3.13.2) did not reveal any significant difference between conditions. Notably, as its strength was reported to index encoding quality (Friese et al., 2013), no difference ($p > 0.5$) was found when considering the cross-frequency coupling between the phase of theta (5 – 8 Hz) in frontal regions and the amplitude of gamma (50 – 80 Hz) in posterior areas in both encoding (Figure 34) and retention (Figure 35) intervals.

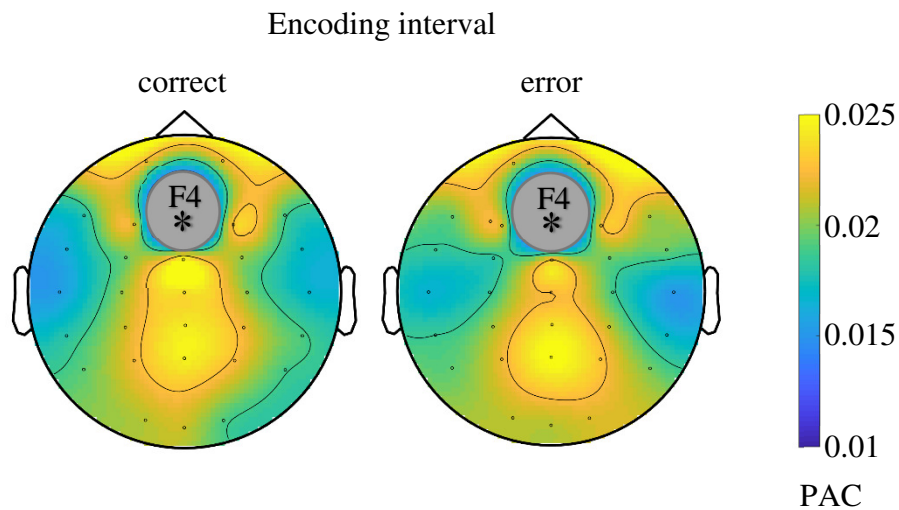


Figure 34: Cross-frequency coupling between the phase of theta (5 – 8 Hz) measured in F4 and the amplitude of gamma (50 – 80 Hz) measured on the remaining channels within the encoding interval. The grey area denotes lack of significant PAC. No significant difference was observed between conditions ($p > 0.5$).

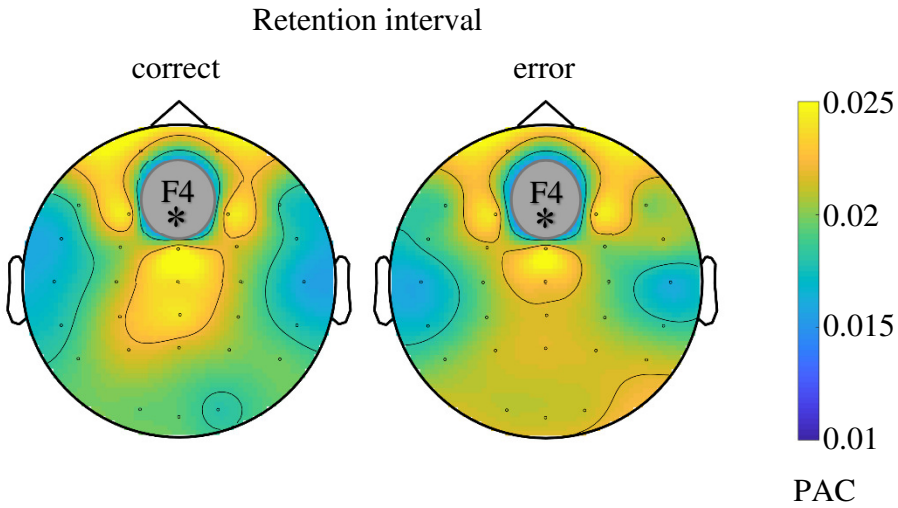


Figure 35: Cross-frequency coupling between the phase of theta (5 – 8 Hz) measured in F4 and the amplitude of gamma (50 – 80 Hz) measured on the remaining channels within the retention interval. The grey area denotes lack of significant PAC. No significant difference was observed between conditions ($p > 0.5$).

CHAPTER 5

DISCUSSION AND CONCLUSION

This study explored the role of cortical brain oscillations in memory by analyzing behavioral and EEG data of healthy volunteers performing a challenging VWM task. Specifically, we tested whether changes in oscillatory activity and connectivity measures during the encoding and retention of four images sequentially presented can predict the quality of memory formation.

We found that theta oscillations during encoding of successful memories exhibited power values in occipital channels that were significantly lower when compared to the incorrect ones. In the following retention interval, errors elicited alpha-beta (ICF) power values higher than those of correct answers in right parieto-occipital channels. Further, we investigated the oscillatory properties of false memory over short-term periods. Our analysis suggested pattern similarities in theta band during encoding between false and successful memories in occipital channels with power values that were lower than the error ones. Conversely, during the retention interval, *false memory* and *error* showed a similar alpha-beta band (ICF) pattern with power levels in right parieto-occipital channels that were higher than those of *correct* answers.

Investigation of the relationship between behavioral and oscillatory properties revealed a positive correlation between average ICF power (within the significant cluster of the retention interval) and mean RT. The behavioral analysis further revealed how RTs of the *error* condition were significantly longer than those of *correct* and *false memory*. The negative correlation between *false memory* and *error* rates revealed that subjects who performed poorly had lower rates of *false memory* responses.

The connectivity analysis revealed significant levels of coherency, as well as significant alpha/gamma PAC and theta/gamma PAC. Yet, these measures did not differ significantly between conditions.

5.1. Correct and Error

Our results showed an association between lower theta power values and successful encoding. For errors, a poor sequential encoding of the stimuli was reflected by higher

theta power values. Involvement of theta oscillations in WM tasks has been widely reported (e.g., Kahana et al., 2001; Jacobs & Kahana, 2010). The observed alpha power decrease accompanied by a simultaneous theta power increase was consistent with the pattern associated with intentional encoding (Mölle et al., 2002) and memory formation (Klimesch et al., 1997b; Osipova et al., 2006). Specifically, theta power increase in occipital channels may reflect the formation of cell assemblies. They are reported to be functionally related to processes such as feature binding and formation of memories (Singer & Gray, 1995; Bastiaansen & Hagoort, 2003; Buzsáki, 2010). Cognitive mechanisms during encoding and retrieval periods vary considerably with respect to the task specificity, hence altering the corresponding oscillatory processes responsible for proper memory formation (Hanslmayr & Staudigl, 2014). Various brain oscillatory studies linked successful memory performances to significant increases in theta band power during encoding (Sederberg et al., 2003; Osipova et al., 2006; White et al., 2013). In contrast, lower levels of theta power corresponding to successful memory formation were also observed depending on the brain region of interest and the time of encoding (Sederberg et al., 2006; Guderian et al., 2009; Burke et al., 2013). Moreover, subbands of theta activity may show opposite tendencies of power levels for correct encoding, i.e., higher power for slow theta ~ 3Hz and lower power for fast theta ~8 Hz (Lega et al., 2012). This is in line with our findings as the difference in theta activity was observed in the upper range (6 – 8 Hz) with lower power levels associated to successful memory performance.

In our task, the fast-paced presentation of detailed grayscale photos led to a challenge in encoding. VWM finite capacity (Miller, 1956; Cowan, 2001; Bays et al., 2011; Oberauer & Eichenberger, 2013) might not be enough to store all information characterizing each presented stimulus. Critically, the fast presentation of images may modify the cognitive strategy in the encoding process. Studies comparing individuals with different memory capacities found that poor performers had actually stored more information (Vogel et al., 2005; Zanto & Gazzaley, 2009; Gaspar et al., 2016). The performance of each subject is also not constant throughout the task and may vary influenced by many factors such as subject's expertise with the encoded category (Moore et al., 2006) relationship between the items (Davachi & Wagner, 2002), encoding conditions (e.g., pace of the presentation, Eng et al., 2005), presence of noise (Dean et al., 2008), distractors (Olivers et al., 2006) and subject's cognitive state (e.g., attention level, Prinzmetal et al., 1986). Thus, considering the context of our study, lower theta power associated with successful memories may be consequential of the encoding strategies that are possibly reflected in task-efficient feature binding during memory formation.

Oscillatory analysis revealed a further difference in the alpha-beta band during the retention interval where the *error* condition elicited higher power values than the *correct* one. The ICF (i.e., the frequency where the observed parieto-occipital pattern was more prominent) varied across subjects and therefore was determined individually. ICF values spread within the range of alpha and beta bands (10 Hz to 26 Hz). Alpha peak frequency in posterior regions has been shown to be subject-dependent and to increase with higher cognitive load (Haegens et al., 2014). The observed oscillatory activity in the retention

interval is in line with the alpha band inhibition-timing hypothesis (Klimesch et al., 2007). Accordingly, the alpha-beta band activity may reflect the suppression of the visual input via disengagement of the visual dorsal pathway (Vanni et al., 1997; Cooper et al., 2003; Tuladhar et al., 2007; Jokisch and Jensen, 2007; Scheeringa et al., 2009).

In our study, alpha-beta band activity was lateralized to the right parieto-occipital channels. Among studies reporting lateralization of alpha activity in the posterior regions, Bonnefond & Jensen (2012) showed the left-lateralized alpha power enabling the suppression of anticipated distractors (symbols or letters). Alpha oscillations were also found to be modulated by visual attention (Worden et al., 2000). More specifically, prior to the onset of the stimulus, alpha power increase was observed over the occipital regions, ipsilateral to the cued direction of attention, aiming to suppress irrelevant stimuli presented over a to-be-ignored location (Leenders et al., 2018). In a subsequent retention interval, an increase in alpha power contralateral to the irrelevant stimulus was related to WM maintenance processes responsible for suppressing the distractors. Both Jensen et al. (2002) and Scheeringa et al. (2009) reported a right lateralization in the alpha band range during the maintenance phase of a verbal WM task. These studies indicate the excitatory/inhibitory roles of alpha band. As our study used complex visual stimuli centrally located on the screen, the lateralization cannot be explained by shifts in visual attention or by factors concerning the spatial location of the stimuli.

The oscillatory power asymmetry taken with the inhibitory function of alpha band suggests an active role of the contralateral regions belonging to the left hemisphere during the retention interval in our study. Parra et al. (2014) reported the engagement of left posterior cortical areas during maintenance in VWM of multi-feature objects. They identified BOLD activity in the left fusiform gyrus (near the LOC) and left parietal cortex related to the maintenance of the binding of visual features. In a transcranial alternating current stimulation (tACS) study, Tseng et al. (2016) demonstrated the recruitment of similar regions of left temporal and parietal cortex, when binding of perceptual features is realized within VWM.

Higher levels of alpha-beta activity recorded for *error* may be indicative of an inefficient allocation of WM storage. This view is supported by the positive correlation of inhibitory alpha power and memory load reported during WM maintenance over task-irrelevant regions (Jensen et al., 2002; Tuladhar et al., 2007). The positive correlation between alpha-beta (ICF) power in retention and RTs further supports the idea that higher alpha activity values may reflect an inefficient WM performance. Similarly, a positive correlation between alpha power and RT in the retention interval was also reported by Roux et al. (2012).

We would like to note that the *error* condition includes also trials where either of the two target probes was recognized correctly. As a poor encoding sequence may include stimuli that were encoded properly, the oscillatory contrast between *correct* and *error* conditions likely weakens. However, this would not affect the character of the reported oscillatory markers distinguishing erroneously and correctly encoded trials in essence.

5.2. False Memory

As “memory is often accurate” (Slotnick & Schacter, 2004) by its nature, a lower rate is expected for false and erroneous memories compared to the correct responses. Inducing high rates of false memory responses is especially challenging for paradigms in STM. Some studies such as Atkins & Reuter-Lorenz (2011) and Melnik et al. (2017) have used strategies of extra distractors of math questions engaging cognitive faculties in order to increase false memory rates. But there was still no comparable number of trials with regard to correctly answered trials in those studies. Despite the cognitively demanding task involving fast-paced encoding and two different probes to be answered, an average false memory rate of $9.75 \pm 5.30\%$ could be obtained in our study.

Due to insufficient number of *false memory* trials, we were not able to make a direct statistical comparison with the other conditions. However, we assessed potential similarities of *false memory* with *correct* and/or *error* by adding in turn *false memory* trials to *correct* (contrasted with *error*) and *error* (contrasted with *correct*) conditions. The balanced number of trials and the increased SNR for the conditions enabled us to perform meaningful comparisons.

Our analysis suggested similarities regarding the encoding pattern between false and successful memories. This observation upheld the idea that proper encoding is a prerequisite for associative false memories. The negative correlation between *error* and *false memory* rates is further in line with the idea that even over short-term periods, false memories may be a byproduct of adaptive processes allowing an efficient functioning of the human memory system (Schacter et al., 2011).

While false memories shared similar oscillatory characteristics with successful memories during encoding, they had similar tendencies with *error* responses within the retention interval. That is, common errors and false memories both showed higher alpha-beta power when compared to *correct* answers. Whereas higher power for errors indicates an inefficient use of WM storage, this may not be so for false memories. Considering the finding that posterior alpha power increases with WM load during retention (Jensen et al., 2002; Tuladhar et al., 2007), it possibly reflects extra load caused by pre-existing semantic associations (Koutstaal et al., 2003) and/or prototypical perceptual features (Gutchess & Schacter, 2012) elicited by the encoded stimuli.

Please note that, the scope of our task comprised all encoded items within the same category. Different category items would modify the encoding mechanism altogether, which would increase the variability between the conditions. Moreover, that would likely lead to insufficient number of erroneous trials to be compared in oscillatory analysis as unrelated probe items are notoriously recognized with much higher rates. A series of studies assessed the effect of relatedness on STM and showed that rates of false recognitions for related lures were significantly higher than those of unrelated ones (e.g., Coane et al., 2007; Atkins and Reuter-Lorenz, 2008; Flegal et al., 2010; Iidaka et al., 2014; Melnik et al., 2017).

5.3. Connectivity

5.3.1. Coherency

The studied task revealed significant theta and alpha coherency between occipital channels and frontal areas. Within the retention interval subjects more consistently recorded significant levels of coherency (Table 3). As discussed in Section 3.13.1, the coherency measure is non-directional, thus it indicates the degree of synchrony between channels with no information pertaining to the leading source. Our observations are compatible with earlier studies suggesting that the phase synchronization of theta and alpha bands between different brain regions may reflect central executive functions of WM (Sauseng et al., 2005a; Klimesch et al., 2008). More specifically, a state of alpha equilibrium – reflected by increased phase synchronization – would enhance the communication between cortical areas (Klimesch et al., 2007). It has been proposed that synchronous theta phase coherence may reflect top-down mechanisms through which central executive areas exert control over task-relevant regions (Sauseng et al., 2004; Sauseng et al., 2010).

Compatible are also our observations concerning connectivity within the beta frequencies, as research highlighted the importance for WM of beta phase synchronization by showing strengthened coherence between frontal and parietal areas during WM maintenance (Babiloni et al., 2004). It has been hypothesized that beta phase synchronization reflects associations between local assemblies related to stimulus representations (Fell & Axmacher, 2011).

5.3.2. Phase-amplitude coupling

Significant values of theta (3 – 5 Hz) to gamma (30 – 60 Hz) PAC were observed throughout both encoding and retention intervals. Even though the strength of cross-frequency coupling could not index task performance, its presence remains consistent with previous studies that linked theta/gamma PAC to the retention in WM of sequentially encoded items (Canolty et al., 2006; Jacobs & Kahana, 2009; Fuentemilla et al., 2010; Lisman & Jensen, 2013).

A significant alpha (8 – 14 Hz) to gamma (60 – 120 Hz) PAC was measured throughout the task and higher levels were observed for the encoding interval, when compared to retention, that differed significantly for channel O1. The reported pattern is compatible with previous connectivity investigations where processing of visuo-spatial information was characterized by the strengthening of the cross-frequency coupling between alpha phase and gamma power in posterior areas (Voytek et al., 2010; Roux & Uhlhaas, 2014; Park et al., 2016).

These observations reinforce the idea that the interaction between slow and fast oscillations covers a relevant role in the coordination of information processing.

Theta/gamma PAC (for sequentially presented information) and alpha/gamma PAC (for spatially distributed information) may reflect distinct WM networks whose enrollment depends on WM content (Roux & Uhlhaas, 2014). Alternatively, with reference to the alpha-gamma coupling, it may induce a cortical state that facilitates visual encoding (Park et al., 2016).

5.4. Limitations and Future Research

When investigating the phenomenon of false memory, studies typically use well known lists where, for each entry, the relationships between items (lure included) are known (e.g., backward/forward associative strength of DRM lists). Our study used photographic stimuli from a wide range of categories. As no publicly available dataset satisfied our experimental requirements, we have built one specific to our task. The downside of this decision was the lack of associative or similarity measures describing the relationships between items, thus, for example, the lures were items chosen arbitrarily among the studied categories. Furthermore, as cognitive models are refined by using stimuli with specific characteristics, the complexity of our dataset made the results more difficult to be interpreted within the scope of perceptual and WM theories. It is also important to consider that the oscillatory analyses of our research were conducted at a channel level. The inability to map the observed results over precise brain locations further reduced our capacity to explain them within theoretical contexts.

Future research may want to adopt a different dataset to systematically manipulate perceptual features (e.g., color, shape, orientation) or semantic content of each item. The definition of associative or similarity measures would enable to investigate their relationship with oscillatory data. Finally, by modifying the recognition interval of our task, it would be possible to study oscillatory characteristics associated with the decision process following the presentation of the probes. All these changes may contribute to refine our findings pertaining to VWM errors and to clarify the relationship between EEG oscillatory activity and perceptual and semantic properties of the encoded stimuli.

5.5. Conclusions

In this study, we aimed to identify oscillatory markers distinguishing successful and erroneous visual memories and investigate oscillatory properties characterizing the phenomenon of false memory over short-term periods. We reported of a theta power increase in occipital channels that may reflect the formation of cell assemblies linked to feature binding or formation of memories. We demonstrated how theta power could index the quality of encoding. Our results suggested that the smaller theta power observed for correct responses correspond to an optimal encoding. On the contrary, the inefficient encoding of erroneous trials was accompanied with higher theta power values. False memories revealed a similar trend and contrasted with the pattern characterizing the other

memory errors. Thus, a proper encoding strategy may leave participants more vulnerable to false memories.

The inhibitory alpha-beta power observed in the retention interval was higher for erroneous memories suggesting that errors are characterized by an inefficient allocation of WM storage. On the other hand, higher alpha-beta power levels for false memories indicate the failure to manage the extra load induced by the encoded stimuli. The negative correlation between the rates of *error* and *false memory* further implies that the latter is an undesired outcome of adaptive processes responsible for the efficient functioning of memory.

REFERENCES

- Aggleton, J.P., Shaw, C., and Gaffan, E.A. (1992). The performance of postencephalitic amnesic subjects on two behavioural tests of memory: concurrent discrimination learning and delayed matching-to-sample. *Cortex*, 28, 359-372. doi: 10.1016/S0010-9452(13)80146-3
- Anllo-Vento, L., and Hillyard, S.A. (1996). Selective attention to the color and direction of moving stimuli: electrophysiological correlates of hierarchical feature selection. *Perception & psychophysics*, 58, 191-206. doi: 10.3758/BF03211875
- Atkins, A.S., and Reuter-Lorenz, P.A. (2008). False working memories? Semantic distortion in a mere 4 seconds. *Memory & Cognition*, 36, 74-81. doi: 10.3758/MC.36.1.74
- Atkins, A.S., and Reuter-Lorenz, P.A. (2011). Neural mechanisms of semantic interference and false recognition in short-term memory. *NeuroImage*, 56, 1726-1734. doi: 10.1016/j.neuroimage.2011.02.048
- Axmacher, N., Mormann, F., Fernández, G., Cohen, M.X., Elger, C.E., and Fell, J. (2007). Sustained neural activity patterns during working memory in the human medial temporal lobe. *Journal of Neuroscience*, 27, 7807-7816. doi: 10.1523/JNEUROSCI.0962-07.2007

- Axmacher, N., Henseler, M.M., Jensen, O., Weinreich, I., Elger, C.E., and Fell, J. (2010). Cross-frequency coupling supports multi-item working memory in the human hippocampus. *Proceedings of the National Academy of Sciences*, 107, 3228-3233. doi: 10.1073/pnas.0911531107
- Baars, B.J. (1997). In the theatre of consciousness. Global workspace theory, a rigorous scientific theory of consciousness. *Journal of Consciousness Studies*, 4, 292-309.
- Babiloni, C., Babiloni, F., Carducci, F., Cincotti, F., Vecchio, F., Cola, B., Rossi, S., Miniussi, C., and Rossini, P.M. (2004). Functional frontoparietal connectivity during short-term memory as revealed by high-resolution EEG coherence analysis. *Behavioral neuroscience*, 118, 687. doi: 10.1037/0735-7044.118.4.687
- Baddeley, A.D. (2003). Working memory: looking back and looking forward. *Nature reviews neuroscience*, 4, 829-839. doi: 10.1038/nrn1201
- Baddeley, A.D. (2012). Working Memory: Theories, Models, and Controversies. *Annual Review of Psychology*, 1-29. doi: 10.1146/annurev-psych-120710-100422
- Baddeley, A.D., and Hitch, G. (1974). Working Memory. In Bower G.H. (Ed), *Psychology of Learning and Motivation Vol. 8* (pp. 47-89). Academic Press. doi: 10.1016/S0079-7421(08)60452-1
- Baddeley, A.D., Eysenck, M. W., & Anderson, M. C. (2009). *Memory*. London: Psychology Press. doi: 10.4324/9781315749860
- Baioui, A., Ambach, W., Walter, B., and Vaitl, D. (2012). Psychophysiology of false memories in a Deese-Roediger-McDermott paradigm with visual scenes. *PloS one*, 7, e30416. doi: 10.1371/journal.pone.0030416
- Barnard, P.J. (1985). Interactive Cognitive Subsystems: A Psycholinguistic Approach to Short-Term Memory. *Progress in the Psychology of Language*, 197-258.
- Bartlett, F., and Kintsch, W. (1995). *Remembering: A Study in Experimental and Social Psychology*. Cambridge: Cambridge University Press. doi:10.1017/CBO9780511759185
- Bastiaansen, M., and Hagoort, P. (2003). Event-induced theta responses as a window on the dynamics of memory. *Cortex*, 39, 967-992. doi: 10.1016/S0010-9452(08)70873-6
- Bays, P.M., Wu, E.Y., and Husain, M. (2011). Storage and binding of object features in visual working memory. *Neuropsychologia*, 49, 1622-1631. doi: 10.1016/j.neuropsychologia.2010.12.023

- Beckett, K. (1996). Culture and the politics of signification: The case of child sexual abuse. *Social problems*, 43, 57-76. doi: 10.2307/3096894
- Bell, A.J., and Sejnowski, T.J. (1995). An information-maximization approach to blind separation and blind deconvolution. *Neural computation*, 7, 1129-1159. doi: 10.1162/neco.1995.7.6.1129
- Bell, A.H., Hadj-Bouziane, F., Frihauf, J.B., Tootell, R.B., and Ungerleider, L.G. (2009). Object representations in the temporal cortex of monkeys and humans as revealed by functional magnetic resonance imaging. *Journal of neurophysiology*, 101, 688-700. doi: 10.1152/jn.90657.2008
- Bettcher, B.M., Mungas, D., Patel, N., Eloffson, J., Dutt, S., Wynn, M., Watson, C.L., Stephens, M., Walsh, C.M., and Kramer, J.H. (2016). Neuroanatomical substrates of executive functions: Beyond prefrontal structures. *Neuropsychologia*, 85, 100-109. doi: 10.1016/j.neuropsychologia.2016.03.001
- Bonnefond, M., and Jensen, O. (2012). Alpha oscillations serve to protect working memory maintenance against anticipated distracters. *Current biology*, 22, 1969-1974. doi: 10.1016/j.cub.2012.08.029
- Brainard, D.H. (1997). The Psychophysics toolbox. *Spatial vision*, 10, 433-436. doi: 10.1163/156856897X00357
- Brainerd, C.J., and Reyna, V.F. (2002). Fuzzy-trace theory and false memory. *Current Directions in Psychological Science*, 11, 164-169. doi: 10.1111/1467-8721.00192
- Brainerd, C.J., and Reyna, V.F. (2005). The science of false memory. New York: Oxford University Press. doi: 10.1093/acprof:oso/9780195154054.001.0001
- Brass, M., Ullsperger, M., Knoesche, T.R., Von Cramon, D.Y., and Phillips, N.A. (2005). Who comes first? The role of the prefrontal and parietal cortex in cognitive control. *Journal of cognitive neuroscience*, 17, 1367-1375. doi: 10.1162/0898929054985400
- Broadbent, D.E. (1958). Perception and communication. Elmsford, NY, US: Pergamon Press. doi: 10.1037/10037-000
- Broadbent, D.E., Cooper, P.F., FitzGerald, P., and Parkes, K.R. (1982). The cognitive failures questionnaire (CFQ) and its correlates. *British journal of clinical psychology*, 21, 1-16. doi: 10.1111/j.2044-8260.1982.tb01421.x
- Bundesen, C. (1990). A theory of visual attention. *Psychological review*, 97, 523. doi: 10.1037/0033-295X.97.4.523

- Burke, J.F., Zaghoul, K.A., Jacobs, J., Williams, R.B., Sperling, M.R., Sharan, A.D., and Kahana, M.J. (2013). Synchronous and asynchronous theta and gamma activity during episodic memory formation. *Journal of Neuroscience*, 33, 292-304. doi: 10.1523/JNEUROSCI.2057-12.2013
- Buzsáki, G. (1996). The hippocampo-neocortical dialogue. *Cerebral cortex*, 6, 81-92. doi: 10.1093/cercor/6.2.81
- Buzsáki, G. (2010). Neural syntax: cell assemblies, synapsembles, and readers. *Neuron*, 68, 362-385. doi: 10.1016/j.neuron.2010.09.023
- Buzsáki, G., and Draguhn, A. (2004). Neuronal oscillations in cortical networks. *Science*, 304, 1926-1929. doi: 10.1126/science.1099745
- Buzsáki, G., and Wang, X.J. (2012). Mechanisms of gamma oscillations. *Annual review of neuroscience*, 35, 203-225. doi: 10.1146/annurev-neuro-062111-150444
- Canolty, R.T., Edwards, E., Dalal, S.S., Soltani, M., Nagarajan, S.S., Kirsch, H.E., Berger, M.S., Barbaro N.M., and Knight, R.T. (2006). High gamma power is phase-locked to theta oscillations in human neocortex. *Science*, 313, 1626-1628. doi: 10.1126/science.1128115
- Carpenter, P.A., Just, M.A., and Reichle, E.D. (2000). Working memory and executive function: Evidence from neuroimaging. *Current opinion in neurobiology*, 10, 195-199. doi: 10.1016/S0959-4388(00)00074-X
- Carrigan, N., and Barkus, E. (2016). A systematic review of cognitive failures in daily life: Healthy populations. *Neuroscience & Biobehavioral Reviews*, 63, 29-42. doi: 10.1016/j.neubiorev.2016.01.010
- Chen, H., Voss, J.L., and Guo, C. (2012). Event-related brain potentials that distinguish false memory for events that occurred only seconds in the past. *Behavioral and Brain Functions*, 8, 36. doi: 10.1186/1744-9081-8-36
- Coane, J.H., McBride, D.M., Raulerson III, B.A., and Jordan, J.S. (2007). False memory in a short-term memory task. *Experimental Psychology*, 54, 62-70. doi: 10.1027/1618-3169.54.1.62
- Cohen, D. (1968). Magnetoencephalography: evidence of magnetic fields produced by alpha-rhythm currents. *Science*, 161, 784-786. doi: 10.1126/science.161.3843.784
- Cohen, M.X. (2014). Analyzing neural time series data: theory and practice. Cambridge, MA: The MIT Press.

- Cohen, J.R., Sreenivasan, K.K., and D'Esposito, M. (2012). Correspondence between stimulus encoding-and maintenance-related neural processes underlies successful working memory. *Cerebral Cortex*, 24(3), 593-599. doi: 10.1093/cercor/bhs339
- Collins, A.M., and Loftus, E.F. (1975). A spreading-activation theory of semantic processing. *Psychological review*, 82, 407-428. doi: 10.1037/0033-295X.82.6.407
- Cooper, N.R., Croft, R.J., Dominey, S.J., Burgess, A.P., and Gruzelier, J.H. (2003). Paradox lost? Exploring the role of alpha oscillations during externally vs. internally directed attention and the implications for idling and inhibition hypotheses. *International Journal of Psychophysiology*, 47, 65-74. doi: 10.1016/S0167-8760(02)00107-1
- Cowan, N. (1999). An Embedded-Processes Model of Working Memory. In Miyake, A. and Shah, P. (Eds.), *Models of Working Memory: Mechanisms of Active Maintenance and Executive Control* (pp. 62-101). Cambridge: Cambridge University Press. doi: 10.1017/CBO9781139174909.006
- Cowan, N. (2001). The magical number 4 in short-term memory: A reconsideration of mental storage capacity. *Behavioral and brain sciences*, 24, 87-185. doi: 10.1017/S0140525X01003922
- Creem, S. H., & Proffitt, D. R. (2001). Defining the cortical visual systems:“what”,“where”, and “how”. *Acta psychologica*, 107(1-3), 43-68. doi: 10.1016/S0001-6918(01)00021-X
- Crone, N.E., Boatman, D., Gordon, B., and Hao, L. (2001). Induced electrocorticographic gamma activity during auditory perception. *Clinical neurophysiology*, 112, 565-582. doi: 10.1016/S1388-2457(00)00545-9
- Davachi, L., and Wagner, A.D. (2002). Hippocampal contributions to episodic encoding: insights from relational and item-based learning. *Journal of neurophysiology*, 88, 982-990. doi: 10.1152/jn.2002.88.2.982
- De Valois, R.L. (1960). Color vision mechanisms in the monkey. *The Journal of general physiology*, 43, 115. doi: 10.1085/jgp.43.6.115
- Dean, G. M., Dewhurst, S. A., and Whittaker, A. (2008). Dynamic visual noise interferes with storage in visual working memory. *Experimental psychology*, 55, 283-289. doi: 10.1027/1618-3169.55.4.283
- Deese, J. (1959). On the prediction of occurrence of particular verbal intrusions in immediate recall. *Journal of experimental psychology*, 58, 17-22. doi: 10.1037/h0046671

- Demiralp, T., Bayraktaroglu, Z., Lenz, D., Junge, S., Busch, N.A., Maess, B., Ergen, M., and Herrmann, C.S. (2007). Gamma amplitudes are coupled to theta phase in human EEG during visual perception. *International journal of psychophysiology*, 64, 24-30. doi: 10.1016/j.ijpsycho.2006.07.005
- DePrince, A.P., Allard, C.B., Oh, H., and Freyd, J.J. (2004). What's in a name for memory errors? Implications and ethical issues arising from the use of the term "false memory" for errors in memory for details. *Ethics & Behavior*, 14, 201-233. doi: 10.1207/s15327019eb1403_1
- Desimone, R., and Duncan, J. (1995). Neural mechanisms of selective visual attention. *Annual review of neuroscience*, 18, 193-222. doi: 10.1146/annurev.ne.18.030195.001205
- Deutsch, J.A., and Deutsch, D. (1963). Attention: Some theoretical considerations. *Psychological review*, 70, 80. doi: 10.1037/h0039515
- Eichenbaum, H. (2004). Hippocampus: cognitive processes and neural representations that underlie declarative memory. *Neuron*, 44, 109-120. doi: 10.1016/j.neuron.2004.08.028
- Eng, H.Y., Chen, D., and Jiang, Y. (2005). Visual working memory for simple and complex visual stimuli. *Psychonomic bulletin & review*, 12, 1127-1133. doi: 10.3758/BF03206454
- Engel, A.K., and Fries, P. (2010). Beta-band oscillations — signalling the status quo? *Current opinion in neurobiology*, 20, 156-165. doi: 10.1016/j.conb.2010.02.015
- Engle, R.W., and Kane, M.J. (2004). Executive Attention, Working Memory Capacity, and a Two-Factor Theory of Cognitive Control. *Psychology of Learning and Motivation*, 145-200. doi: 10.1016/S0079-7421(03)44005-X
- Eriksson, J., Vogel, E.K., Lansner, A., Bergström, F., and Nyberg, L. (2015). Neurocognitive architecture of working memory. *Neuron*, 88, 33-46. doi: 10.1016/j.neuron.2015.09.020
- Federmeier, K.D., and Kutas, M. (2002). Picture the difference: Electrophysiological investigations of picture processing in the two cerebral hemispheres. *Neuropsychologia*, 40, 730-747. doi: 10.1016/S0028-3932(01)00193-2
- Fell, J., and Axmacher, N. (2011). The role of phase synchronization in memory processes. *Nature reviews neuroscience*, 12, 105. doi: 10.1038/nrn2979
- Fernández, T., Harmony, T., Rodríguez, M., Bernal, J., Silva, J., Reyes, A., and Marosi, E. (1995). EEG activation patterns during the performance of tasks involving

- different components of mental calculation. *Electroencephalography and clinical Neurophysiology*, 94, 175-182. doi: 10.1016/0013-4694(94)00262-J
- Fernández, T., Harmony, T., Mendoza, O., López-Alanís, P., Marroquín, J. L., Otero, G., and Ricardo-Garcell, J. (2012). Event-related EEG oscillations to semantically unrelated words in normal and learning disabled children. *Brain and cognition*, 80, 74-82. doi: 10.1016/j.bandc.2012.04.008
- Flegal, K.E., Atkins, A.S., and Reuter-Lorenz, P.A. (2010). False memories seconds later: The rapid and compelling onset of illusory recognition. *Journal of Experimental Psychology: Learning, Memory, and Cognition*, 36, 1331. doi: 10.1037/a0019903
- Flegal, K.E., and Reuter-Lorenz, P.A. (2014). Get the gist? The effects of processing depth on false recognition in short-term and long-term memory. *Memory & cognition*, 42, 701-711. doi: 10.3758/s13421-013-0391-9
- Florian, G., and Pfurtscheller, G. (1995). Dynamic spectral analysis of event-related EEG data. *Electroencephalography and clinical neurophysiology*, 95, 393-396. doi: 10.1016/0013-4694(95)00198-8
- Foxe, J.J., and Snyder, A.C. (2011). The role of alpha-band brain oscillations as a sensory suppression mechanism during selective attention. *Frontiers in psychology*, 2, 154. doi: 10.3389/fpsyg.2011.00154
- Freunberger, R., Klimesch, W., Doppelmayr, M., and Höller, Y. (2007). Visual P2 component is related to theta phase-locking. *Neuroscience letters*, 426, 181-186. doi: 10.1016/j.neulet.2007.08.062
- Friedenberg, J. (2013). *Visual Attention and Consciousness*. New York: Psychology Press. doi: 10.4324/9780203073858
- Fries, P., Reynolds, J.H., Rorie, A.E., and Desimone, R. (2001). Modulation of oscillatory neuronal synchronization by selective visual attention. *Science*, 291, 1560-1563. doi: 10.1126/science.1055465
- Friese, U., Köster, M., Hassler, U., Martens, U., Trujillo-Barreto, N., and Gruber, T. (2013). Successful memory encoding is associated with increased cross-frequency coupling between frontal theta and posterior gamma oscillations in human scalp-recorded EEG. *Neuroimage*, 66, 642-647. doi: 10.1016/j.neuroimage.2012.11.002
- Fuentemilla, L., Penny, W.D., Cashdollar, N., Bunzeck, N., and Düzel, E. (2010). Theta-coupled periodic replay in working memory. *Current Biology*, 20, 606-612. doi: 10.1016/j.cub.2010.01.057
- Gaspar, J.M., Christie, G.J., Prime, D.J., Jolicœur, P., and McDonald, J.J. (2016). Inability to suppress salient distractors predicts low visual working memory capacity.

- Proceedings of the National Academy of Sciences*, 113, 3693-3698. doi: 10.1073/pnas.1523471113
- Gazzaley, A., and Nobre, A.C. (2012). Top-down modulation: Bridging selective attention and working memory. *Trends in cognitive sciences*, 16, 129-135. doi: 10.1016/j.tics.2011.11.014
- Gevins, A., Smith, M.E., McEvoy, L., and Yu, D. (1997). High-resolution EEG mapping of cortical activation related to working memory: effects of task difficulty, type of processing, and practice. *Cerebral cortex*, 7, 374-385. doi: 10.1093/cercor/7.4.374
- Gibson, J.J. (1950). *The Perception of the Visual World*. Oxford, England: Houghton Mifflin. doi: 10.2307/1419017
- Gibson, J.J. (2015). *The Ecological Approach to Visual Perception*. New York: Psychology Press. doi: 10.4324/9781315740218
- Goldman, R.I., Stern, J.M., Engel Jr, J., and Cohen, M.S. (2002). Simultaneous EEG and fMRI of the alpha rhythm. *Neuroreport*, 13, 2487. doi: 10.1097/00001756-200212200-00022
- Grill-Spector, K., Kourtzi, Z., and Kanwisher, N. (2001). The lateral occipital complex and its role in object recognition. *Vision research*, 41, 1409-1422. doi: 10.1016/S0042-6989(01)00073-6
- Gross, J. (2014). Analytical methods and experimental approaches for electrophysiological studies of brain oscillations. *Journal of neuroscience methods*, 228, 57-66. doi: 10.1016/j.jneumeth.2014.03.007
- Gross, J., Schmitz, F., Schnitzler, I., Kessler, K., Shapiro, K., Hommel, B., and Schnitzler, A. (2004). Modulation of long-range neural synchrony reflects temporal limitations of visual attention in humans. *Proceedings of the national Academy of Sciences*, 101, 13050-13055. doi: 10.1073/pnas.0404944101
- Gruber, T., Tsivilis, D., Montaldi, D., and Müller, M.M. (2004). Induced gamma band responses: an early marker of memory encoding and retrieval. *Neuroreport*, 15, 1837-1841. doi: 10.1097/01.wnr.0000137077.26010.12
- Guderian, S., Schott, B.H., Richardson-Klavehn, A., and Düzel, E. (2009). Medial temporal theta state before an event predicts episodic encoding success in humans. *Proceedings of the National Academy of Sciences*, 106, 5365-5370. doi: 10.1073/pnas.0900289106
- Gutchess, A.H., and Schacter, D.L. (2012). The neural correlates of gist-based true and false recognition. *Neuroimage*, 59, 3418-3426. doi: 10.1016/j.neuroimage.2011.11.078

- Haegens, S., Osipova, D., Oostenveld, R., and Jensen, O. (2010). Somatosensory working memory performance in humans depends on both engagement and disengagement of regions in a distributed network. *Human brain mapping*, 31, 26-35. doi: 10.1002/hbm.20842
- Haegens, S., Cousijn, H., Wallis, G., Harrison, P.J., and Nobre, A.C. (2014). Inter- and intra-individual variability in alpha peak frequency. *Neuroimage*, 92, 46-55. doi: 10.1016/j.neuroimage.2014.01.049
- Halliday, D.M., Rosenberg, J.R., Amjad, A.M., Breeze, P., Conway, B.A., and Farmer, S.F. (1995). A framework for the analysis of mixed time series/point process data—theory and application to the study of physiological tremor, single motor unit discharges and electromyograms. *Progress in biophysics and molecular biology*, 64, 237. doi: 10.1016/S0079-6107(96)00009-0
- Hämäläinen, M., Hari, R., Ilmoniemi, R.J., Knuutila, J., and Lounasmaa, O.V. (1993). Magnetoencephalography—theory, instrumentation, and applications to noninvasive studies of the working human brain. *Reviews of modern Physics*, 65, 413. doi: 10.1103/RevModPhys.65.413
- Hanslmayr, S., Aslan, A., Staudigl, T., Klimesch, W., Herrmann, C.S., and Bäuml, K.H. (2007). Prestimulus oscillations predict visual perception performance between and within subjects. *Neuroimage*, 37, 1465-1473. doi: 10.1016/j.neuroimage.2007.07.011
- Hanslmayr, S., Gross, J., Klimesch, W., and Shapiro, K.L. (2011). The role of alpha oscillations in temporal attention. *Brain research reviews*, 67, 331-343. doi: 10.1016/j.brainresrev.2011.04.002
- Hanslmayr, S., and Staudigl, T. (2014). How brain oscillations form memories — a processing based perspective on oscillatory subsequent memory effects. *Neuroimage*, 85, 648-655. doi: 10.1016/j.neuroimage.2013.05.121
- Harmony, T. (2013). The functional significance of delta oscillations in cognitive processing. *Frontiers in integrative neuroscience*, 7, 83. doi: 10.3389/fnint.2013.00083
- Harmony, T., Fernández, T., Silva, J., Bernal, J., Díaz-Comas, L., Reyes, A., Marosi, E., Rodríguez, Mario and Rodríguez, Miguel. (1996). EEG delta activity: an indicator of attention to internal processing during performance of mental tasks. *International journal of psychophysiology*, 24, 161-171. doi: 10.1016/S0167-8760(96)00053-0
- Harrison, S.A., and Tong, F. (2009). Decoding reveals the contents of visual working memory in early visual areas. *Nature*, 458, 632-635. doi: 10.1038/nature07832

- Herrmann, C.S., Munk, M.H., and Engel, A.K. (2004). Cognitive functions of gamma-band activity: memory match and utilization. *Trends in cognitive sciences*, 8, 347-355. doi: 10.1016/j.tics.2004.06.006
- Hipp, J.F., and Siegel, M. (2013). Dissociating neuronal gamma-band activity from cranial and ocular muscle activity in EEG. *Frontiers in human neuroscience*, 7, 338. doi: 10.3389/fnhum.2013.00338
- Howard, M.W., Rizzuto, D.S., Caplan, J.B., Madsen, J.R., Lisman, J., Aschenbrenner-Scheibe, R., Schulze-Bonhage, A., and Kahana, M.J. (2003). Gamma oscillations correlate with working memory load in humans. *Cerebral cortex*, 13, 1369-1374. doi: 10.1093/cercor/bhg084
- Hsieh, L.T., and Ranganath, C. (2014). Frontal midline theta oscillations during working memory maintenance and episodic encoding and retrieval. *Neuroimage*, 85, 721-729. doi: 10.1016/j.neuroimage.2013.08.003
- Hyvärinen, A. (1999). Fast and robust fixed-point algorithms for independent component analysis. *IEEE transactions on Neural Networks*, 10, 626-634. doi: 10.1109/72.761722
- Hyvärinen, A., and Oja, E. (2000). Independent component analysis: algorithms and applications. *Neural networks*, 13, 411-430. doi: 10.1016/S0893-6080(00)00026-5
- Iidaka, T., Harada, T., and Sadato, N. (2014). False memory for face in short-term memory and neural activity in human amygdala. *Brain research*, 1591, 74-85. doi: 10.1016/j.brainres.2014.10.003
- Israel, L., and Schacter, D.L. (1997). Pictorial encoding reduces false recognition of semantic associates. *Psychonomic Bulletin & Review*, 4, 577-581. doi: 10.3758/BF03214352
- Jacobs, J., and Kahana, M.J. (2009). Neural representations of individual stimuli in humans revealed by gamma-band electrocorticographic activity. *Journal of Neuroscience*, 29, 10203-10214. doi: 10.1523/JNEUROSCI.2187-09.2009
- Jacobs, J., and Kahana, M.J. (2010). Direct brain recordings fuel advances in cognitive electrophysiology. *Trends in cognitive sciences*, 14, 162-171. doi: 10.1016/j.tics.2010.01.005
- Jensen, O., Gelfand, J., Kounios, J., and Lisman, J.E. (2002). Oscillations in the alpha band (9–12 Hz) increase with memory load during retention in a short-term memory task. *Cerebral cortex*, 12, 877-882. doi: 10.1093/cercor/12.8.877

- Jensen, O., and Tesche, C.D. (2002). Frontal theta activity in humans increases with memory load in a working memory task. *European journal of Neuroscience*, 15, 1395-1399. doi: 10.1046/j.1460-9568.2002.01975.x
- Jensen, O., Kaiser, J., and Lachaux, J.P. (2007). Human gamma-frequency oscillations associated with attention and memory. *Trends in neurosciences*, 30, 317-324. doi: 10.1016/j.tins.2007.05.001
- Jensen, O., and Mazaheri, A. (2010). Shaping functional architecture by oscillatory alpha activity: gating by inhibition. *Frontiers in human neuroscience*, 4, 186. doi: 10.3389/fnhum.2010.00186
- Jokisch, D., and Jensen, O. (2007). Modulation of gamma and alpha activity during a working memory task engaging the dorsal or ventral stream. *Journal of Neuroscience*, 27, 3244-3251. doi: 10.1523/JNEUROSCI.5399-06.2007
- Jones, T.C., Bartlett, J.C., and Wade, K.A. (2006). Nonverbal conjunction errors in recognition memory: Support for familiarity but not for feature bundling. *Journal of Memory and Language*, 55, 138-155. doi: 10.1016/j.jml.2006.01.002
- Jonides, J., Lewis, R.L., Nee, D.E., Lustig, C.A., Berman, M.G., and Moore, K.S. (2008). The Mind and Brain of Short-Term Memory. *Annual Review of Psychology*, 193-224. doi: 10.1146/annurev.psych.59.103006.093615
- Kahana, M.J., Seelig, D., and Madsen, J.R. (2001). Theta returns. *Current opinion in neurobiology*, 11, 739-744. doi: 10.1016/S0959-4388(01)00278-1
- Kastner, S., and Ungerleider, L.G. (2000). Mechanisms of visual attention in the human cortex. *Annual review of neuroscience*, 23, 315-341.
- Killebrew, K.W., Gurariy, G., Peacock, C.E., Berryhill, M.E., and Caplovitz, G. P. (2018). Electrophysiological correlates of encoding processes in a full-report visual working memory paradigm. *Cognitive, Affective, & Behavioral Neuroscience*, 18, 353-365. doi: 10.3758/s13415-018-0574-8
- Klimesch, W. (1996). Memory processes, brain oscillations and EEG synchronization. *International journal of psychophysiology*, 24, 61-100. doi: 10.1016/S0167-8760(96)00057-8
- Klimesch, W. (1997). EEG-alpha rhythms and memory processes. *International Journal of psychophysiology*, 26, 319-340. doi: 10.1016/S0167-8760(97)00773-3
- Klimesch, W. (1999). EEG alpha and theta oscillations reflect cognitive and memory performance: A review and analysis. *Brain research reviews*, 29, 169-195. doi: 10.1016/S0165-0173(98)00056-3

- Klimesch, W. (2000). Theta frequency, synchronization and episodic memory performance. In Miller, R. (Ed.), *Time and the Brain* Vol. 3 (pp. 262-279). Singapore: Harwood Academic Publishers. doi: 10.4324/9780203304570_chapter_8
- Klimesch, W., Doppelmayr, M., Pachinger, T., and Ripper, B. (1997a). Brain oscillations and human memory: EEG correlates in the upper alpha and theta band. *Neuroscience letters*, 238, 9-12. doi: 10.1016/S0304-3940(97)00771-4
- Klimesch, W., Doppelmayr, M., Schimke, H., and Ripper, B. (1997b). Theta synchronization and alpha desynchronization in a memory task. *Psychophysiology*, 34, 169-176. doi: 10.1111/j.1469-8986.1997.tb02128.x
- Klimesch, W., Russegger, H., Doppelmayr, M., and Pachinger, T. (1998). A method for the calculation of induced band power: implications for the significance of brain oscillations. *Electroencephalography and Clinical Neurophysiology/Evoked Potentials Section*, 108, 123-130. doi: 10.1016/S0168-5597(97)00078-6
- Klimesch, W., Sauseng, P., and Hanslmayr, S. (2007). EEG alpha oscillations: The inhibition–timing hypothesis. *Brain research reviews*, 53, 63-88. doi: 10.1016/j.brainresrev.2006.06.003
- Klimesch, W., Freunberger, R., Sauseng, P., and Gruber, W. (2008). A short review of slow phase synchronization and memory: evidence for control processes in different memory systems? *Brain research*, 1235, 31-44. doi: 10.1016/j.brainres.2008.06.049
- Klimesch, W., Fellinger, R., and Freunberger, R. (2011). Alpha oscillations and early stages of visual encoding. *Frontiers in psychology*, 2, 118. doi: 10.3389/fpsyg.2011.00118
- Kopell, N., Whittington, M.A., and Kramer, M.A. (2011). Neuronal assembly dynamics in the beta frequency range permits short-term memory. *Proceedings of the National Academy of Sciences*, 108, 3779-3784. doi: 10.1073/pnas.1019676108
- Kourtzi, Z., and Kanwisher, N. (2001). Representation of perceived object shape by the human lateral occipital complex. *Science*, 293, 1506-1509. doi: 10.1126/science.1061133
- Koutstaal, W., and Schacter, D.L. (1997). Gist-based false recognition of pictures in older and younger adults. *Journal of Memory and Language*, 37, 555-583. doi: 10.1006/jmla.1997.2529
- Koutstaal, W., Schacter, D.L., and Brenner, C. (2001). Dual task demands and gist-based false recognition of pictures in younger and older adults. *Journal of Memory and Language*, 44, 399-426. doi: 10.1006/jmla.2000.2734

- Koutstaal, W., Reddy, C., Jackson, E.M., Prince, S., Cendan, D.L., and Schacter, D.L. (2003). False recognition of abstract versus common objects in older and younger adults: Testing the semantic categorization account. *Journal of Experimental Psychology: Learning, Memory, and Cognition*, 29, 499. doi: 10.1037/0278-7393.29.4.499
- Kumaran, D., and Maguire, E.A. (2006). The dynamics of hippocampal activation during encoding of overlapping sequences. *Neuron*, 49, 617-629. doi: 10.1016/j.neuron.2005.12.024
- Lamme, V.A. (2003). Why visual attention and awareness are different. *Trends in cognitive sciences*, 7, 12-18. doi: 10.1016/S1364-6613(02)00013-X
- Lange, J., Oostenveld, R., and Fries, P. (2013). Reduced occipital alpha power indexes enhanced excitability rather than improved visual perception. *Journal of Neuroscience*, 33, 3212-3220. doi: 10.1523/JNEUROSCI.3755-12.2013
- Laufs, H., Kleinschmidt, A., Beyerle, A., Eger, E., Salek-Haddadi, A., Preibisch, C., and Krakow, K. (2003). EEG-correlated fMRI of human alpha activity. *Neuroimage*, 19, 1463-1476. doi: 10.1016/S1053-8119(03)00286-6
- Leenders, M.P., Lozano-Soldevilla, D., Roberts, M.J., Jensen, O., and De Weerd, P. (2018). Diminished alpha lateralization during working memory but not during attentional cueing in older adults. *Cerebral Cortex*, 28, 21-32. doi: 10.1093/cercor/bhw345
- Lefebvre, C.D., Marchand, Y., Eskes, G.A., and Connolly, J.F. (2005). Assessment of working memory abilities using an event-related brain potential (ERP)-compatible digit span backward task. *Clinical Neurophysiology*, 116, 1665-1680. doi: 10.1016/j.clinph.2005.03.015
- Lega, B.C., Jacobs, J., and Kahana, M. (2012). Human hippocampal theta oscillations and the formation of episodic memories. *Hippocampus*, 22, 748-761. doi: 10.1002/hipo.20937
- Linden, D.E., Bittner, R.A., Muckli, L., Waltz, J.A., Kriegeskorte, N., Goebel, R., Singer, W., and Munk, M.H. (2003). Cortical capacity constraints for visual working memory: Dissociation of fMRI load effects in a fronto-parietal network. *Neuroimage*, 20, 1518-1530. doi: 10.1016/j.neuroimage.2003.07.021
- Lisman, J. (2010). Working memory: the importance of theta and gamma oscillations. *Current Biology*, 20, R490-R492. doi: 10.1016/j.cub.2010.04.011
- Lisman, J.E., and Idiart, M.A. (1995). Storage of 7 plus/minus 2 short-term memories in oscillatory subcycles. *Science*, 267, 1512.

- Lisman, J.E., and Jensen, O. (2013). The theta-gamma neural code. *Neuron*, 77, 1002-1016. doi: 10.1016/j.neuron.2013.03.007
- Lopes da Silva, F.H. (2013). EEG and MEG: relevance to neuroscience. *Neuron*, 80, 1112-1128. doi: 10.1016/j.neuron.2013.10.017
- Luck, S.J. (2005). An introduction to the event-related potential technique. Cambridge, MA: The MIT Press.
- Luck, S.J., and Hillyard, S.A. (1994). Electrophysiological correlates of feature analysis during visual search. *Psychophysiology*, 31, 291-308. doi: 10.1111/j.1469-8986.1994.tb02218.x
- Luck, S.J., and Hollingworth, A. (2008). Visual Memory. New York: Oxford University Press. doi: 10.1093/acprof:oso/9780195305487.001.0001
- Makeig, S., Bell, A.J., Jung, T.P., and Sejnowski, T.J. (1996). Independent component analysis of electroencephalographic data. Touretzky, D.S., Mozer, M.C., and Hasselmo M.E. (Eds.), *Advances in Neural Information Processing Systems 8: Proceedings of the 1995 Conference Vol. 8* (pp. 145-151). Cambridge, MA: MIT Press.
- Mapelli, I., and Özkurt, T.E. (2019). Brain Oscillatory Correlates of Visual Short-Term Memory Errors. *Frontiers in Human Neuroscience*, 13, 33. doi: 10.3389/fnhum.2019.00033
- Maris, E., and Oostenveld, R. (2007). Nonparametric statistical testing of EEG-and MEG-data. *Journal of neuroscience methods*, 164, 177-190. doi: 10.1016/j.jneumeth.2007.03.024
- Maris E., van Vugt M., and Kahana M. (2011). Spatially distributed patterns of oscillatory coupling between high-frequency amplitudes and low-frequency phases in human iEEG. *Neuroimage*, 54, 836-850. doi: 10.1016/j.neuroimage.2010.09.029
- Marshall, L., and Born, J. (2007). The contribution of sleep to hippocampus-dependent memory consolidation. *Trends in cognitive sciences*, 11, 442-450. doi: 10.1016/j.tics.2007.09.001
- Mayer, J.S., Bittner, R.A., Nikolić, D., Bledowski, C., Goebel, R., and Linden, D.E. (2007). Common neural substrates for visual working memory and attention. *Neuroimage*, 36, 441-453. doi: 10.1016/j.neuroimage.2007.03.007
- Meador, K.J., Ray, P.G., Echaz, J.R., Loring, D.W., and Vachtsevanos, G.J. (2002). Gamma coherence and conscious perception. *Neurology*, 59, 847-854. doi: 10.1212/WNL.59.6.847

- Medendorp, W.P., Kramer, G.F., Jensen, O., Oostenveld, R., Schoffelen, J.M., and Fries, P. (2007). Oscillatory activity in human parietal and occipital cortex shows hemispheric lateralization and memory effects in a delayed double-step saccade task. *Cerebral cortex*, 17, 2364-2374. doi: 10.1093/cercor/bhl145
- Melnik, N., Mapelli, I., and Özkurt, T.E. (2017). Modulation of alpha oscillations is required for the suppression of semantic interference. *Neurobiology of Learning and Memory*, 144, 11-18. doi: j.nlm.2017.05.007
- Merker, B. (2013). Cortical gamma oscillations: the functional key is activation, not cognition. *Neuroscience & Biobehavioral Reviews*, 37, 401-417. doi: 10.1016/j.neubiorev.2013.01.013
- Michalareas, G., Vezoli, J., Van Pelt, S., Schoffelen, J.M., Kennedy, H., and Fries, P. (2016). Alpha-beta and gamma rhythms subserve feedback and feedforward influences among human visual cortical areas. *Neuron*, 89, 384-397. doi: 10.1016/j.neuron.2015.12.018
- Miller, G.A. (1956). The magical number seven, plus or minus two: Some limits on our capacity for processing information. *Psychological review*, 63, 81. doi: 10.1037/h0043158
- Miller R. (1991). Cortico-hippocampal interplay and the representation of contexts in the brain. *Studies of Brain Function Vol. 17*. Berlin: Springer. doi: 10.1007/978-3-662-21732-0
- Millett, D. (2001). Hans Berger: From psychic energy to the EEG. *Perspectives in biology and medicine*, 44, 522-542. doi: 10.1353/pbm.2001.0070
- Milner, A.D., and Goodale, M.A. (2006). *The visual brain in action*. New York: Oxford University Press. doi: 10.1093/acprof:oso/9780198524724.001.0001
- Milner, A.D., and Goodale, M.A. (2008). Two visual systems re-viewed. *Neuropsychologia*, 46, 774-785. doi: 10.1016/j.neuropsychologia.2007.10.005
- Mitchell, D.J., McNaughton, N., Flanagan, D., and Kirk, I.J. (2008). Frontal-midline theta from the perspective of hippocampal “theta”. *Progress in neurobiology*, 86, 156-185. doi: 10.1016/j.pneurobio.2008.09.005
- Mölle, M., Marshall, L., Fehm, H.L., and Born, J. (2002). EEG theta synchronization conjoined with alpha desynchronization indicate intentional encoding. *European Journal of Neuroscience*, 15, 923-928. doi: 10.1046/j.1460-9568.2002.01921.x
- Moore, C.D., Cohen, M.X., and Ranganath, C. (2006). Neural mechanisms of expert skills in visual working memory. *Journal of Neuroscience*, 26, 11187-11196. doi: 10.1523/JNEUROSCI.1873-06.2006

- Müller, M.M., Gruber, T., and Keil, A. (2000). Modulation of induced gamma band activity in the human EEG by attention and visual information processing. *International Journal of Psychophysiology*, 38, 283-299. doi: 10.1016/S0167-8760(00)00171-9
- Neuper, C., and Pfurtscheller, G. (2001). Event-related dynamics of cortical rhythms: frequency-specific features and functional correlates. *International journal of psychophysiology*, 43, 41-58. doi: 10.1016/S0167-8760(01)00178-7
- Nichols, E.A., Kao, Y.C., Verfaellie, M., & Gabrieli, J.D. (2006). Working memory and long-term memory for faces: Evidence from fMRI and global amnesia for involvement of the medial temporal lobes. *Hippocampus*, 16, 604-616. doi: 10.1002/hipo.20190
- Nolte, G., Bai, O., Wheaton, L., Mari, Z., Vorbach, S., and Hallett, M. (2004). Identifying true brain interaction from EEG data using the imaginary part of coherency. *Clinical neurophysiology*, 115, 2292-2307. doi: 10.1016/j.clinph.2004.04.029
- Norman, D.A. (1968). Toward a theory of memory and attention. *Psychological review*, 75, 522. doi: 10.1037/h0026699
- Oberauer, K., and Eichenberger, S. (2013). Visual working memory declines when more features must be remembered for each object. *Memory & Cognition*, 41, 1212-1227. doi: 10.3758/s13421-013-0333-6
- Obleser, J., Wöstmann, M., Hellbernd, N., Wilsch, A., and Maess, B. (2012). Adverse listening conditions and memory load drive a common alpha oscillatory network. *Journal of Neuroscience*, 32, 12376-12383. doi: 10.1523/JNEUROSCI.4908-11.2012
- Olivers, C. N., Meijer, F., and Theeuwes, J. (2006). Feature-based memory-driven attentional capture: visual working memory content affects visual attention. *Journal of Experimental Psychology: Human Perception and Performance*, 32, 1243. doi: 10.1037/0096-1523.32.5.1243
- Olszewska, J.M., Reuter-Lorenz, P.A., Munier, E., and Bendler, S.A. (2015). Misremembering what you see or hear: Dissociable effects of modality on short- and long-term false recognition. *Journal of Experimental Psychology: Learning, Memory, and Cognition*, 41, 1316. doi: 10.1037/xlm0000115
- Onton, J., Delorme, A., and Makeig, S. (2005). Frontal midline EEG dynamics during working memory. *Neuroimage*, 27, 341-356. doi: 10.1016/j.neuroimage.2005.04.014
- Oostenveld, R., Fries, P., Maris, E., and Schoffelen, J.M. (2011). FieldTrip: Open source software for advanced analysis of MEG, EEG, and invasive electrophysiological

- data. *Computational intelligence and neuroscience*, 2011, 1-9. doi: 10.1155/2011/156869
- Osaka, N., Osaka, M., Kondo, H., Morishita, M., Fukuyama, H., and Shibasaki, H. (2004). The neural basis of executive function in working memory: An fMRI study based on individual differences. *Neuroimage*, 21, 623-631. doi: 10.1016/j.neuroimage.2003.09.069
- Osipova, D., Takashima, A., Oostenveld, R., Fernández, G., Maris, E., and Jensen, O. (2006). Theta and gamma oscillations predict encoding and retrieval of declarative memory. *Journal of neuroscience*, 26, 7523-7531. doi: 10.1523/JNEUROSCI.1948-06.2006
- Özkurt, T.E., and Schnitzler, A. (2011). A critical note on the definition of phase–amplitude cross-frequency coupling. *Journal of Neuroscience methods*, 201, 438-443. doi: 10.1016/j.jneumeth.2011.08.014
- Özkurt, T.E. (2012). Statistically reliable and fast direct estimation of phase-amplitude cross-frequency coupling. *IEEE Transactions on Biomedical Engineering*, 59, 1943-1950. doi: 10.1109/TBME.2012.2194783
- Palmer, S.E. (1999). *Vision science: Photons to phenomenology*. Cambridge, MA: The MIT Press.
- Palva, J.M., Monto, S., Kulashekhar, S., and Palva, S. (2010). Neuronal synchrony reveals working memory networks and predicts individual memory capacity. *Proceedings of the National Academy of Sciences*, 107, 7580-7585. doi: 10.1073/pnas.0913113107
- Palva, S., Kulashekhar, S., Hämäläinen, M., and Palva, J.M. (2011). Localization of cortical phase and amplitude dynamics during visual working memory encoding and retention. *Journal of Neuroscience*, 31, 5013-5025. doi: 10.1523/JNEUROSCI.5592-10.2011
- Park, H., Lee, D.S., Kang, E., Kang, H., Hahm, J., Kim, J.S., Chung, C.K., Jiang, H., Gross, J., and Jensen, O. (2016). Formation of visual memories controlled by gamma power phase-locked to alpha oscillations. *Scientific reports*, 6, 28092. doi: 10.1038/srep28092
- Parra, M.A., Della Sala, S., Logie, R.H., and Morcom, A.M. (2014). Neural correlates of shape–color binding in visual working memory. *Neuropsychologia*, 52, 27-36. doi: 10.1016/j.neuropsychologia.2013.09.036
- Pasternak, T., and Greenlee, M.W. (2005). Working memory in primate sensory systems. *Nature Reviews Neuroscience*, 6, 97. doi: 10.1038/nrn1603

- Pfurtscheller, G., and Lopes da Silva, F.H. (1999). Event-related EEG/MEG synchronization and desynchronization: basic principles. *Clinical neurophysiology*, 110, 1842-1857. doi: 10.1016/S1388-2457(99)00141-8
- Posner, M.I., and Snyder, C.R.R. (1975). Facilitation and inhibition in the processing of signals. *Attention and performance V*, 669–682.
- Prinzmetal, W., Presti, D. E., and Posner, M. I. (1986). Does attention affect visual feature integration? *Journal of Experimental Psychology: Human Perception and Performance*, 12, 361-369. doi: 10.1037/0096-1523.12.3.361
- Race, E., LaRocque, K.F., Keane, M.M., and Verfaellie, M. (2013). Medial temporal lobe contributions to short-term memory for faces. *Journal of Experimental Psychology: General*, 142, 1309. doi: 10.1037/a0033612
- Raghavachari, S., Kahana, M.J., Rizzuto, D.S., Caplan, J.B., Kirschen, M.P., Bourgeois, B., Madsen, J. R., and Lisman, J. E. (2001). Gating of human theta oscillations by a working memory task. *Journal of Neuroscience*, 21, 3175-3183. doi: 10.1523/JNEUROSCI.21-09-03175.2001
- Raghavachari, S., Lisman, J.E., Tully, M., Madsen, J.R., Bromfield, E., and Kahana, M.J. (2006). Theta oscillations in human cortex during a working-memory task: Evidence for local generators. *Journal of Neurophysiology*, 95, 1630-1638. doi: 10.1152/jn.00409.2005
- Rihs, T.A., Michel, C.M., & Thut, G. (2007). Mechanisms of selective inhibition in visual spatial attention are indexed by α -band EEG synchronization. *European Journal of Neuroscience*, 25, 603-610. doi: 10.1111/j.1460-9568.2007.05278.x
- Rizzuto, D.S., Madsen, J.R., Bromfield, E.B., Schulze-Bonhage, A., Seelig, D., Aschenbrenner-Scheibe, R., and Kahana, M.J. (2003). Reset of human neocortical oscillations during a working memory task. *Proceedings of the national academy of Sciences*, 100, 7931-7936. doi: 10.1073/pnas.0732061100
- Roediger, H.L., and McDermott, K.B. (1995). Creating false memories: Remembering words not presented in lists. *Journal of experimental psychology: Learning, Memory, and Cognition*, 21, 803-814. doi: 10.1037/0278-7393.21.4.803
- Roux, F., Wibral, M., Mohr, H.M., Singer, W., and Uhlhaas, P.J. (2012). Gamma-band activity in human prefrontal cortex codes for the number of relevant items maintained in working memory. *Journal of Neuroscience*, 32, 12411-12420. doi: 10.1523/JNEUROSCI.0421-12.2012
- Roux, F., and Uhlhaas, P.J. (2014). Working memory and neural oscillations: alpha-gamma versus theta-gamma codes for distinct WM information? *Trends in cognitive sciences*, 18, 16-25. doi: 10.1016/j.tics.2013.10.010

- Sauseng, P., Klimesch, W., Doppelmayr, M., Hanslmayr, S., Schabus, M., and Gruber, W.R. (2004). Theta coupling in the human electroencephalogram during a working memory task. *Neuroscience letters*, 354, 123-126. doi: 10.1016/j.neulet.2003.10.002
- Sauseng, P., Klimesch, W., Schabus, M., and Doppelmayr, M. (2005a). Fronto-parietal EEG coherence in theta and upper alpha reflect central executive functions of working memory. *International Journal of Psychophysiology*, 57, 97-103. doi: 10.1016/j.ijpsycho.2005.03.018
- Sauseng, P., Klimesch, W., Stadler, W., Schabus, M., Doppelmayr, M., Hanslmayr, S., Gruber, W.R., and Birbaumer, N. (2005b). A shift of visual spatial attention is selectively associated with human EEG alpha activity. *European Journal of Neuroscience*, 22, 2917-2926. doi: 10.1111/j.1460-9568.2005.04482.x
- Sauseng, P., Hoppe, J., Klimesch, W., Gerloff, C., and Hummel, F.C. (2007). Dissociation of sustained attention from central executive functions: local activity and interregional connectivity in the theta range. *European Journal of Neuroscience*, 25, 587-593. doi: 10.1111/j.1460-9568.2006.05286.x
- Sauseng, P., Griesmayr, B., Freunberger, R., and Klimesch, W. (2010). Control mechanisms in working memory: a possible function of EEG theta oscillations. *Neuroscience & Biobehavioral Reviews*, 34, 1015-1022. doi: 10.1016/j.neubiorev.2009.12.006
- Schacter, D.L., Guerin, S.A., and Jacques, P.L.S. (2011). Memory distortion: an adaptive perspective. *Trends in cognitive sciences*, 15, 467-474. doi: 10.1016/j.tics.2011.08.004
- Scheeringa, R., Petersson, K.M., Oostenveld, R., Norris, D.G., Hagoort, P., and Bastiaansen, M.C. (2009). Trial-by-trial coupling between EEG and BOLD identifies networks related to alpha and theta EEG power increases during working memory maintenance. *Neuroimage*, 44, 1224-1238. doi: 74710.1016/j.neuroimage.2008.08.041
- Seamon, J.G., Luo, C.R., Schlegel, S.E., Greene, S.E., and Goldenberg, A.B. (2000). False memory for categorized pictures and words: The category associates procedure for studying memory errors in children and adults. *Journal of Memory and Language*, 42, 120-146. doi: 10.1006/jmla.1999.2676
- Sederberg, P.B., Kahana, M.J., Howard, M.W., Donner, E.J., and Madsen, J.R. (2003). Theta and gamma oscillations during encoding predict subsequent recall. *Journal of Neuroscience*, 23, 10809-10814. doi: 10.1523/JNEUROSCI.23-34-10809.2003
- Sederberg, P.B., Schulze-Bonhage, A., Madsen, J.R., Bromfield, E.B., McCarthy, D.C., Brandt, A., Tully, M.S., and Kahana, M. J. (2006). Hippocampal and neocortical

- gamma oscillations predict memory formation in humans. *Cerebral Cortex*, 17, 1190-1196. doi: 10.1093/cercor/bhl030
- Serences, J.T., Ester, E.F., Vogel, E.K., and Awh, E. (2009). Stimulus-specific delay activity in human primary visual cortex. *Psychological science*, 20, 207-214. doi: 10.1111/j.1467-9280.2009.02276.x
- Siegel, M., Engel, A.K., and Donner, T.H. (2011). Cortical network dynamics of perceptual decision-making in the human brain. *Frontiers in human neuroscience*, 5, 21. doi: 10.3389/fnhum.2011.00021
- Singer, W., and Gray, C.M. (1995). Visual feature integration and the temporal correlation hypothesis. *Annual review of neuroscience*, 18, 555-586. doi: 10.1146/annurev.ne.18.030195.003011
- Singer, W. (2009). Distributed processing and temporal codes in neuronal networks. *Cognitive neurodynamics*, 3, 189-196. doi: 10.1007/s11571-009-9087-z
- Slotnick, S.D., and Schacter, D L. (2004). A sensory signature that distinguishes true from false memories. *Nature neuroscience*, 7, 664. doi:10.1038/nn1252
- Spitzer, B., and Haegens, S. (2017). Beyond the status Quo: a role for beta oscillations in endogenous content (Re-) activation. *eneuro*, 4 ENEURO-0170. doi: 10.1523/ENEURO.0170-17.2017
- Sporns, O. (2010). *Networks of the Brain*. Cambridge, MA: The MIT Press.
- Stipacek, A., Grabner, R., Neuper, C., Fink, A., and Neubauer, A. (2003). Sensitivity of human EEG alpha band desynchronization to different working memory components and increasing levels of memory load. *Neuroscience letters*, 353, 193-196. doi: 10.1016/j.neulet.2003.09.044
- Stone, J.V. (2012). *Vision and brain: How we perceive the world*. Cambridge, MA: The MIT Press.
- Tallon-Baudry, C., Bertrand, O., Peronnet, F., and Pernier, J. (1998). Induced γ -band activity during the delay of a visual short-term memory task in humans. *Journal of Neuroscience*, 18, 4244-4254. doi: 10.1523/JNEUROSCI.18-11-04244.1998
- Tallon-Baudry, C., Kreiter, A., and Bertrand, O. (1999). Sustained and transient oscillatory responses in the gamma and beta bands in a visual short-term memory task in humans. *Visual neuroscience*, 16, 449-459. doi: 10.1017/S0952523899163065
- Tallon-Baudry, C., Bertrand, O., and Fischer, C. (2001). Oscillatory synchrony between human extrastriate areas during visual short-term memory maintenance. *Journal*

- of Neuroscience*, 21, RC177-RC177. doi: 10.1523/JNEUROSCI.21-20-j0008.2001
- Thut, G., Nietzel, A., Brandt, S.A., and Pascual-Leone, A. (2006). α -Band electroencephalographic activity over occipital cortex indexes visuospatial attention bias and predicts visual target detection. *Journal of Neuroscience*, 26, 9494-9502. doi: 10.1523/JNEUROSCI.0875-06.2006
- Treisman, A. M. (1964). Verbal cues, language, and meaning in selective attention. *The American journal of psychology*, 77, 206-219. doi: 10.2307/1420127
- Tseng, P., Chang, Y.T., Chang, C.F., Liang, W.K., and Juan, C.H. (2016). The critical role of phase difference in gamma oscillation within the temporoparietal network for binding visual working memory. *Scientific reports*, 6, 32138. doi: 10.1038/srep32138
- Tuladhar, A.M., Huurne, N.T., Schoffelen, J.M., Maris, E., Oostenveld, R., and Jensen, O. (2007). Parieto-occipital sources account for the increase in alpha activity with working memory load. *Human brain mapping*, 28, 785-792. doi: 10.1002/hbm.20306
- Ungerleider, L.G., and Haxby, J.V. (1994). 'What' and 'where' in the human brain. *Current opinion in neurobiology*, 4, 157-165. doi: 10.1016/0959-4388(94)90066-3
- Van Dijk, H., Schoffelen, J.M., Oostenveld, R., and Jensen, O. (2008). Prestimulus oscillatory activity in the alpha band predicts visual discrimination ability. *Journal of Neuroscience*, 28, 1816-1823. doi: 10.1523/JNEUROSCI.1853-07.2008
- van Oosterom, A. (1991). History and evolution of methods for solving the inverse problem. *Journal of Clinical Neurophysiology*, 8, 371-380. doi: 10.1097/00004691-199110000-00002
- Vanni, S., Revonsuo, A., and Hari, R. (1997). Modulation of the parieto-occipital alpha rhythm during object detection. *Journal of Neuroscience*, 17, 7141-7147. doi: 10.1523/JNEUROSCI.17-18-07141.1997
- Voytek, B., Canolty, R.T., Shestyuk, A., Crone, N., Parvizi, J., and Knight, R.T. (2010). Shifts in gamma phase-amplitude coupling frequency from theta to alpha over posterior cortex during visual tasks. *Frontiers in human neuroscience*, 4, 191. doi: 10.3389/fnhum.2010.00191
- Vrba, J., and Robinson, S.E. (2001). Signal processing in magnetoencephalography. *Methods*, 25, 249-271. doi: 10.1006/meth.2001.1238

- Waldhauser, G.T., Johansson, M., and Hanslmayr, S. (2012). Alpha/beta oscillations indicate inhibition of interfering visual memories. *Journal of Neuroscience*, 32, 1953-1961. doi: 10.1523/JNEUROSCI.4201-11.2012
- Wang, X.J. (2010). Neurophysiological and computational principles of cortical rhythms in cognition. *Physiological reviews*, 90, 1195-1268. doi: 10.1152/physrev.00035.2008
- White, T.P., Jansen, M., Doege, K., Mullinger, K.J., Park, S.B., Liddle, E.B., Gowland, P.A., Francis, S.T., Bowtell, R., and Liddle, P.F. (2013). Theta power during encoding predicts subsequent-memory performance and default mode network deactivation. *Human brain mapping*, 34, 2929-2943. doi: 10.1002/hbm.22114
- Worden, M.S., Foxe, J.J., Wang, N., and Simpson, G.V. (2000). Anticipatory biasing of visuospatial attention indexed by retinotopically specific-band electroencephalography increases over occipital cortex. *Journal of Neuroscience*, 20, 1-6. doi: <http://dx.doi.org/10.1523/JNEUROSCI.20-06-j0002.2000>
- Wróbel, A. (2000). Beta activity: A carrier for visual attention. *Acta neurobiologiae experimentalis*, 60, 247-260.
- Wyart, V., and Tallon-Baudry, C. (2008). Neural dissociation between visual awareness and spatial attention. *Journal of Neuroscience*, 28, 2667-2679. doi: 10.1523/JNEUROSCI.4748-07.2008
- Wyart, V., and Tallon-Baudry, C. (2009). How ongoing fluctuations in human visual cortex predict perceptual awareness: baseline shift versus decision bias. *Journal of Neuroscience*, 29(27), 8715-8725. doi: 10.1523/JNEUROSCI.0962-09.2009
- Yuan, P., and Raz, N. (2014). Prefrontal cortex and executive functions in healthy adults: A meta-analysis of structural neuroimaging studies. *Neuroscience & Biobehavioral Reviews*, 42, 180-192. doi: 10.1016/j.neubiorev.2014.02.005
- Yuval-Greenberg, S., Tomer, O., Keren, A.S., Nelken, I., and Deouell, L.Y. (2008). Transient induced gamma-band response in EEG as a manifestation of miniature saccades. *Neuron*, 58, 429-441. doi: 10.1016/j.neuron.2008.03.027
- Zanto, T.P., and Gazzaley, A. (2009). Neural suppression of irrelevant information underlies optimal working memory performance. *Journal of Neuroscience*, 29, 3059-3066. doi: 10.1523/JNEUROSCI.4621-08.2009

APPENDIX A

PRE-EXPERIMENT QUESTIONNAIRE

PARTICIPANT'S FORM		Date: _____
GENERAL INFORMATION		
Subject Name: _____	Phone: _____	
Subject ID: _____	E-Mail: _____	
Gender: F <input type="checkbox"/> M <input type="checkbox"/>	Handedness: L <input type="checkbox"/> R <input type="checkbox"/>	
Age: _____		
MEDICAL HISTORY		
Vision: _____	Drugs: _____	
Hearing: _____	Smoking: _____	
Sleep: _____	Alcohol: _____	
Physical Exercise: _____	Coffee/Tea: _____	
Menstruation Period: <input type="checkbox"/>		
EDUCATION INFORMATION		
University: _____	Mother Tongue: _____	
Department: _____	Other Languages: _____ /5	
Level: UG <input type="checkbox"/> BS <input type="checkbox"/>	_____ /5	
MS <input type="checkbox"/> PhD <input type="checkbox"/>		

APPENDIX B

PARTICIPANTS' INFORMATION

Subject ID	Age	Gender	Task Success Rate (%)	Task False Memory Rate (%)	Task Error Rate (%)
1	26	F	41.6667	4.1667	49.0741
2	38	F	50.4630	12.5000	37.0370
3	27	M	52.7778	9.7222	37.5000
4	21	M	69.4444	10.6481	19.9074
5	24	M	48.1481	16.6667	35.1852
6	24	F	55.0926	1.8519	38.8889
7	22	F	55.5556	10.6481	27.7778
8	20	M	49.5370	6.0185	41.2037
9	25	F	41.2037	18.5185	39.3519
10	21	M	56.9444	7.8704	35.1852
11	26	M	50.0000	5.5556	44.4444
12	24	F	51.3889	21.2963	26.8519
13	21	F	56.9444	9.7222	32.4074
14	21	F	49.5370	4.1667	46.2963
15	25	M	50.9259	6.4815	42.5926
16	23	F	46.2963	4.6296	49.0741

17	23	M	45.3704	6.0185	48.6111
18	21	M	44.4444	9.2593	45.3704
19	24	M	56.9444	6.4815	36.5741
20	24	M	50.9259	7.8704	41.2037
21	28	F	52.3148	20.3704	26.8519
22	22	F	50.9259	13.8889	35.1852
23	22	M	62.0370	10.1852	27.7778
24	20	M	46.2963	8.7963	44.9074
25	24	M	58.7963	4.6296	33.7963
26	19	M	47.6852	5.5556	40.7407
27	18	F	47.6852	6.0185	45.8333
28	25	M	49.0741	5.5556	45.3704
Pilot 1	37	F	47.2222	1.8519	50.9259
Pilot 2	28	F	43.5185	16.2037	39.8148
Pilot 3	30	F	54.1667	14.8148	31.0185
Pilot 4	37	M	54.6296	17.5926	27.7778
Pilot 5	27	F	45.8333	15.7407	37.5000
Pilot 6	28	M	53.7037	10.1852	36.1111

Table 4: Participants' information and task performance, i.e., success (*correct*), *false memory* and *error* rates.

APPENDIX C

RESPONSE TIMES

Subject ID	Response Time for Correct (s)	Response Time for False Memory (s)	Response Time for Error (s)
1	1.5514	1.8828	1.7989
2	1.7049	1.4882	1.9935
3	0.6242	0.6472	0.7862
4	0.6998	0.7159	0.7267
5	1.2746	1.3602	1.4139
6	1.1795	1.4262	1.2145
7	1.3362	1.2655	1.6290
8	1.1186	1.2747	1.3105
9	1.3461	1.3618	1.6204
10	0.8943	0.9106	0.9473
11	1.2447	1.3233	1.4398
12	1.3068	1.2352	1.6472
13	1.0295	0.8676	1.1364
14	1.2989	1.2555	1.4498
15	1.0653	1.2013	1.1366
16	0.8512	0.7426	1.1711

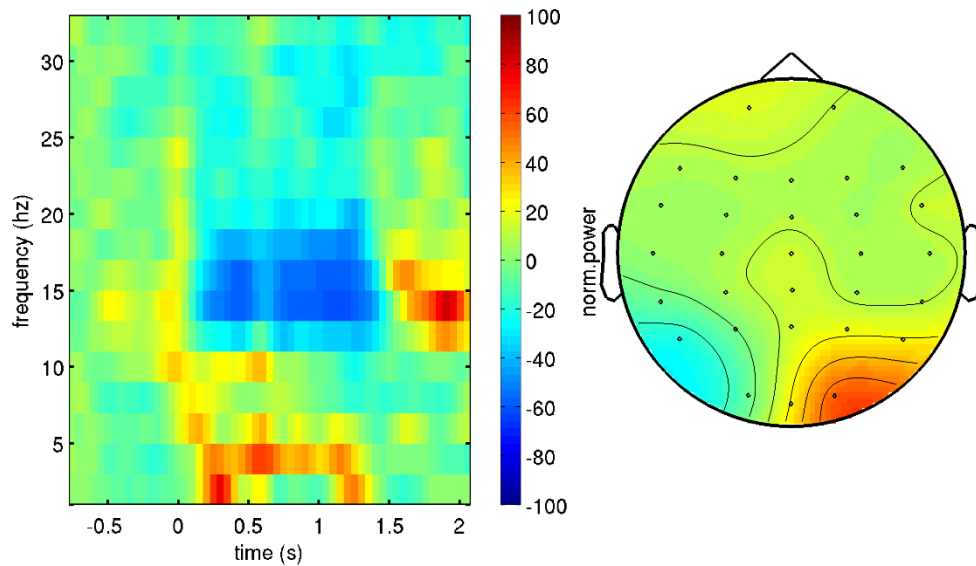
17	0.9051	1.1935	1.0613
18	1.1976	1.5783	1.2646
19	1.1332	1.0012	1.2425
20	0.9742	0.9533	1.0512
21	1.4456	1.5841	1.7905
22	1.2653	1.2910	1.5356
23	0.8745	0.9131	0.9430
24	0.8344	0.7559	0.9303
25	1.0748	0.8694	1.4233
26	1.4675	1.1647	1.8104
27	1.0487	1.1868	1.4972
28	0.6328	0.4001	0.7331
Pilot 1	1.0585	1.1531	1.0558
Pilot 2	1.2802	1.1089	1.4671
Pilot 3	1.2770	1.1656	1.5682
Pilot 4	1.1559	0.8671	1.3489
Pilot 5	1.2028	1.2951	1.6294
Pilot 6	0.9951	0.9839	0.9541

Table 5: Averaged response times for each condition and all subjects.

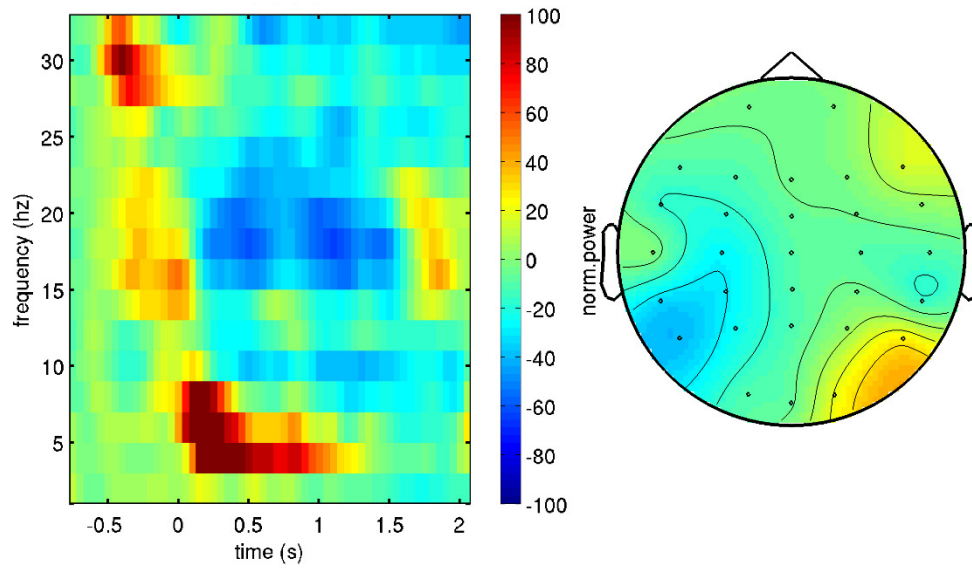
APPENDIX D

Figure 36: Time-frequency representations and topographical plots for each subject. Power values have been normalized considering the (percentage) variation from the mean baseline (see Section 3.6). The time $t = 0$ s corresponds to the onset of the first stimulus to be encoded. At $t = 1$ s the retention interval begins. Finally, the time $t = 2$ s is the earliest probe onset (Figure 11). The power values plotted in the time-frequency portraits are averaged over the posterior right channels (P4, P8, O2). The topographical plots highlight the spatial distribution of the power estimated within the time interval [1.55, 1.75] for the specific individual central frequencies (see Section 3.9).

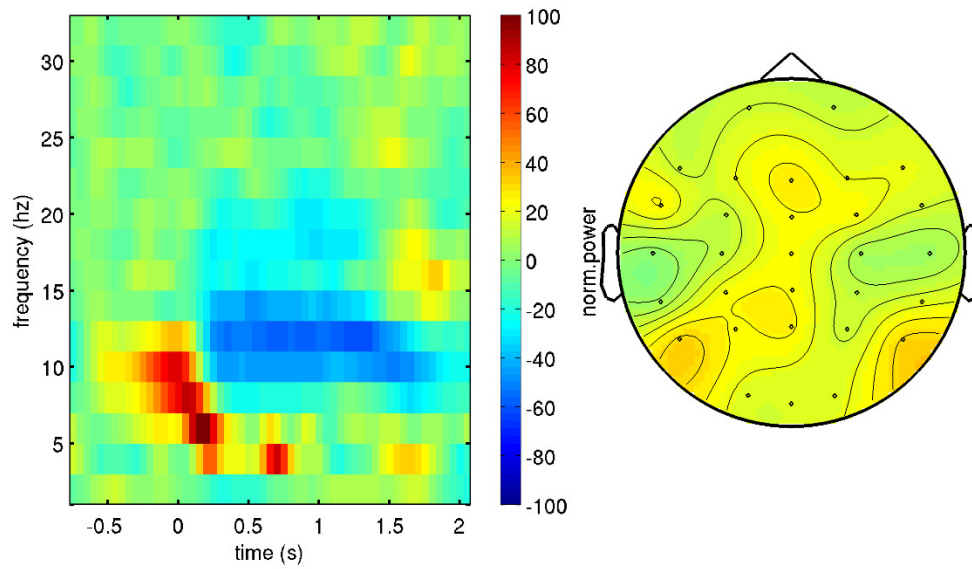
Subject 01 – ICF = 14 Hz, ICF Bandwidth = [12, 18] Hz



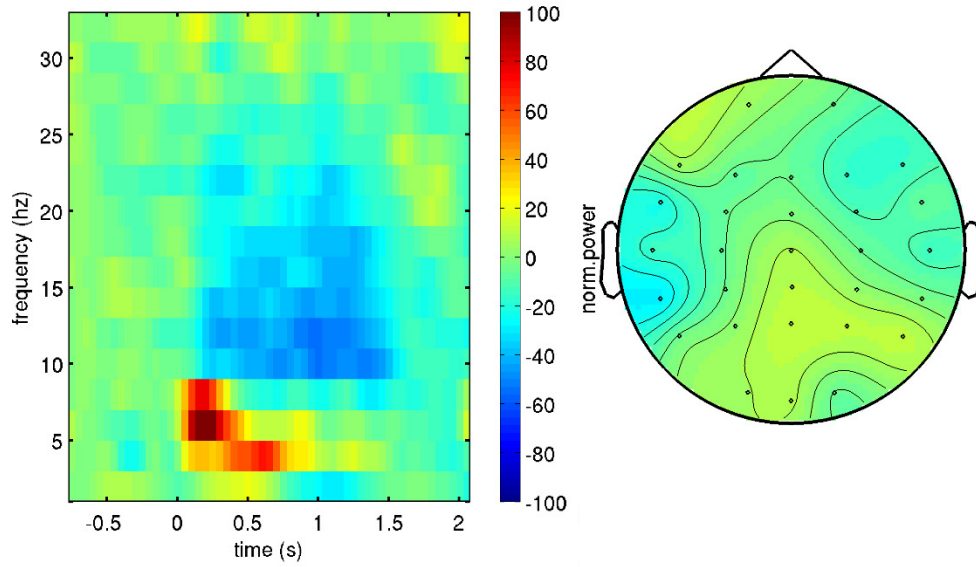
Subject 02 – ICF = 20 Hz, ICF Bandwidth = [16, 20] Hz



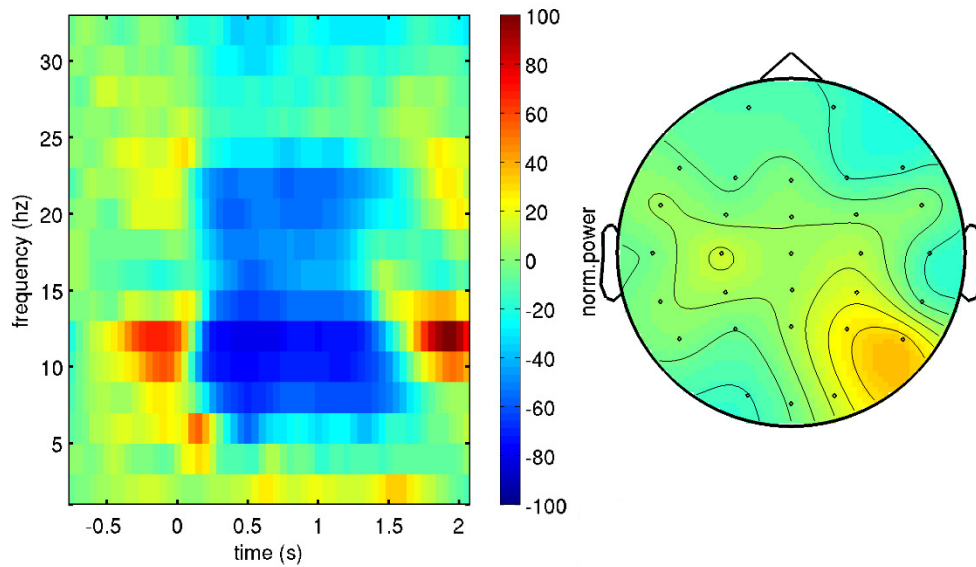
Subject 03 – ICF = 16 Hz, ICF Bandwidth = [14, 16] Hz



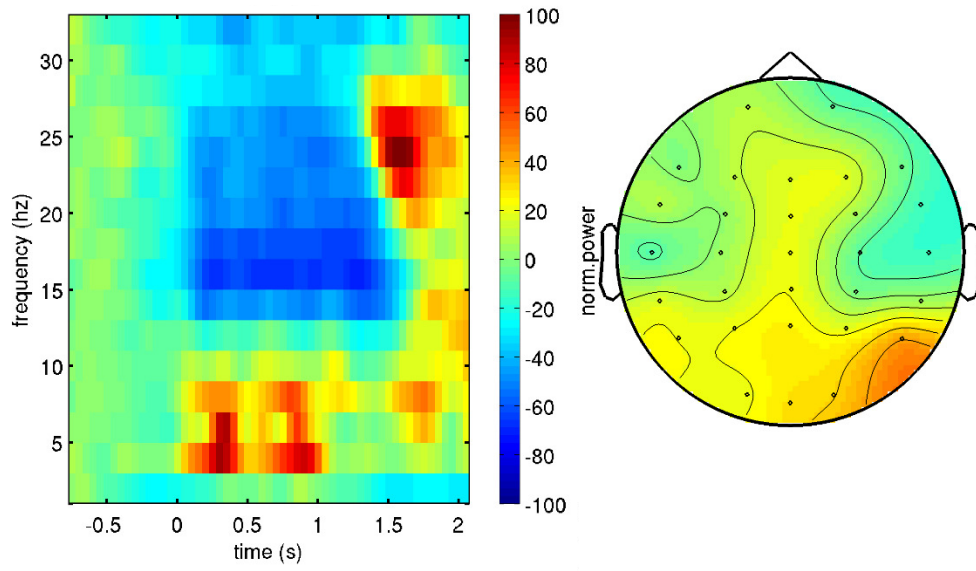
Subject 04 – ICF = 24 Hz, ICF Bandwidth = [24, 24] Hz



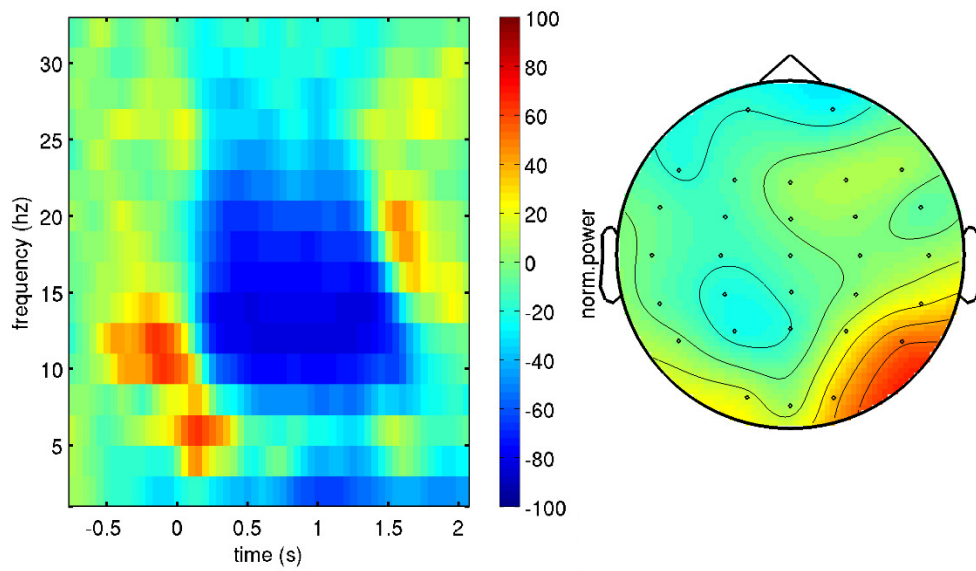
Subject 05 – ICF = 14 Hz, ICF Bandwidth = [12, 14] Hz



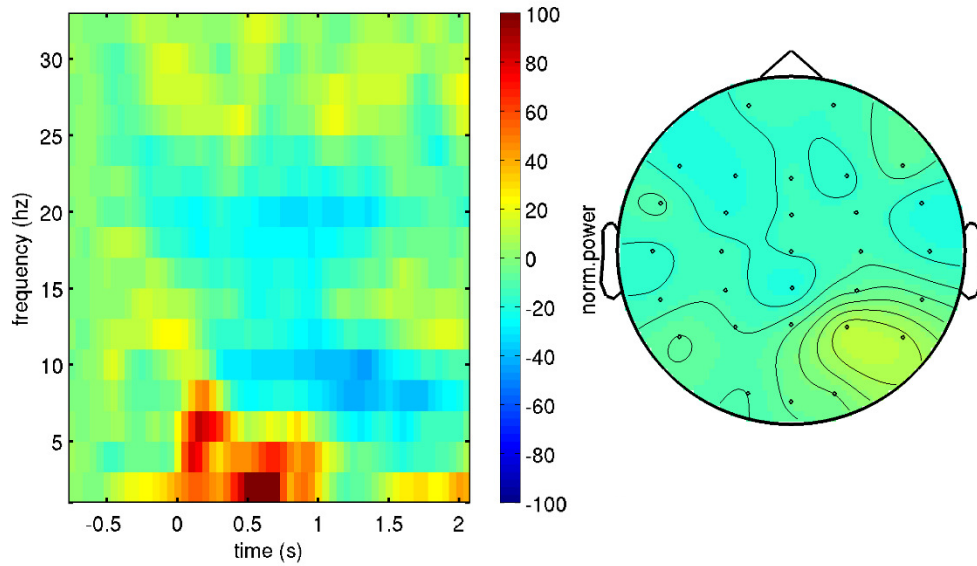
Subject 6 – ICF = 26 Hz, ICF Bandwidth = [20, 28] Hz



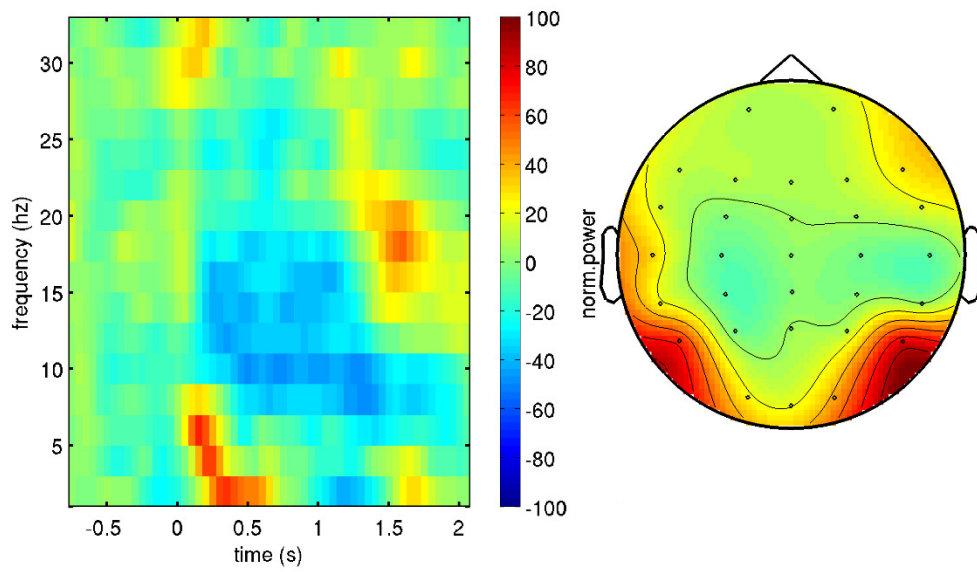
Subject 7 – ICF = 20 Hz, ICF Bandwidth = [16, 22] Hz



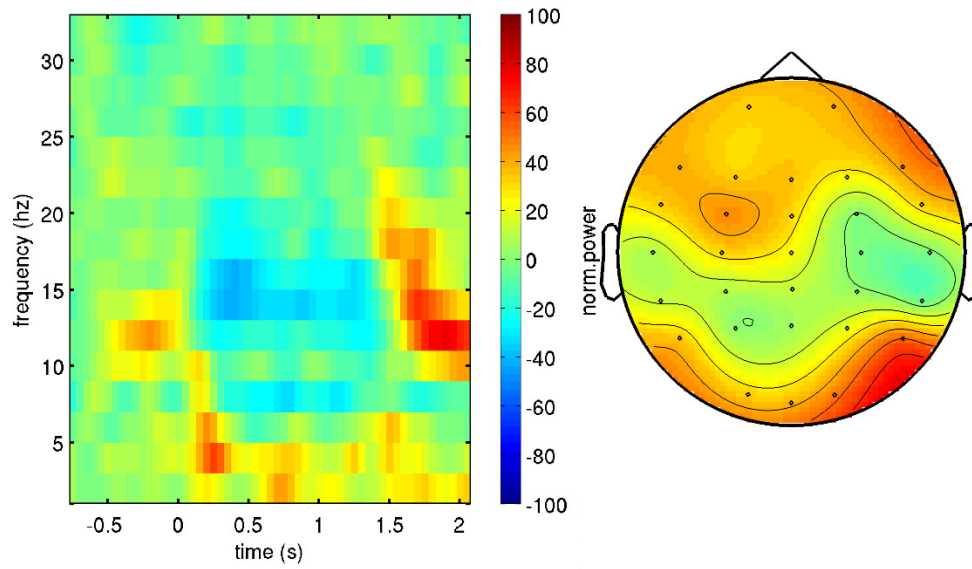
Subject 8 – ICF = 12 Hz, ICF Bandwidth = [10, 16] Hz



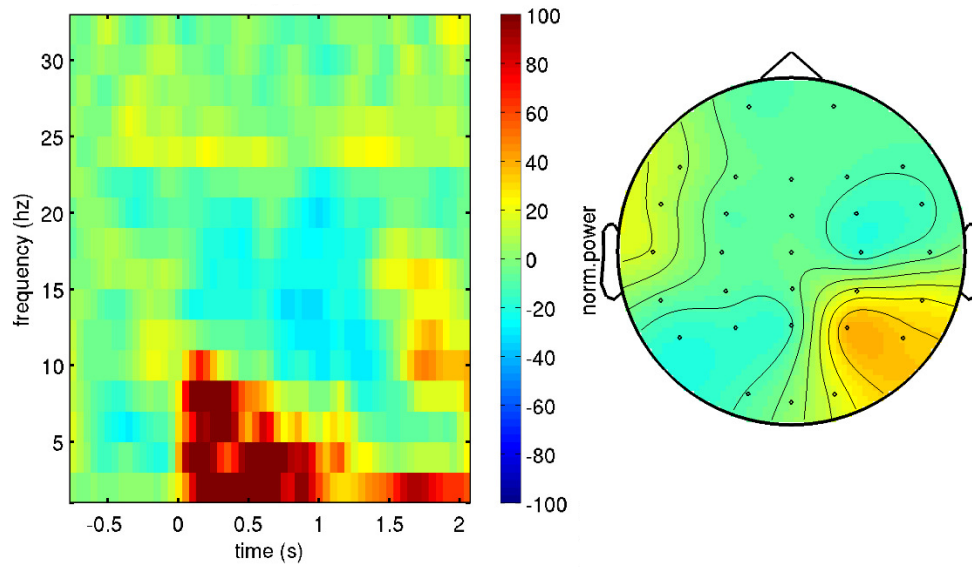
Subject 9 – ICF = 18 Hz, ICF Bandwidth = [14, 22] Hz



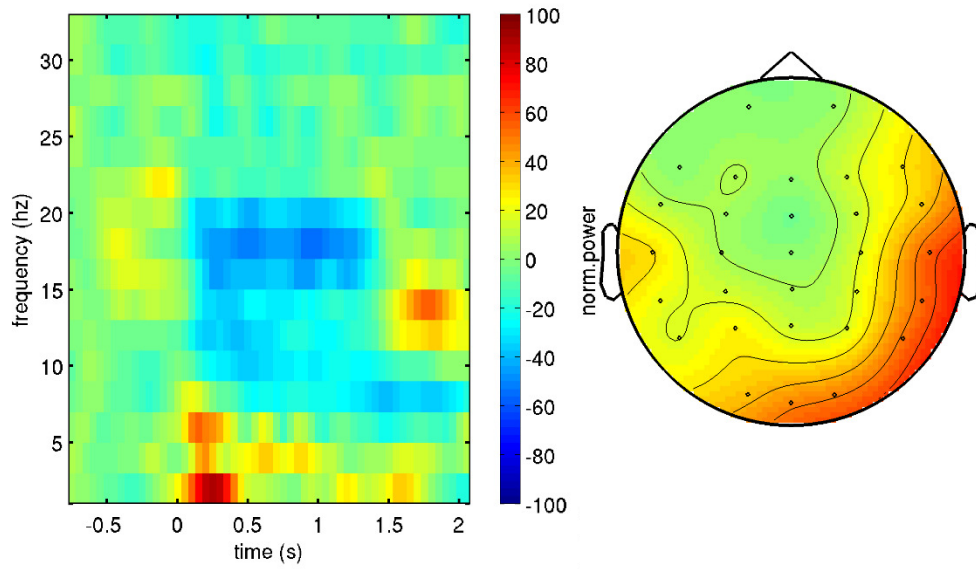
Subject 10 – ICF = 18 Hz, ICF Bandwidth = [12, 20] Hz



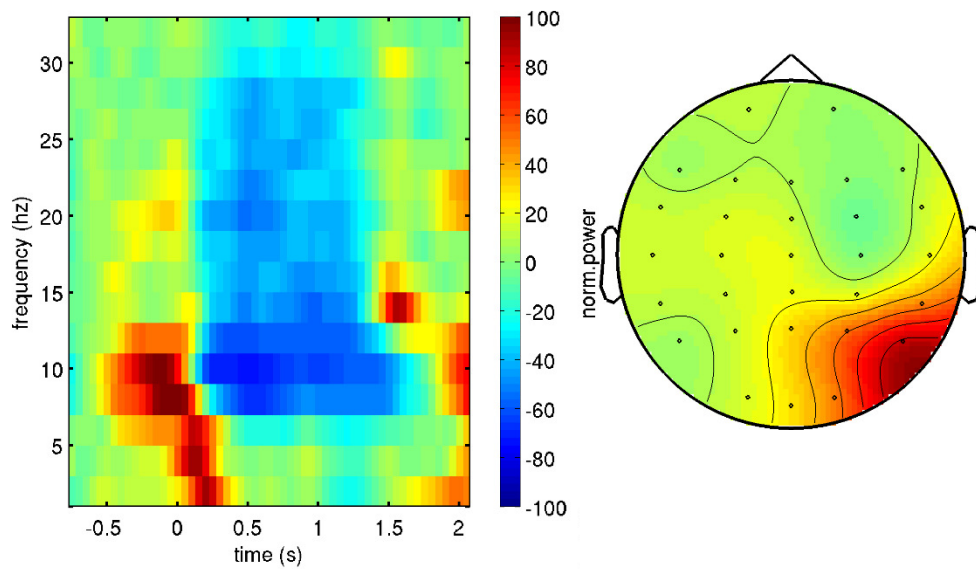
Subject 11 – ICF = 10 Hz, ICF Bandwidth = [8, 12] Hz



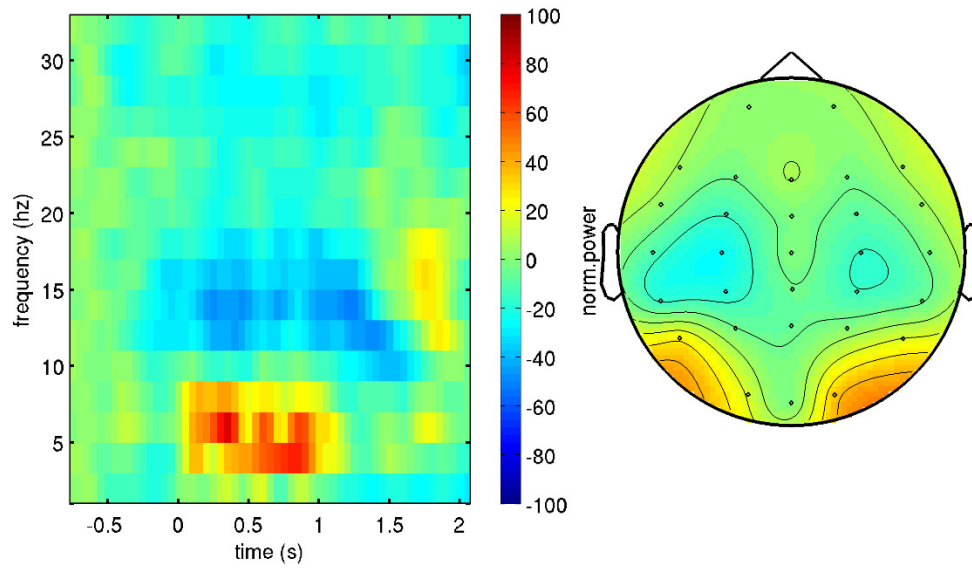
Subject 12 – ICF = 14 Hz, ICF Bandwidth = [14, 18] Hz



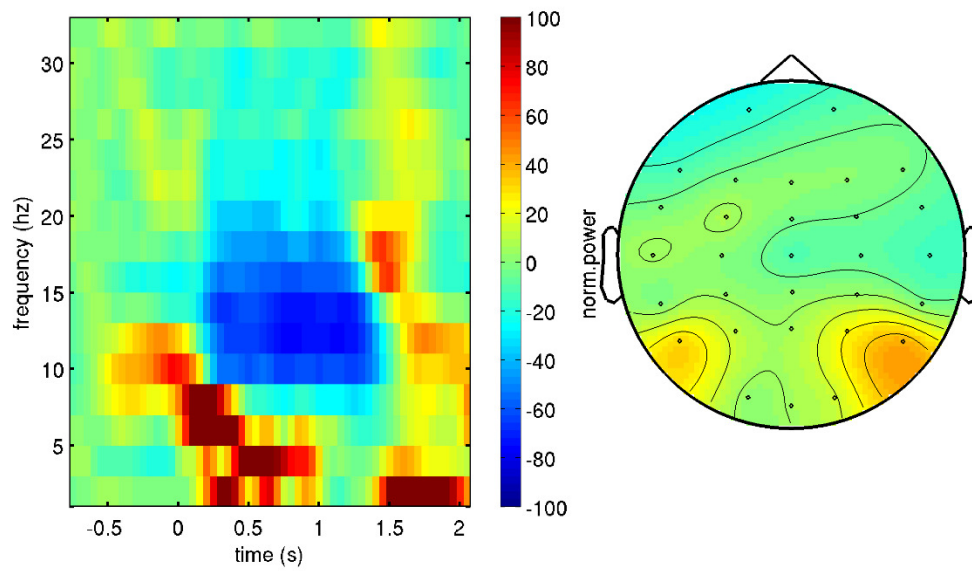
Subject 13 – ICF = 14 Hz, ICF Bandwidth = [14, 18] Hz



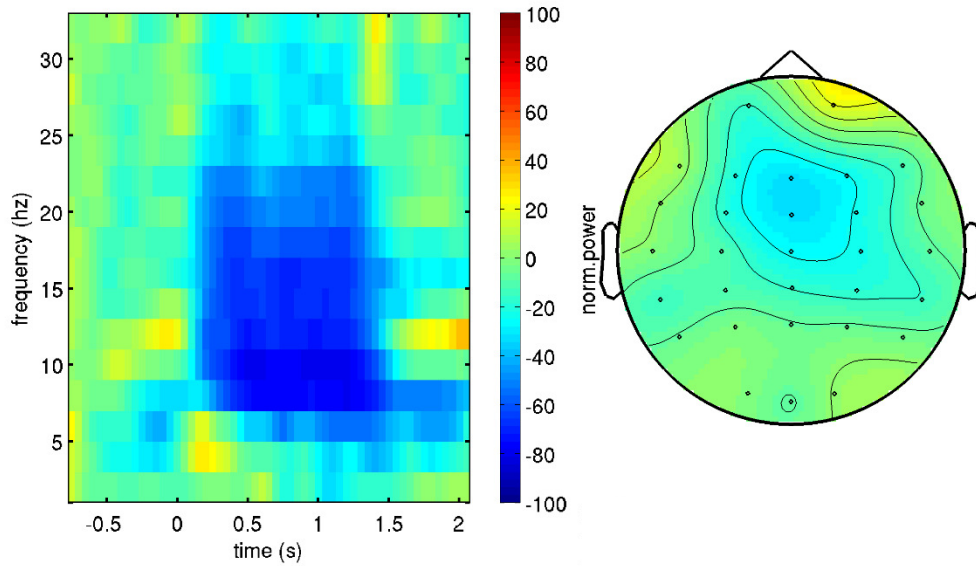
Subject 14 – ICF = 16 Hz, ICF Bandwidth = [12, 18] Hz



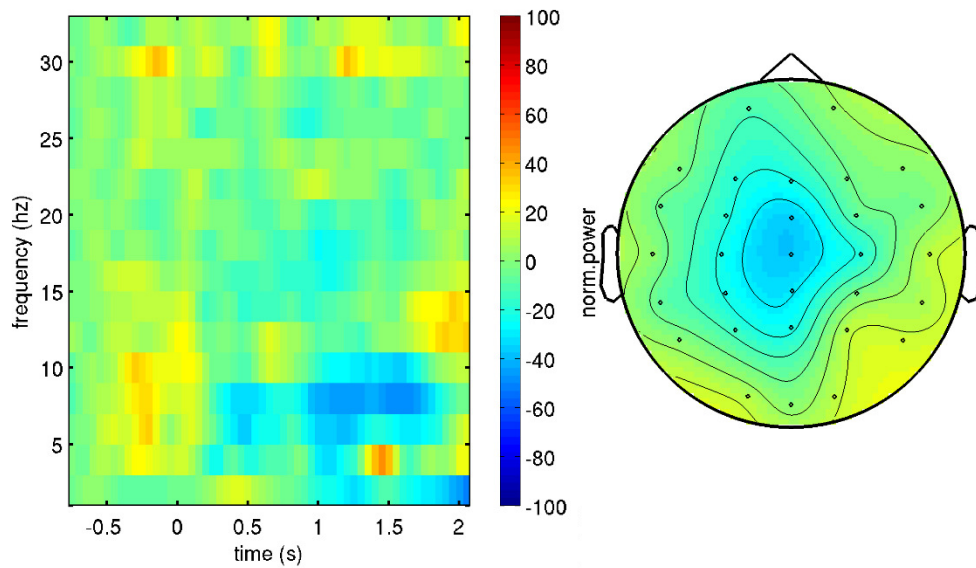
Subject 15 – ICF = 18 Hz, ICF Bandwidth = [16, 20] Hz



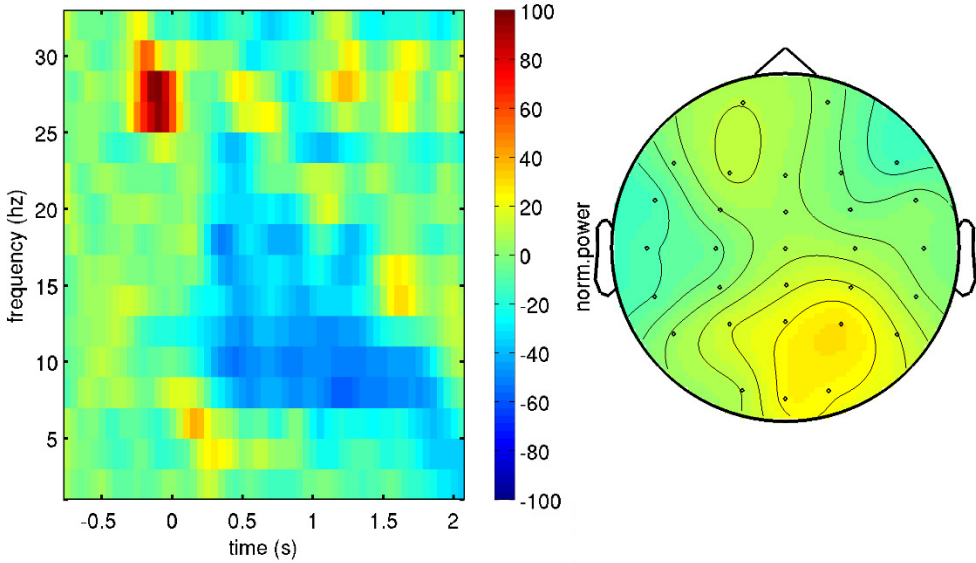
Subject 16 – ICF = 20 Hz, ICF Bandwidth = [20, 22] Hz



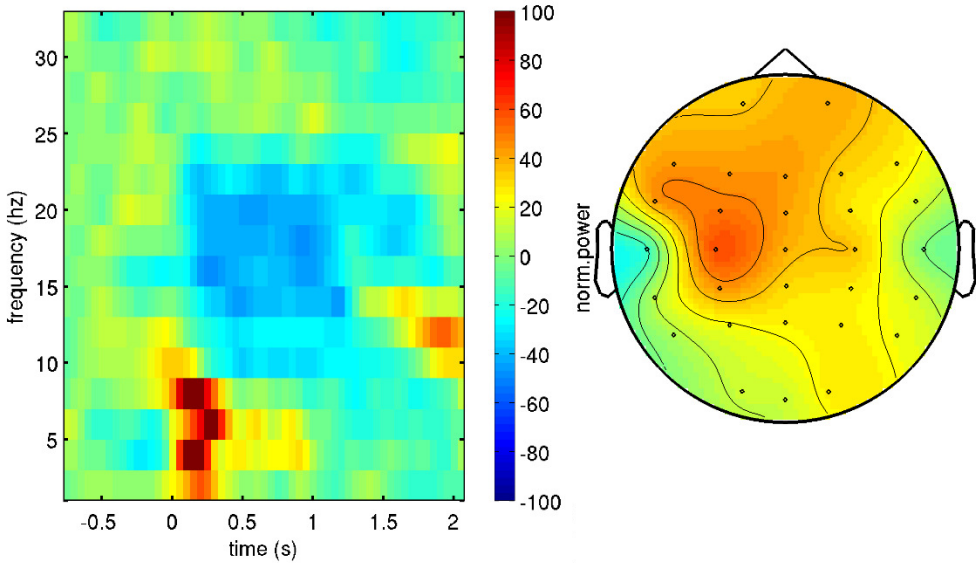
Subject 17 – ICF = 14 Hz, ICF Bandwidth = [14, 14] Hz



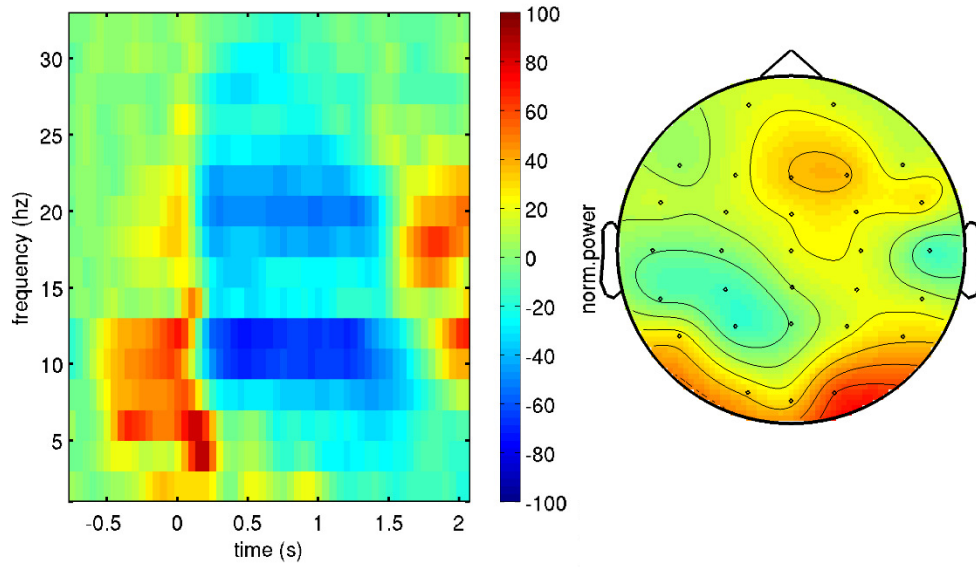
Subject 18 – ICF = 14 Hz, ICF Bandwidth = [14, 14] Hz



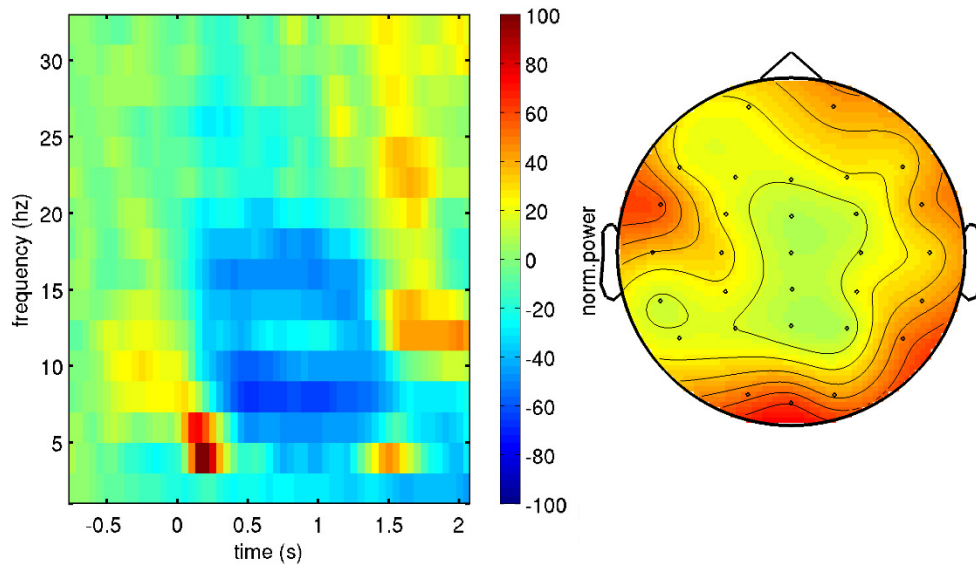
Subject 19 – ICF = 14 Hz, ICF Bandwidth = [12, 14] Hz



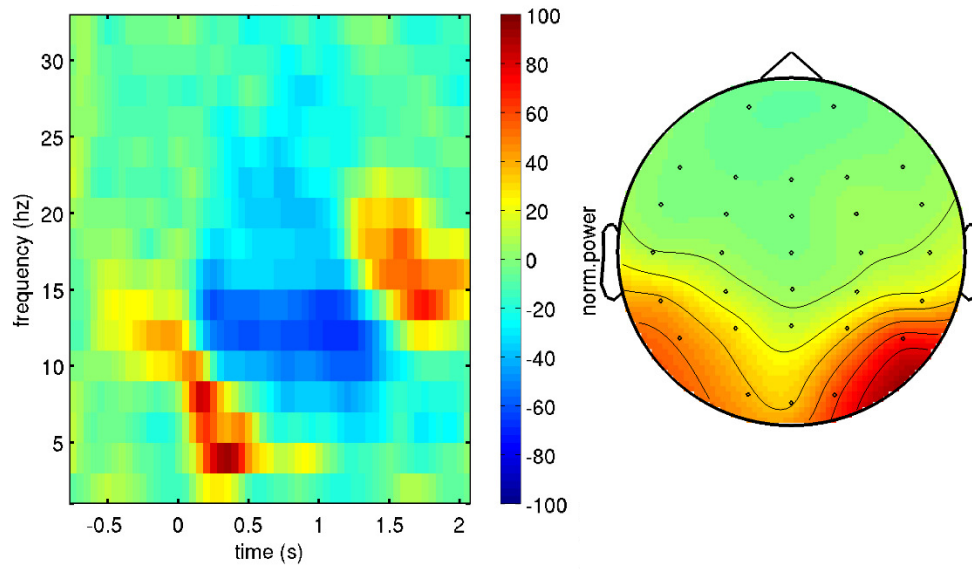
Subject 20 – ICF = 18 Hz, ICF Bandwidth = [16, 18] Hz



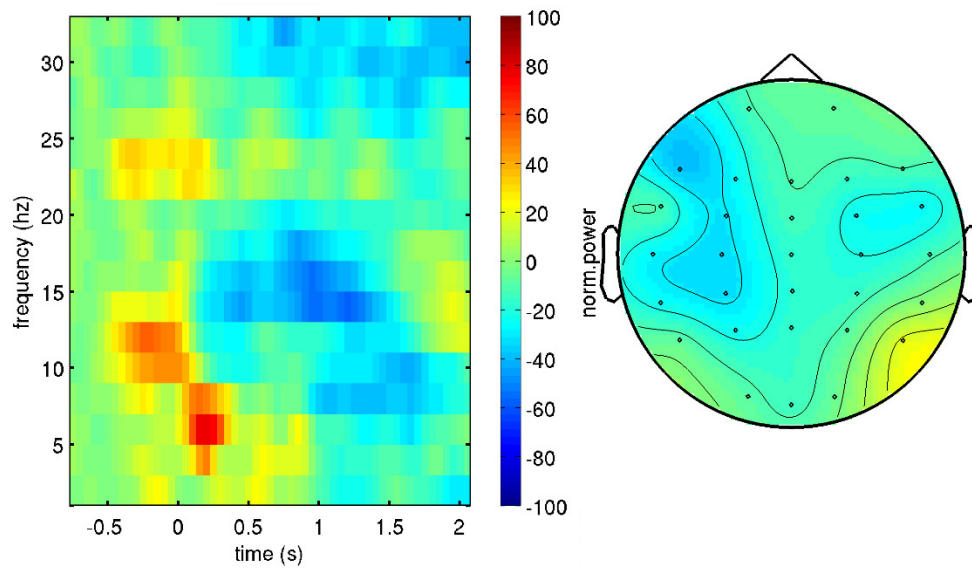
Subject 21 – ICF = 14 Hz, ICF Bandwidth = [14, 16] Hz



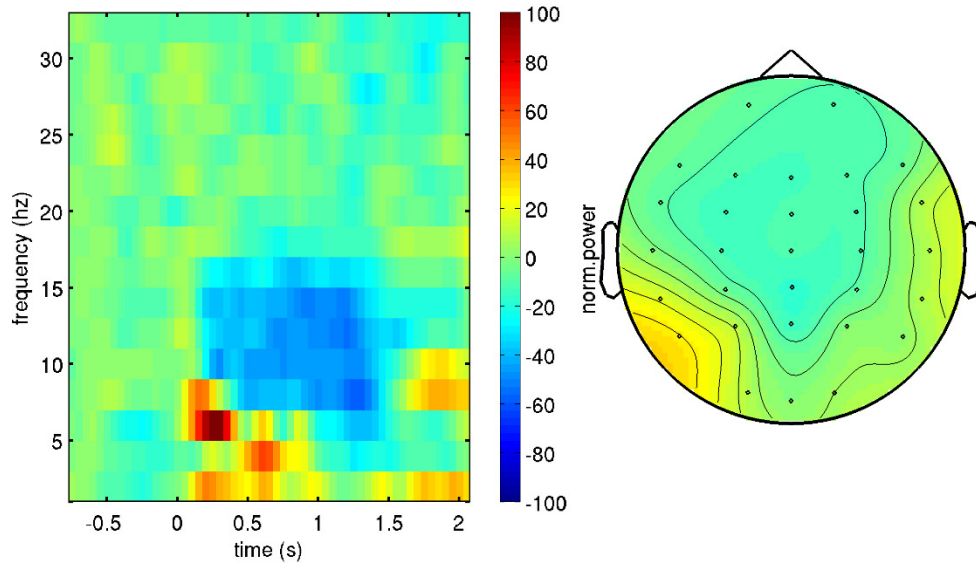
Subject 22 – ICF = 14 Hz, ICF Bandwidth = [12, 22] Hz



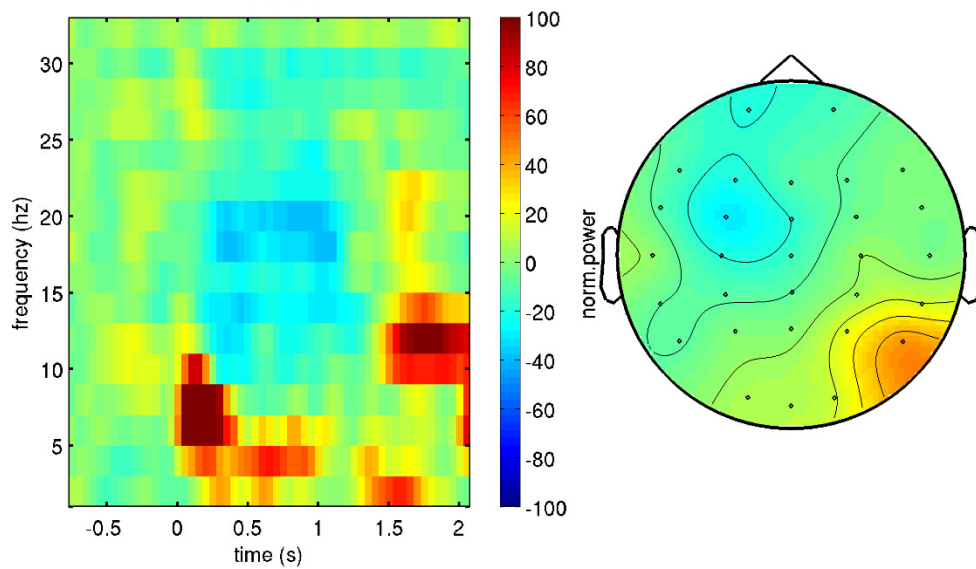
Subject 23 – ICF = 18 Hz, ICF Bandwidth = [16, 18] Hz



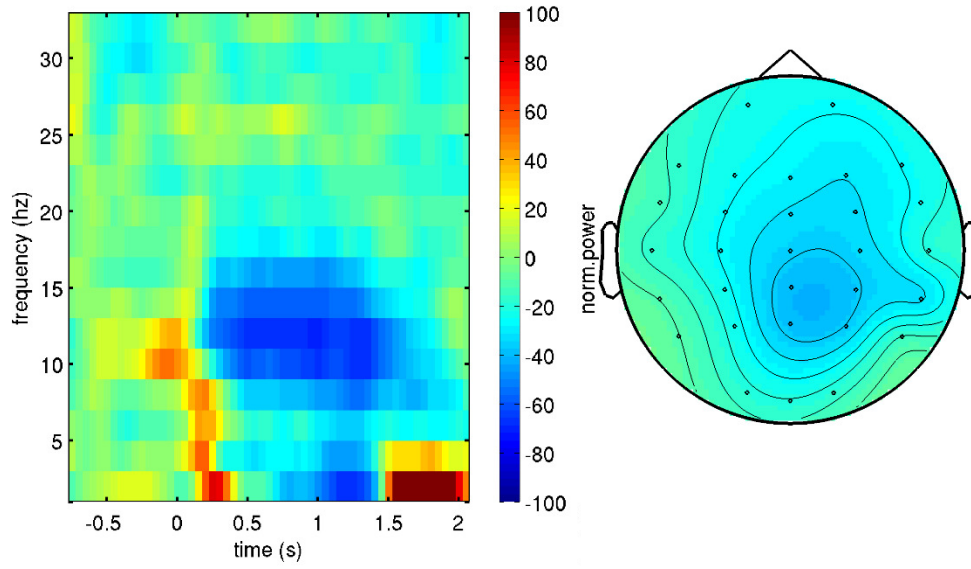
Subject 24 – ICF = 10 Hz, ICF Bandwidth = [10, 10] Hz



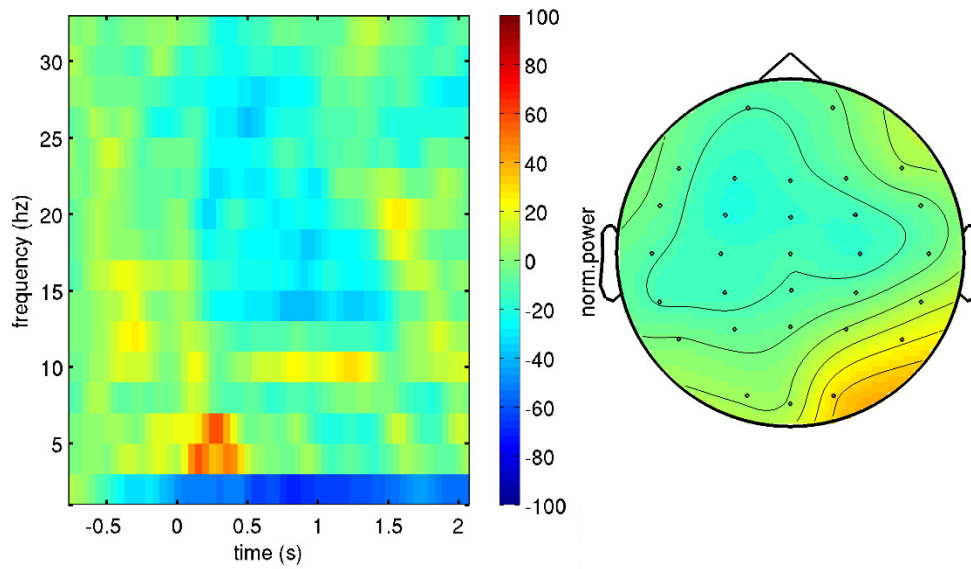
Subject 25 – ICF = 20 Hz, ICF Bandwidth = [14, 20] Hz



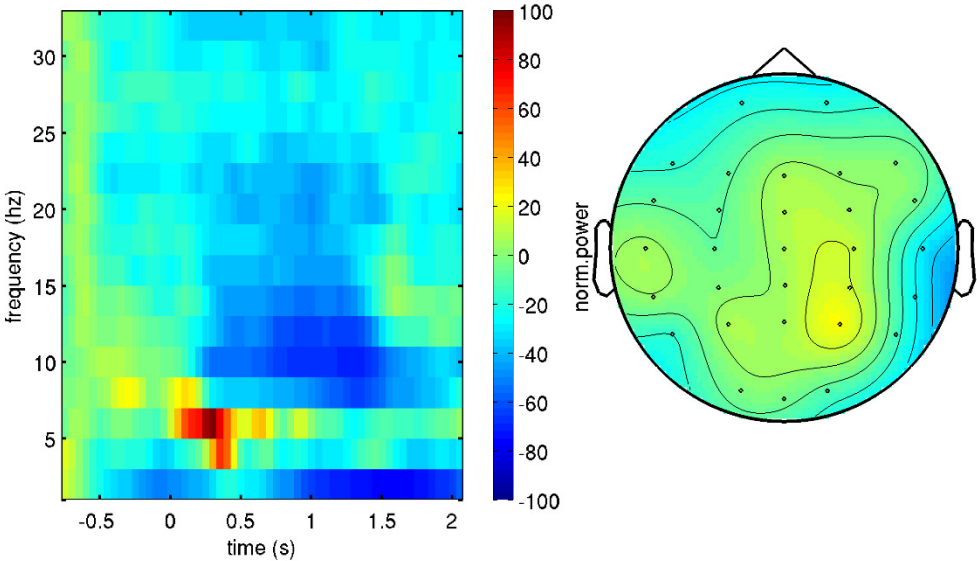
Subject 26 – ICF = 16 Hz, ICF Bandwidth = [16, 16] Hz



Subject 27 – ICF = 20 Hz, ICF Bandwidth = [18, 22] Hz



Subject 28 – ICF = 14 Hz, ICF Bandwidth = [14, 14] Hz



CURRICULUM VITAE

CONTACTS

Mobile (TR): +90 530 876 27 55

Mobile (IT): +39 331 844 94 26

E-mail: igormapelli@gmail.com

PERSONAL

Date of birth: 21/12/1978

Nationality/Citizenship: Italian

EDUCATION

2010 – 2019: Ph. D. Medical Informatics, METU, Ankara (TR)

Thesis title: “Brain Oscillatory Analysis of Visual Working Memory Errors”

1997 – 2008: M. Sc. Computer Science, Università degli Studi di Torino, Torino (IT)

(note: inclusive of BS)

Thesis title: “Genetic Clustering for Feature Selection”

Pre-university studies: Industrial technical certificate

LANGUAGE SKILLS

Italian:

Native language

English:

Understanding:

Listening: proficient user (C2)

Reading: proficient user (C2)

Speaking:

Spoken interaction: proficient user (C2)

Spoken production: proficient user (C2)

Writing:

proficient user (C2)

French:

Understanding:

Listening: proficient user (C2)

Reading: proficient user (C2)

Speaking:

Spoken interaction: proficient user (C1)

Spoken production: proficient user (C1)

Writing:

independent user (B2)

Turkish:

Elementary level

WORK EXPERIENCE

- **2013 –** : Laboratory assistant
 - **Main activities:** While performing my research duties to complete the Ph. D. requirements I have contributed to establish the Neurosignal laboratory at the METU Informatics Institute. Other than the data collection and analysis related to the thesis, I help with the maintenance and update of the EEG system, computers and others laboratory equipment. When experiments are scheduled, I help with subjects' preparation and system settings. Throughout the experiment I monitor the efficiency of the entire system to ensure that data are recorded successfully.
 - **Software used:** MATLAB, PSYCHTOOLBOX, FIELDTRIP, WEKA, SPSS, OFFICE, BRAINVISION SOFTWARE, WINDOWS, LINUX
 - **Scientific supervisor:** Assoc. Prof. Dr. Tolga Esat Özkurt

- **July 2008 – June 2009:** Temporary researcher
 - **Name of employer:** Università degli studi di Torino
 - **Employer's address:** Via Bogino n.9, Torino (IT)
 - **Main activities:** Developing computer models to ensure the traceability and valorization of production quality in certain fruit types (apples) cultivated in the region of Piedmont (Italy). Analysis of many components (morphological, chemical, physical, sensorial) for varieties recognition and yield characterization. Defining criteria to form a traceability system through the specification of distinguishing characteristics. Data mining process has been used for the characterization of effective parameters. WEKA has been the primary analysis instrument. In the end, using JAVA, I developed an application which resorts to digitalized images as input to calculate the dimension of the fruits.
 - **Software used:** WEKA, JAVA, NETBEANS, ECLIPSE, DERBY, WINDOWS, OS X
 - **Scientific supervisor:** Assoc. Prof. Dr. Marco Botta

- **November 2005 – March 2006:** Technical specialist and reprographer
 - **Name of employer:** Service Trade S.r.l. for TOROC (TORino Organising Committee)
 - **Employer's address:** Via Larga n.15, Milano (IT)
 - **Main activities:** Printers diagnostic, maintenance and management techniques for Torino 2006 Olympic Winter Games and Paralympic Winter Games.

- **1996:** Internship
 - **Name of employer:** Mairie de Sallanches (FR)
 - **Main activities:** Technical assistance

RESEARCH INTEREST

- Neural oscillations (EEG/MEG)
- Biomedical signal processing
- Statistical signal processing
- Networks of the brain
- Artificial intelligence
- Data mining
- Brain computer interface

PROJECT INVOLVED

TÜBİTAK 3501 (#112E562)	Researcher	Brain Oscillatory Analysis of Short Term Auditory and Visual False Memories	01/04/2013 – 01/10/2015
----------------------------	------------	---	----------------------------

LIST OF PUBLICATION

Journals

- Mapelli, I., and Özkurt, T.E. (2019). Brain Oscillatory Correlates of Visual Short-Term Memory Errors. *Frontiers in Human Neuroscience*, 13, 33. doi: 10.3389/fnhum.2019.00033
- Duzcu, H., Özkurt, T.E., Mapelli, I., and Hohenberger, A. (2019). N1 and P2 peak dependent temporal expectation and response discrimination in interval timing. *Acta Neurobiologiae Experimentalis*, Under Review.
- Melnik, N., Mapelli, I., and Özkurt, T.E. (2017). Modulation of alpha oscillations is required for the suppression of semantic interference. *Neurobiology of Learning and Memory*, 144, 11-18. doi: j.nlm.2017.05.007

National Conferences (Turkey)

- Mapelli, I., and Özkurt, T.E., "Classification of living and non-living objects from MEG recordings", *21st IEEE Signal Processing and Communication Applications Conference (SIU 2013)*.
- Eken, A., Mapelli, I., Saraçaydın, G., Kantar, E., Çobanoğlu, O., Kayalar, A.A., and Gökçay, D., "Representation of pain in somatosensory cortex: preliminary results from fNIRS", *21st IEEE Signal Processing and Communication Applications Conference (SIU 2013)*.

Abstracts

- Göktepe, G., Mapelli, I., and Özkurt, T.E., "Would somatosensory stimuli increase LTM performance? A preliminary EEG study", *International Conference for Cognitive Neuroscience*, Amsterdam, Netherlands, 2017.
- Mapelli, I., and Özkurt, T.E., "Alpha and Theta Synchronization Between Occipital and Frontal Regions Distinguish Errors in a Visual Working Memory Task", *BIOMAG 2016 - 20th International Conference on Biomagnetism*, Seoul, Korea, 2016.
- Mapelli, I., Melnik, N., and Özkurt, T.E., "Alpha activity in the posterior regions distinguishes visual false memories and other memory errors", *OHBM*, Hawaii, USA, 2015.

- Melnik, N., Mapelli, I., and Özkurt, T.E., "Alpha activity reflects semantic interference resolution in an auditory working memory task", *OHBM*, Hawaii, USA, 2015.
- Mapelli, I., Özer, S., and Özkurt, T.E., "Brain oscillatory analysis of gist-based short-term false memory for visual stimuli: a preliminary study", *1st Joint Turkish-German Symposium on Human Neuroscience*, Berlin, Germany, 2014.
- Mapelli, I., and Özkurt, T.E., "Feature extraction and selection for an efficient classification of MEG recordings", *INCF 2013 – Neuroinformatics Congress*, Stockholm, Sweden, 2013.
- Özkurt, T.E., Mapelli, I., and Schnitzler, A., "Efficient estimation of cross-frequency coupling from Parkinson's disease recordings", *BIOMAG 2012 - 18th International Conference on Biomagnetism*, Paris, France, 2012.

ATTENDED WORKSHOPS

- Toolkit of Cognitive Neuroscience: advanced data analysis and source modelling of EEG and MEG data, Donders Centre for Cognitive Neuroimaging, Nijmegen, The Netherlands, April 8-11, 2013

OTHER

Reviewer for the journal *Frontiers in Neuroscience*.